Surface Structure and Reactivity of Platinum in the Oxidation of Ammonia

Von der Naturwissenschaftlichen Fakultät der Gottfried Wilhelm Leibniz
Universität Hannover zur Erlangung des Grades
Doktor der Naturwissenschaften
(Dr. rer. nat.)
genehmigte Dissertation

von
Master of Engineering
Yingfeng Zeng
geboren am 28. 11. 1974 in Nanchang, China

February 2008

Referent: Prof. Dr. R. Imbihl
Koreferent: Prof. Dr. H. Pfnür
Tag der Promotion: 13. 02. 2008

To my parents, my wife Liqin and our daughter Cunhui

Kurzzusammenfassung

Diese Dissertation war Teil eines Projektes, das sich die Überwindung der Druck- und Materiallücke zwischen Einkristallstudien im UHV und der technischen Katalyse am Beispiel der katalytischen Ammoniak-Oxidation an Platin zum Ziel gesetzt hatte. In einem UHV-System wurde deshalb der Druck systematisch variiert von 10^{-6} mbar bis zum 10^{-2} mbar-Bereich. Die Kinetik der Reaktion und reaktions-induzierte Substratänderungen wurden in diesem Druckbereich verfolgt durch Ratenmessungen über ein differentiell gepumptes Quadrupolmassenspektrometer, über Austrittsarbeitsmessungen mittels einer Kelvin-Sonde und über die Beugung niederenergetischer Elektronen (LEED).

Die Kinetik der katalytischen Ammoniakoxidation wurde studiert an Pt(533), Pt(443), Pt(865), Pt(100) und an einer polykristallinen Platinfolie. Die höchste katalytische Aktivität wies die Pt-Folie auf, danach nahm die Aktivität in der Reihenfolge Pt(865), Pt(533), Pt(443) und Pt(100) ab. Offenbar erhöhen Oberflächendefekte wie atomare Stufen oder Kinken die Aktivität in dieser Reaktion. Unter Reaktionsbedingungen konnten die reaktiven Haftkoeffizienten der reagierenden Gase bestimmt werden: $s_{reac}(O_2)$ erreicht 0.14 auf der Platinfolie. Ganz allgemein ist bei niedriger Temperatur und kleinem Verhältnis der Reaktanten O_2/NH_3 die N_2-Bildung bevorzugt, während bei hoher Temperatur und großem Verhältnis O_2/NH_3 die NO-Bildung dominiert.

In Abhängigkeit vom Gesamtdruck, der Temperatur und dem O_2/NH_3-Verhältnis verursacht die Reaktion eine mehr oder wenige schwere Umstrukturierung der Oberfläche. Es zeigte sich, dass die reaktions-induzierte Umstrukturierung der Oberfläche verbunden war mit einer Hysterese der Reaktionsrate bei Heiz-Kühl-Zyklen. Eine sehr breite Hysterese von etwa 70 K Breite tritt bei Pt(100) auf, die auf den wohlbekannten 1×1 ↔ hex Phasenübergang von Pt(100) zurückgeführt werden kann. Die reaktions-induzierte Restrukturierung der katalytischen Oberfläche nimmt tendenziell mit steigendem Gesamtdruck zu. Dabei beobachtet man aber eine nicht-monotone Abhängigkeit vom Gesamtdruck. Auf beiden Orientierungen, Pt(533) und Pt(443), findet man bei 10^{-3} mbar eine Hysterese verbunden mit einer ungeordneten Oberfläche, aber bei 10^{-2} mbar verschwindet diese Hysterese bei beiden Orientierungen verbunden mit der Ausbildung einer teilweise geordneten Oberfläche.

Die raumzeitliche Dynamik der katalytischen Ammoniakoxidation an Pt(100) und Pt(443) wurde mittels Photoelektonenemissionsmikroskopie (PEEM) untersucht. Reaktionsfronten und räumlich homogen ablaufende Übergänge wurden an Pt(100) gefunden, während keinerlei Strukturbildung an Pt(443) beobachtet wurde. Offensichtlich sind die nicht-linearen Phänomene an Pt(100) auf den 1×1 ↔ hex Phasenübergang von Pt(100) zurückzuführen.

Schlüsselwörter: Platin, Ammoniak-Oxidation, Katalyse, Pt(865), Pt(533), Pt(443), Pt(100), Platinfolie, Hysterese, Ammoniak, NO, Stickstoff, Umstrukturierung, Phasenübergang, Strukturempfindlichkeit, Drucklücke, Materiallücke

Abstract

This work was part of an effort to bridge the pressure gap and material gap between model catalysts and technical catalysis in catalytic ammonia oxidation. The pressure was increased systematically from UHV to close to the mbar range and the state of the surface was monitored by utilizing various *in situ* techniques. The kinetics and reaction-induced restructuring were followed in 10^{-6} – 10^{-2} mbar range using rate measurement via a quadrupole mass spectrometer, work function measurement via a Kelvin probe and low energy electron diffraction (LEED) to gain insight into the structure sensitivity of the reaction.

The kinetics of ammonia oxidation were studied on Pt(533), Pt(443), Pt(865), Pt(100) and the Pt foil. The highest catalytic activity was found on the Pt foil, then the activity decreased in the order Pt(865), Pt(533), Pt(443), and Pt(100). Evidently atomic steps and kinks enhance the catalytic activity. The reaction sticking coefficients of the reactants were determined under reaction conditions, s_{reac} (O_2) reaches 0.14 on a Pt foil. Quite generally, low temperature and a low O_2/NH_3 ratio of the feed gas favor N_2 formation; high temperature and a high ratio O_2/NH_3 lead to preferred NO formation. No N_2O was detected in the pressure range studied here.

Depending on the total pressure, the temperature and $p(O_2)/p(NH_3)$ conditions severe restructuring of the Pt surface occurred under reaction conditions. The restructuring was favored to be associated with a hysteresis in the reaction rate upon cyclic variation of the temperature. A rather broad hysteresis occurred on Pt(100) where the well known 1×1 ↔ hex surface phase transition is connected with two surface states with strongly different catalytic activity, i. e. oxygen sticking. On Pt(443) no LEED detectable substrate changes and no rate hysteresis occurred below 10^{-3} mbar. But above 10^{-3} mbar a substantial hysteresis effect were seen. The restructuring which tends to increase with rising total pressure was found to depend in a non-monotonic way on the total pressure. So on both orientations, Pt(533) and Pt(443), a hysteresis was present at 10^{-3} mbar, but vanished again at 10^{-2} mbar. LEED showed a disordered surface at 10^{-3} mbar.

The spatiotemporal dynamic of ammonia oxidation on Pt(100) and Pt(443) have been studied by photoelectron emission microscopy (PEEM) in a UHV system. Reaction fronts and spatially homogeneous transition were observed on Pt(100), while the reaction proceeds spatially homogeneous over Pt(443). Apparently the nonlinear phenomena of the reaction on Pt(100) can assigned to the phase transition from the active 1×1 to the inactive hex phase of Pt(100).

Keywords: Platinum, Ammonia-Oxidation, Catalysts, Pt(533), Pt(443), Pt(865), Pt(100), Pt Foil, Hysteresis, Ammonia, NO, Nitrogen, Phase Transition, Structure Sensitivity, Restructuring, Pressure Gap, Material Gap

Contents

CHAPTER 1 INTRODUCTION....1

CHAPTER 2 EXPERIMENTAL TECHNIQUES....7

2.1 INTRODUCTION....7
2.2 NOTATION OF SURFACE STRUCTURES....8
2.3 LOW ENERGY ELECTRON DIFFRACTION (LEED)....9
2.3.1 Experimental Set-up of LEED....10
2.3.2 Basic Theory of LEED....11
2.3.3 Diffraction and reciprocal space....12
2.3.4 Characterization of Stepped Surface from the LEED Pattern....13
2.4 AUGER ELECTRON SPECTROSCOPY (AES)....15
2.4.1 The Auger process....15
2.4.2 The AES instrumentation....17
2.5 KELVIN PROBE MEASUREMENT....17
2.5.1 Work function changes induced by adsorbates....17
2.5.2 Work function change measurement....18
2.5.3 Experimental setup of Kelvin probe....20
2.6 PHOTOELECTRON EMISSION MICROSCOPY (PEEM)....21
2.6.1 Application of PEEM....21
2.6.2 Instrumentation of PEEM....23
2.7 TEMPERATURE PROGRAMMED TECHNIQUES....24
2.8 SCANNING ELECTRON MICROSCOPE (SEM)....25

CHAPTER 3 EXPERIMENTAL SETUP....27

3.1 INTRODUCTION....27
3.2 THE UHV SYSTEM....27
3.2.1 Ultrahigh Vacuum....31
3.3 SAMPLES AND PREPARATION....31
3.3.1 Structural models and LEED patterns of clean surface....32
3.3.2 The standard procedure for cleaning surfaces....33
3.4 GAS CALIBRATION....33
3.5 RATE MEASUREMENT....35
3.5.1 Calculation of reaction rate....35
3.5.2 Reaction sticking coefficient....36
3.5.3 Order of reaction....37

3.6 High Pressure Reaction Cell 37

CHAPTER 4 THE STEADY-STATE KINETICS OF AMMONIA OXIDATION OVER PT 39

4.1 Introduction 39
4.2 Oxygen and Ammonia Adsorption over Pt 40
4.2.1 NH_3 on Pt(443) 40
4.2.2 Oxygen on Pt(443) 47
4.3 Stationary Reaction Kinetics 52
4.3.1 Temperature dependence and influence of reactant ratio 52
4.3.1.1 Pt(865) 52
4.3.1.2 Pt(100) 59
4.3.1.3 Pt foil 66
4.3.1.4 Pt(533) and Pt(443) 69
4.3.2 Partial Pressure Dependence 72
4.3.2.1 Oxygen 72
4.3.2.2 Ammonia 75
4.3.3 Work Function Measurement during Ammonia Oxidation 77
4.4 Reaction Mechanism 81
4.5 Summary and Conclusion 84

CHAPTER 5 STRUCTURE SENSITIVE REACTION – AMMONIA OXIDATION ON PT 87

5.1 Introduction 87
5.2 Structure Sensitivity of the Reaction Rate 89
5.3 Influence of Total Pressure 96
5.4 Stability of surface structure 104
5.4.1 Adsorption on Pt(443) 105
5.4.2 Under Reaction Condition 107
5.4.2.1 LEED Studies 107
5.4.2.2 SEM Studies 109
5.5 Overview of Hysteresis and LEED Pattern Change after Reaction 111
5.6 Summary and Conclusion 113

CHAPTER 6 SUMMARY 115

REFERENCE 119

LIST OF ABBREVIATIONS 125

LIST OF PUBLICATIONS 127

CURRICULUM VITAE 129

ACKNOWLEDGEMENTS 131

Chapter 1 Introduction

Heterogeneously catalyzed reactions contain purely chemical and purely physical processes. For the catalytic process to take place, the starting material must be transported to the catalyst. Thus apart from the actual chemical reaction, diffusion, adsorption and desorption processes are of importance for the progress of the overall reaction [1].

Surface structure of a catalyst is very difficult to study under working conditions, i.e., at ambient or elevated gas pressure. Apparently, the UHV approach has the advantageous whole arsenal of surface analytical techniques being available to characterize the catalyst. Over the past years, many surface science techniques have been developed to provide atomic level information on surface structure (atomic and electronic), the surface composition with ever improving spatial and time resolution. Most of these techniques involve the use of electron, photon, or ion scattering and detection [2-5]. The drawback of this approach is the need for a high vacuum working environment. Several gaps between catalysis and traditional surface science have been identified:

(1) the materials gap; (2) the pressure gap.

Surface science has reached a degree of maturity that allows the correlation of precise knowledge of surface structure and composition with macroscopic catalytic properties [6]. Using model system with increasing degree of complexity, i.e., single crystal surfaces with different orientation, bimetallic surfaces and planar oxide-metal systems, is one strategy to try to bridge the materials gap. Closing the pressure gap can be achieved by virtue of surface sensitive techniques that work in the presence of a gas phase at high pressure. Since the 1980s, many researchers have devoted

attention to solving the pressure and material gap problem in order to efficiently use the results of model studies to explain or even predict specific features of catalytic systems [7-9].

Bridging the gaps between ideal and real system in heterogeneous catalysis is the purpose of the priority program 1091 of the Deutsche Forschungsgemeinschaft (DFG- SPP-1091) which provided the framework for this study. The goal of the program is to gain insights into the so-called pressure and material gap by investigating systems with different degree of ideality. Ammonia oxidation on platinum catalyst was chosen as one example for such a reaction. Catalytic ammonia oxidation was investigated by (a) theory applying DFT to single crystal surfaces [10], (b) studies under UHV and intermediate pressure conditions with different orientation single crystal faces [11-16], (c) transient low pressure experiments on Pt gauze [17], and (d) close to atmospheric pressure experiments over polycrystalline Pt gauze and foil [18].

The industrial application of ammonia oxidation over platinum based gauze catalysts is a highly optimized process, reaching yields of nitric oxide between 94 and 98% [19]. Nitric acid is an important intermediate in fertilizer production as well as for nitration and oxidation reactions in the production of dye, pharmaceuticals and explosives. Industrial application started with the development of a process for nitric acid production by Ostwald. The catalytic oxidation of ammonia over platinum is a key step, both in industrial manufacturing of nitric acid and in environmental chemistry where ammonia is removed in the so-called selective catalytic reduction process [20].

In ammonia oxidation, molecular nitrogen, NO and water are the main products of ammonia oxidation over platinum under UHV conditions. N_2 products is formed between 500 and 800 K, mainly NO is produced at high temperature and at high oxygen partial pressure [21-24]. To a small extent also N_2O is formed, in particular, N_2O is reported for studies at pressures above 10^{-1} mbar [25]. The reason for the

pressure dependence of N_2O formation was not fully understood yet, which illustrates the difficulty in comparing low and high-pressure studies. The following reactions take place [18]:

(R1) $4NH_3 + 5O_2 \rightarrow 4NO + 6H_2O$ $\Delta_rH_{298K} = -907$ kJ/mol

(R2) $4NH_3 + 3O_2 \rightarrow 2N_2 + 6H_2O$ $\Delta_rH_{298K} = -1266$ kJ/mol

(R3) $2NH_3 + 2O_2 \rightarrow N_2O + 3H_2O$ $\Delta_rH_{298K} = -1104$ kJ/mol

The secondary reactions of ammonia oxidation can be used for the elimination of NO_x emissions.

(R4) $2NH_3 + 3\ N_2O \rightarrow \quad 4\ N_2 + 3H_2O$ $\Delta_rH_{298K} = -877$ kJ/mol

(R5) $2NH_3 + 6\ NO \rightarrow \quad 5\ N_2 + 6H_2O$ $\Delta_rH_{298K} = -1808$ kJ/mol

Many studies of catalytic ammonia oxidation have been performed on single crystal Pt [21, 26, 27], polycrystalline Pt [28, 29], supported Pt [30, 31], and Pt-Rh alloys [32]. Although ammonia oxidation has already been highly optimized in the industry, the mechanism on molecular level are still far from being understood well.

In order to gain a certain insight of ammonia oxidation on Pt, many studies have been conducted in UHV systems. The oxidation of ammonia comprises a number of steps.

Adsorption and decomposition of ammonia on Pt, dissociative adsorption of oxygen, and NO adsorption and dissociation, were studied.

Ammonia adsorption and decomposition have been investigated on polycrystalline Pt [33], single crystal Pt planes [10, 34-44] and supported Pt [31, 45]. Three thermal desorption peaks were found following adsorption at 90 K. They are attributed to multilayers of solid ammonia at 100 K, to the weakly chemisorbed molecular ammonia at 150 K and the chemisorbed molecular ammonia in the 170 to 450 K temperature range, respectively [37]. Generally, for the adsorption state of ammonia on Pt surface, at low coverage, NH_3 is strongly bound to the surface via

nitrogen like “inverted umbrella”; at high coverage ammonia appears to be hydrogen-bonded to the initial layer of ammonia. Although ammonia adsorption is believed to be molecular, steady state ammonia decomposition on Pt occurs above 400 K, which indicates that dissociative adsorption does occur at elevated temperatures. After comparison of the decomposition ability of different orientations, it was found that high-index Miller planes are more reactive for the decomposition of ammonia [38]. Using periodic density functional theory (DFT) calculations Novell-Leruth et al. studied adsorbed NH_x species on Pt(100) and Pt(111) surfaces. It was found that Pt(100) has a higher affinity for NH_2 species, whereas NH species are preferred over Pt(111) [42].

Adsorption and dissociation of NO on different orientation Pt single crystal surfaces have been studied using experimental techniques and DFT slab calculations [46-56]. These results show that both the presence of steps and the orientation of the steps are important to activate NO, NO on Pt(100) has stronger bonding and much higher decomposition ability than Pt(111) and Pt(110). Decreasing of oxygen coverage could suppress recombinative desorption of NO, part of the NO molecules adsorbed on the step sites dissociates around 450 K on Pt(533). Adsorption states of NO on the Pt(111) step surface were elucidated by using infrared reflection absorption spectroscopy (IRAS), STM and DFT calculation. On the (111) terrace, NO molecules are adsorbed at fcc-hollow, hcp-hollow and on-top sites. On the other hand, NO molecules adsorb at the twofold bridge sites of a step [52].

The secondary reaction of ammonia, i.e. NO reduction by NH_3 on Pt has been studied frequently as a model reaction for the selective catalytic reduction process (SCR). This reaction follows two main pathways, leading to N_2 and H_2O, and to N_2O and H_2O. This reaction system also gives rise to nonlinear behavior, such as rate oscillations and spatio-temporal pattern formation [50, 57-60].

Ammonia oxidation was studied under reaction conditions, ranging from UHV to atmospheric pressure, with single crystals and with polycrystalline Pt or Pt-Rh alloys.

Single crystal studies of the $NH_3 + O_2$ have been carried out with the orientations Pt(100) [22, 61], Pt(111) [21], and the stepped Pt surfaces [26], Pt(443), Pt(533) [14] and Pt(410) [62]. Most of the proposed reaction mechanisms were based on that originally suggested by Fogel et al., who suggested that NO formation plays a key role in the formation of products [23]. Mieher et al. proposed that the reaction proceeds via the oxygen atoms stripping hydrogen of NH_3 followed by the recombination of nitrogen atoms with oxygen, to form NO, or with other nitrogen atoms, to form N_2 [63]. In their mechanism NO was not intermediate for N_2 formation. Ammonia activation on Pt(111) was studied by Offermans et al. by means of DFT calculations . They have shown that beside O_{ad}, OH_{ad} plays an important role in the activation of ammonia leading to the dehydrogenation [10].

The structure of a metal catalyst surface is not rigid under reaction conditions, but changes in response to its changing chemical environment. This restructuring occurs on an atomic level on the time scale of adsorption (10^{-3} sec), on a mesoscopic scale on the order of seconds or on longer time scales leading to morphological changes, to deactivation or activation of catalytic processes [64]. Under industrial conditions Pt catalysts undergo severe morphological changes in the Ostwald process due to the strong exothermicity of the reaction. The restructuring behavior of catalysts is a general phenomena in heterogeneous catalysis, is often associated with an activation or deactivation, or change in the selectivity of a catalyst.

In heterogeneous catalysis, the term “structure sensitivity” was first introduced to indicate the dependence of a catalytic rate on the size of the catalyst particle. As the metal loading of a dispersed, supported catalyst decreases, the mean metal particle size decreases as well. The smaller the particle is, the more edge and corner atoms are exposed [65].

The direct correlation between low coordination sites (present at the steps and kinks) and catalytic activity led to the development of the concept of structure sensitivity. The proposition that highly uncoordinated sites are chemically distinct in

that sense that they are capable of breaking the bonds in the rate determining step of the mechanism. Thermal desorption experiments revealed that stepped surface are often capable of adsorbing and decomposing surface species such as adsorbed hydrocarbons or diatomic gases at significantly lower temperatures than flat surface.

In this thesis, a short introduction of the applied experimental techniques and a description of the experimental setups are presented in chapters 2 and 3, respectively. After the critical review, results are shown in chapter 4 and 5.

In chapter 4 the adsorption and dissociation of oxygen and ammonia on Pt(443) are studied in a UHV system equipped with low energy electron diffraction (LEED), Auger electron spectroscopy (AES), Kelvin probe and photoelectron emission microscopy (PEEM). Here, *in situ* work function measurement, LEED and PEEM measurements permit us to relate the presence of certain adsorbates and the variation of surface structure to the catalytic activity. And the stationary reaction kinetics studies of ammonia oxidation on five different Pt surfaces are presented, Pt(100), Pt(533), Pt(443), Pt(865) and Pt foil. The experiments were systematically performed in the pressure range from 10^{-7} to 10^{-2} mbar.

The activities of ammonia oxidation over Pt surfaces with different structure are compared under identical reaction conditions. The influence of the total pressure on reactivity and selectivity is investigated in the pressure range from UHV to intermediate pressures (10^{-3} to 10^{-2} mbar) for Pt(533), Pt(443), Pt(865)and Pt(100). The variation of the surface structure was studied before and after reaction via LEED in order to compare the stability of surfaces with different orientations. Surface topographical changes are studied via SEM, and element analysis of the catalytic surface is carried out by Energy Dispersive X-ray (EDX) analysis. All these results are described in chapter 5.

Finally, conclusions are drawn, and the efforts to bridge the pressure gap and material gap in ammonia oxidation reaction are briefly summarized in chapter 6.

Chapter 2 Experimental Techniques

2.1 Introduction

Surface characterization is an essential part of surface science and heterogeneous catalysis. Spectroscopy, microscopy, diffraction and methods based on adsorption and desorption or bulk reactions all offer tools to investigate the nature of an active catalyst. With such knowledge we hope to understand catalysts better. In the fundamentally oriented studies in UHV system, model catalysts are applied, which is better defined. With such kind of catalyst we are in the domain of surface science, where a wealth of analytical techniques is available that do not work on technical catalysts. And these surface sensitive techniques can help us to provide different information of catalytic reactions, for example, depending on the variation of structure, morphology, coverage and composition of the surface.

In this work several techniques were used to study the reaction mechanism of ammonia oxidation over Pt model catalysts: low energy electron diffraction (LEED) determining the geometrical surface structure, Auger electron spectroscopy (AES) for the elemental composition of the surface, Kelvin probe measurements giving information about work function changes *in situ* under different conditions, photoelectron emission microscopy (PEEM) for spatio-temporal dynamics studies, traditional temperature-programmed techniques for desorption studies and rate measurement, and scanning electron microscope (SEM) which was used for the observation of the variation of surface morphology. A brief introduction to the principle of the above techniques and their applications in this thesis is presented in

this chapter.

2.2 Notation of Surface Structures

Many of the technologically most important metals possess the face centred cubic (fcc) structure: for example the catalytically important precious metals (Pt, Rh, Pd) all exhibit an fcc structure.

The fcc(100) surface is that obtained by cutting the fcc metal parallel to the front surface of the fcc cubic unit cell - this exposes a surface with an atomic arrangement of 4-fold symmetry, as shown in Fig. 2.1a.

The fcc(110) surface is obtained by cutting the fcc unit cell in a manner that intersects the x and y axes but not the z-axis - this exposes a surface with an atomic arrangement of 2-fold symmetry, as shown in Fig. 2.1b.

The (111) surface is obtained by cutting the fcc metal in such a way that the surface plane intersects the x-, y- and z- axes at the same value - this exposes a surface with an atomic arrangement of 3-fold (apparently 6-fold, hexagonal) symmetry. This layer of surface atoms actually corresponds to one of the close-packed layers on which the fcc structure is based, as shown in Fig. 2.1c.

A notation which is better suited for practical purposes and which is now widely in use was proposed by Lang et al. [66]. In this case the surface is considered as consisting of terraces of low miller index planes ($h_t\,k_t\,l_t$) with constant widths, and step faces of monoatomic height which are characterized by low miller index ($h_s\,k_s\,l_s$). A step with kinks corresponds to a higher-index plane, i.e. its face itself is not planar but stepped. The resulting notation is then n($h_t\,k_t\,l_t$)×($h_s\,k_s\,l_s$), where n gives the number of parallel atom rows forming a terrace. Accordingly the (775)-surface is denoted by $6(111)\times(11\bar{1})$, since 6 atom wide (111) terraces are followed by $(11\bar{1})$ steps. The designation for the (10, 8, 7) surfaces is 7(111)×(310); now the step is formed by a (310) plane which itself is “rough”, i. e. contains kinks. Frequently, the

stepped nature of a surface is marked as postscript (S) to the identification, i.e. for example Pt(S)-[7(111)×(310)] [67].

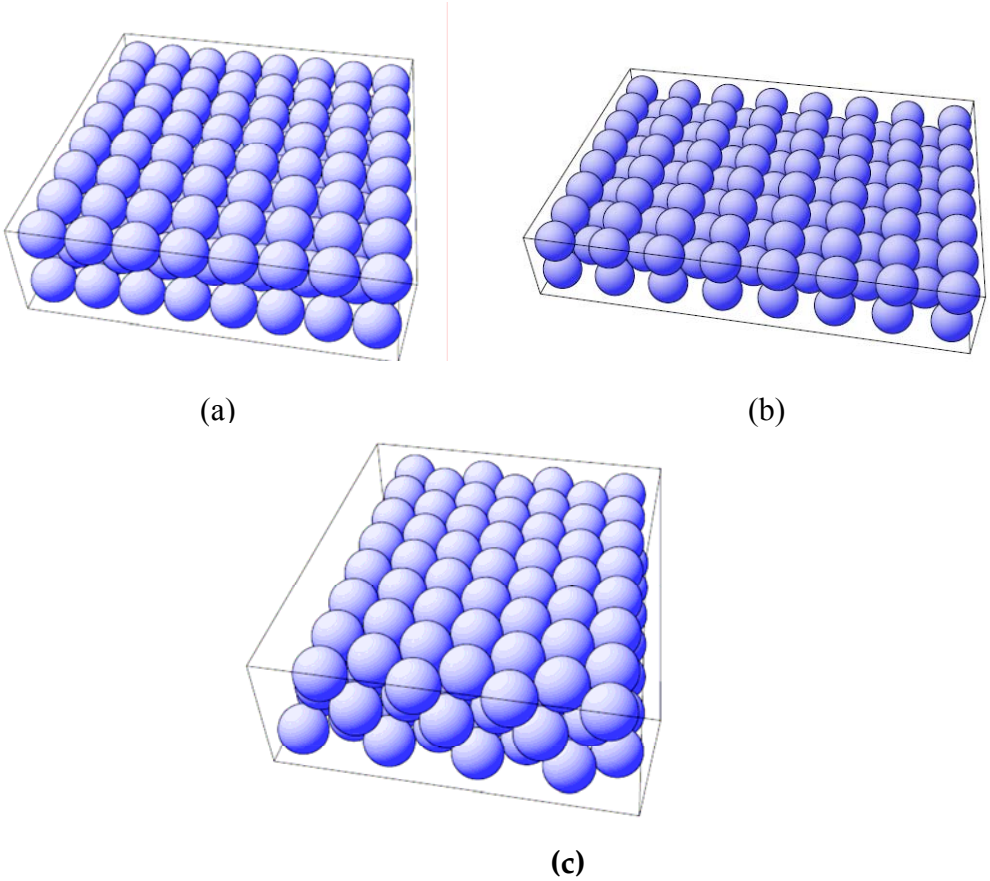

Figure 2.1. Ball model of low Miller index surface of the face centered cubic (fcc) metal: (a) (100), (b) (110), (c) (111).

2.3 Low Energy Electron Diffraction (LEED)

Apart from Auger electron spectroscopy, LEED is the most common technique used in studies of single crystal surface. For a long time it has been the only method to study the structure and morphology of two-dimensional surfaces. It probes the long-range order of periodic surface structures and yields valuable information even without going through complicated analysis if I/V – curves (intensity vs. voltages

curves).

LEED is used as a standard method for the characterization of the surface quality during the sample preparation prior to other UHV experiments.

1. Generally, the structural information given by a LEED pattern result from the position and the intensity of the diffraction spots as well as from the spot profiles.

2. The positions of the surface atoms are obtained from the so-called I-V curves, which means that the spot intensities are measured as a function of the electron energy. Measurements of the spot profiles thus provide important statistical parameters of the surface, such as the average terrace width distribution.

The extreme surface sensitivity of electrons with energies in the range of 50 to 200 eV is one of reason for this capability. With the electrons wavelength of the order of inter atomic distance, as shown in the following equations:

$$\lambda = \frac{h}{\sqrt{2m_e \cdot E(eV)}} \quad , \tag{2.1}$$

where

Planck's constant: $h = 6.62 \times 10^{-34}$ J·s; mass of electron: $m_e = 9.11 \times 10^{-31}$ Kg,

then finally Equ. 2.2 can be derived from the Equ. 2.1

$$\lambda\left(\mathring{\mathrm{A}}\right) = \sqrt{150.4 / E(eV)} \quad , \tag{2.2}$$

the atomic arrangement in the surface unit cell is accessible for the measurement [68].

2.3.1 Experimental Set-up of LEED

A typical LEED experiment setup is shown in Fig. 2.2. Within this standard LEED operation the electron energy can be varied between 0 and 1000 eV. The cathode is a thoriated Iridium hairpin filament, these filaments may be operated up to a pressure in the upper 10^{-5} mbar range. The grids and the screen in the form of calottes with different diameters are arranged concentrically around a common center where the sample surface has to be positioned. On the other hand, a 4-grid

LEED optics can be used as an electron energy analyzer, or more precisely, a retarding field analyzer (RFA). This offers the possibility of recording Auger electron spectra (AES).

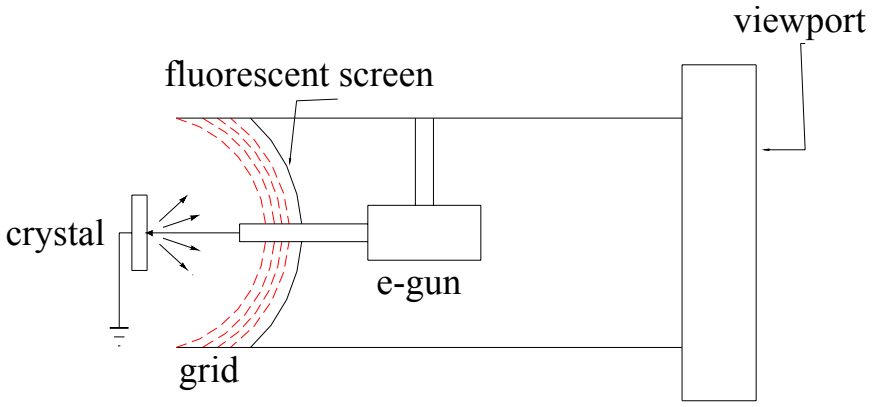

Figure 2.2. Scheme of the experimental set-up for LEED.

2.3.2 Basic Theory of LEED

The basis for the interference of electrons at crystal surfaces is the de Broglie equation $\lambda = h/mv$. In the case of wave scattering at a periodic array in one dimension, constructive interference takes place if the scattered waves from neighboring lattice points have path differences of multiples of the wavelength λ. If the primary wave strikes the surface with an incident angle θ_0, normally incidence θ_0 is zero. Interference of the backscattered waves occurs in direction θ, where θ is given by the condition

$$a(\sin\theta - \sin\theta_0) = d = n\lambda \tag{2.3}$$

then

$$a\sin\theta = n\lambda \tag{2.4}$$

where n - integer (..-1, 0, 1, 2..), a is the distance between the periodically arranged scatterers and n an integer denoting the order of diffraction, which were

shown in the following diagram, Fig. 2.3.

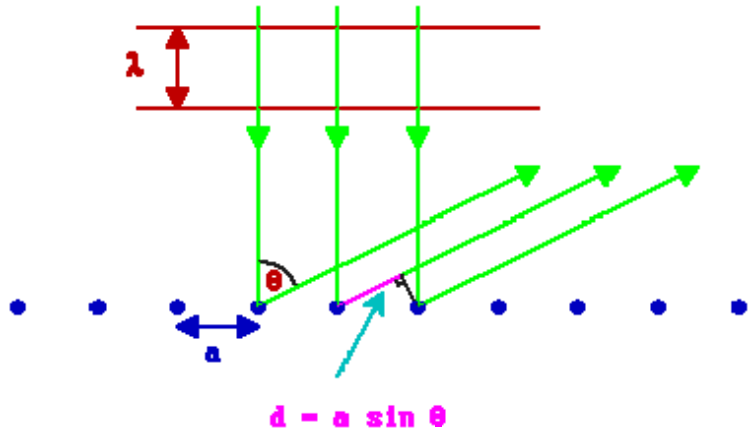

Figure 2.3. Scheme of the diffraction process in one dimension

2.3.3 Diffraction and reciprocal space

According to the Equ. (2.1) and Equ. (2.4), scattered electrons will exhibit an interference pattern with constructive interference in directions with

$$\sin\theta = \frac{nh}{a\sqrt{2m_e E}}, \qquad (2.5)$$

Symbols are defined above. Hence, if the scattered electrons are collected with a fluorescent screen, one observes a pattern of spots. Each spot corresponds to a direction in which constructive interference takes place.

Because of the inverse relationship between interatomic distances and the directions in which constructive interference between the scattered electrons occurs, the separation between LEED spots is large when interatomic distances are small and vice versa: the LEED pattern is a projection of the so called reciprocal lattice. In two-dimensions the construction of the reciprocal lattice is: if a surface lattice is characterized by two base vectors $\vec{a}_1$ and $\vec{a}_2$, the reciprocal lattice follows the definition of the reciprocal lattice vectors $\vec{a}_1^{\,*}$ and $\vec{a}_2^{\,*}$:

$$\vec{a}_i \cdot \vec{a}_j^{\,*} = \delta_{ij} \qquad (2.6)$$

in which

$\vec{a}_i$ are the base vectors of the real lattice (i = 1,2)

$\vec{a}_j^{\,*}$ are the base vectors of the reciprocal lattice (j = 1,2)

δ_{ij} is the Kronecker delta, $\delta_{11} = \delta_{22} = 1$, $\delta_{12} = \delta_{21} = 0$

The observed LEED pattern is a two-dimensional reciprocal lattice of the ordered surface projected onto a two-dimensional real plane. The position of the LEED spots can be determined using an Ewald construction. So from a LEED pattern we can obtain the information about the geometry of the surface and the adsorbates layer [69].

2.3.4 Characterization of Stepped Surface from the LEED Pattern

Surface with regular arrays of steps and kinks may easily be analyzed by LEED. Since each frequently occurring pair distance on the surface gives rise to a corresponding spot distance in the diffraction pattern, the latter will reflect both the periodicities of the atomic configuration on the terraces and of the steps.

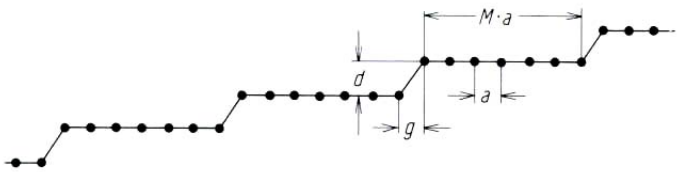

Figure 2.4. Cross section of a surface consisting of terraces separated by periodic steps.

If the terrace is composed of (M＋1) atoms separated by a distance *a*, as shown in Fig. 2.4 [67]. The ratio of the spot separation will simply be given by $a/M \cdot a$, the spot from the flat terrace plane will be split into doublets. According to Henzler LEED patterns from stepped surface may be analyzed, the scattered intensity *I* at an

angle φ is derived:

$$I(\varphi)=\frac{\sin^2\left[\frac{1}{2}ka(M+1)\sin\varphi\right]}{\sin^2\left[\frac{1}{2}\sin\varphi\right]}\times\sum_{m=-\infty}^{+\infty}\delta\left[\tfrac{1}{2}k(M\times a+g)\sin\varphi+\tfrac{1}{2}kd(1+\cos\varphi)-m\pi\right],\quad(2.7)$$

where I is the intensity of electron beam in direction φ, k = 2π/λ, λ is the wavelength of the electron beam, M+1 is the number of atom rows on one terrace and a is the separation of atom rows, d is the step height, and g is the horizontal shift of the top layer of one step compared with the adjacent step [70]. The first term is the normal interference function of a periodic array consisting of (M+1) atoms and exhibits maximum values if $\frac{1}{2}ka\cdot\sin\varphi=n\pi$. The second term represents a sum of δ-function in the limit of an infinite number of steps. This term depends only on the width ($M{\cdot}a$ + g) of the terraces and on the step height d. The separation of two adjacent delta functions derived from Equ. (2.7) is given by:

$$\Delta\varphi=\frac{\lambda}{(Ma+g)\cos\varphi-d\sin\varphi}\quad,\qquad(2.8)$$

which simplifies in the vicinity of the (0,0)-spot (φ=0) to

$$\Delta\varphi_{0,0}\approx\frac{\lambda}{Ma+g}\quad,\qquad(2.9)$$

the terrace width (Ma+g) can then be determined from the magnitude $\Delta\varphi_{0,0}$ of the splitting of the (0,0)-spot.

Upon variation of the electron energy the delta function also tend to pass through the positions of the normal spots, so that at certain wavelengths these are not split. This situation occurs for the (0,0) beam if

$$E_{0,0}=\frac{1.5s^2}{4d^2}\quad,\qquad(2.10)$$

where $E_{0,0}$ are the voltages in volts for observation of a single 00 reflection, d is the step height in nm. For all voltages computed from integer values of s (and an assumed d) single spots at the site of the 00 beam are expected. For half-integral values of s the (0,0)-beam will be split symmetrically into two spots of equal

intensity. By observation of voltages necessary to obtain single and double spots and by application of equation (2.10) the step height can be derived from observation of the LEED pattern alone.

2.4 Auger Electron Spectroscopy (AES)

AES is a common analytical technique used specifically in the study of surfaces and, more generally, in the area of material science. Underlying the spectroscopic technique is the Auger effect. The detection of the first "Auger" electrons was reported in 1923 by the French scientist Pierre Auger. And the use of Auger electrons as a tool for surface analysis was first introduced by Lander in 1953 [71]. In this work, the technique has been used daily to check the cleanliness of the surface, and more importantly it is also used to provide elemental information after reaction.

2.4.1 The Auger process

When a beam of electrons interacts with the atoms in a material, core level electrons can be ejected if the energy of the incident electrons (1 keV ~ 10 keV) is larger than the ionization threshold. Relaxation of ionized atom can occur by filling the core vacancy with an electron from an outer shell. The relaxation energy is then dissipated in either of two ways. It can be given to a second electron, an Auger electron, which is emitted from the atom with a characteristic kinetic energy E_{kin}, as demonstrated in Fig. 2.5, or it can appear as a characteristic X-ray photon, $\Delta E = h\nu$.

The conventional way to assign Auger transitions is to use the X-ray spectroscopic nomenclature. Three electron levels are involved in an Auger transition, each of which is designed by its principal quantum number n. The capital letters K, L, M, N ... are used for states with n = 1, 2, 3, 4 ..., respectively. Different subshells are distinguished using the suffices 1, 2, 3, 4 ... which correspond to the spectroscopic levels $s_{1/2}$, $p_{1/2}$, $p_{3/2}$, $d_{3/2}$, $d_{5/2}$, ..., for example, a vacancy in the $1s_{1/2}$

level be filled by a $2s_{1/2}$ electron and a $2p_{1/2}$ electron be ejected, the corresponding Auger transition would be designated as $K_1L_1L_2$. No matter from where the Auger electron is emitted, three electronic states participate in the process, and with relaxation phenomena neglected, the kinetic energy of the Auger electron can be written

$$E_{kin} = E_1 - E_2 - E_3 \,, \tag{2.11}$$

where E_1 denotes the binding energy of the initial core electron prior to ionization, E_2 that of the electron that fills the core hole, and E_3 the binding energy of the ejected electron. The essence of using Auger electron spectroscopy as an element specific analytical tool is that in each case the emitted electron carries a characteristic energy, which arises from the combination of energetically well defined atomic levels unique for a given atom.

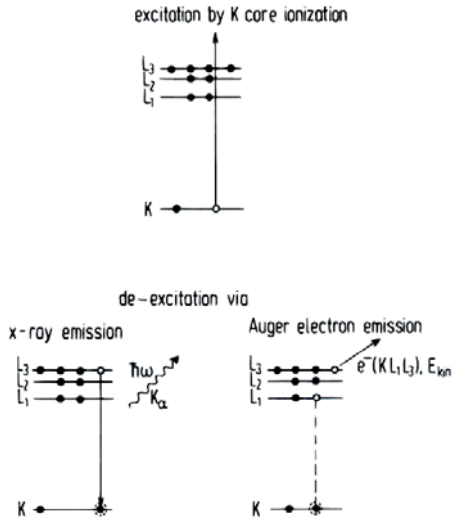

Figure 2.5. Energy-level diagram illustrating the two possible filling mechanisms of a K-shell core hole generated.

For atoms with many electron states, there are many different Auger transitions possible. According to the above process, Auger transitions are assigned by capital letters denoting the shells, whereby subfigures indicate the participating subshells. The sequence of these capitals is chosen according to equation (2.11). Beside KLL

transition, KLM, LMM, MNN, and NOO transitions can occur and lead to a wealth of Auger emission features for Z elements [72].

2.4.2 The AES instrumentation

The retarding field analyzer (RFA) consists of a series of concentric hemispherical grid. The sample is struck by a beam of electrons, and some electron are re-emitted by the sample and travel towards the grids. The first grid is usually grounded. The next grid has a voltage -V applied, so that any electrons lower than this energy are reflected back to the sample or the first (grounded) grid. There are usually more grids for reasons that will not be entered into here. The high energy electrons are detected and form the signal from the RFA. The RFA has a much larger solid angle over which electron may be detected than the cylindrical mirror analyzer (CMA) or concentric hemispherical analyzer (CHA). However, as it collects electrons above a certain energy unlike the CMA or CHA which collect electrons within a range of energies, the RFA suffers from greater noise, a poor signal to noise ratio. In our experiments, this AES is often applied to check the sample after cleaning process.

2.5 Kelvin Probe Measurement

2.5.1 Work function changes induced by adsorbates

The work function is the minimum energy (usually measured in electron volts) needed to remove an electron from a solid to a point outside the solid surface (or energy needed to move an electron from the Fermi energy level in to vacuum). The final electron position is far from the surface on the atomic scale but still close to the solid on the macroscopic scale.

The work function at zero temperature:

$$E\phi = E_{n-1} + E_{vac} - E_n \,, \tag{2.12}$$

or $$E\phi = E_{vac} - E_F \,. \tag{2.13}$$

Even on a clean, well-defined surface in UHV, the microscopic interpretation of Eϕ contains several contributions. On a metal surface a major contribution is due to the fact that the electron density “leaks out” from the relatively rigid framework of positive ion cores. This gives rise to a dipole layer at the surface, which the emitted electron must pass through. Similar effects occur at steps, which thus also modify the work function of a clean surface.

In the case of adsorption, adsorbed atoms and molecules generally have a significant influence on the electronic structure of a surface: they rearrange the electronic charge within the chemical bond and may also add elementary dipoles if the adsorbed molecule has its own static dipole moment. The second contribution is due to the relaxation of the substrate induced by the overlayer. But the latter contribution is very small. At higher coverages due to the interaction of the adsorbates complex depolarization occurs.

2.5.2 Work function change measurement

Work function change (Δφ) measurements are very simple to perform and yet can provide fairly detailed information about microscopic processes. Moreover, the work function is a surface sensitive property, because it contains above all the surface potential.

The Kelvin Probe is an extremely sensitive analytical tool. It measures changes in contact potential difference between a reference material and a sample which depend upon changes in the work function of the material being studied, not the absolute work function. The work function is defined as the amount of energy need to release electrons from the materials surface. Many factors can influence contact potential difference (CPD), including temperature, stress, strain, adsorption or desorption of molecules, depending on the sample material, even photo excitation.

The Kelvin probe method was successfully introduced by Mignolet to follow work function changes during gas adsorption. The physical principle behind it is the followings: one measures the displacement current i_D, which flows inside the connecting wire of a charged plate condenser as soon as the capacitance is periodically modulated. This can be achieved by vibrating one plate with respect to the other (fixed) plate, with frequency ω around a distance d_0 according to:

$$d(t) = d_0 + a\sin\omega t\,. \tag{2.14}$$

A permanent alternating displacement current is thus obtained, which is given as

$$i_D(t) = dQ/dt = -\varepsilon\varepsilon_0 AVa\omega\cos\omega t(d_0 + a\sin\omega t)^{-2}\,, \tag{2.15}$$

where Q= charge on the capacitor; ε, ε_0 = permittivity of the dielectricum and vacuum; A is plate area; V= voltage applied to the capacitor (V equals the contact potential difference, Δφ); d_0 = plate distance with plate at rest; ω = frequency of vibration, and a = amplitude of vibration. According to Equ. 2.15, i_D represent a time-dependent periodic function and differs from zero only if the contact potential difference V has a finite value. Because its magnitude is proportional to V, i_D can be utilized to monitor contact potential differences.

Experimentally, the sample is moved by means of a UHV manipulator in front of an inert reference electrode, which consists of a small gold net plate.

For following work function changes, it is mandatory that the adsorption occurs only at the sample surface; gases must not interact with the reference electrode, the physical operation is as follows, Fig. 2.6. By applying an external voltage V_{ex} between the sample and reference electrode the CPD can be compensated to zero, whereby the two Fermi levels are shifted with respect to each other accordingly. Any adsorption now changes the surface potential of the sample, and its work function leading to build-up of a renewed CPD. The external voltage to compensate this CPD again to zero is then equal to work function change on the sample [72].

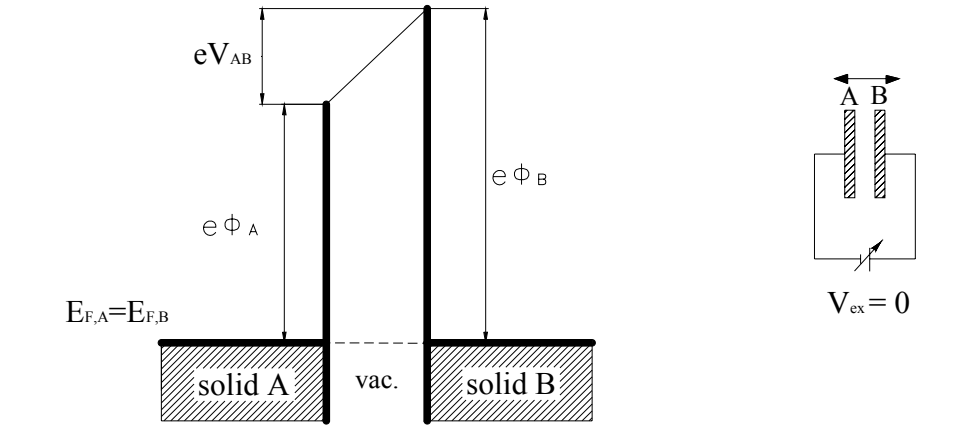

(a)

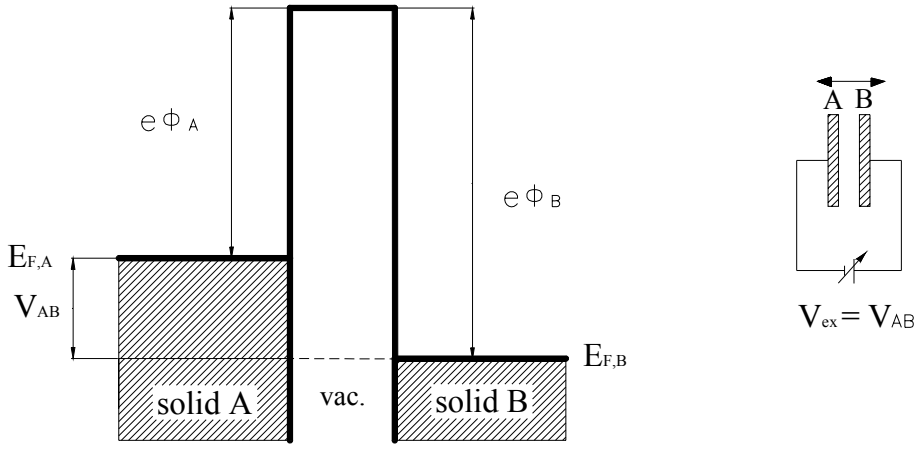

(b)

Figure 2.6. Physical principle of the Kelvin method: electrical potential situation with two different metals A and B connected to form a condenser. Because the Fermi levels equilibrate, a contact potential difference V_{AB} is built up. (a) If an adjustable external voltage V_{ex} is connected to the plates of the capacitor, the CPD V_{AB} can be compensated to zero. Then the condition $V_{AB} = V_{ex}$ holds. (b) In a self-compensating circuitry device, this is achieved automatically using lock-in techniques.

2.5.3 Experimental setup of Kelvin probe

The design of the Kelvin probe used in our lab is shown in Fig. 2.7. A vibrating gold grid is used as reference electrode, the reference electrode is driven by a

piezoceramic. And the setup proposal for Kelvin probe and specimen are also shown.

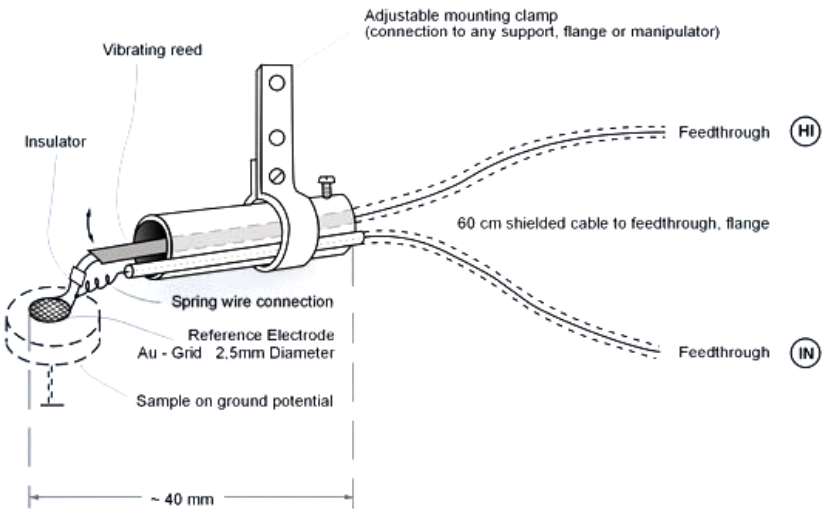

Figure 2.7. Design of Kevin probe and the set-up proposal for Kelvin probe and specimen.

2.6 Photoelectron Emission Microscopy (PEEM)

Photoemission electron microscopy (PEEM) is based on imaging the secondary electrons that are produced in the filling of the core-hole created in the primary photoexcitation processes. These processes depend upon the transition probability from the ground state to the unoccupied states above the Fermi level. High resolution imaging of surfaces and interfaces with topographical, elemental, chemical, orientational and magnetic contrast can be obtained.

2.6.1 Application of PEEM

PEEM provides a real space image of the sample surface under controlled conditions in ultra-high vacuum or in a reactive gas mixture. Real time experiments became possible by the development of an UHV compatible PEEM, which is capable of following work function changes over macroscopic surface areas *in situ*. This technique thus offers the unique opportunity of studying, both the surface

morphology and the geometrical distribution of adsorbed reactants during a heterogeneous catalytic reaction. The contrast of the PEEM image during the reaction is due to local changes of the work function Φ caused by the laterally varying adsorbate concentration.

According to Fowler' theory,

$$Y \propto (h\nu - \Phi)^2, \tag{2.16}$$

where Y is photoelectron yield, hν is the photo energy and Φ is the work function. As shown in Fig. 2.8, the wavy line approaching the sample under about 75^o from the

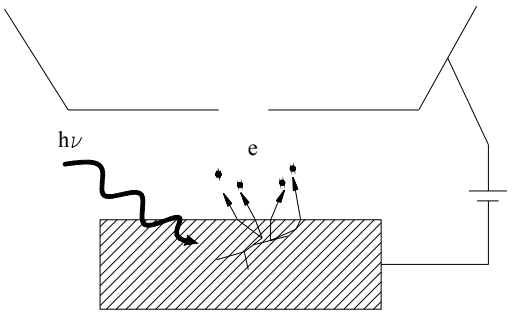

Figure 2.8. Schematic drawing on the principle of PEEM.

surface normal represent UV-light. It is possible to determine the absolute work function of the surface, clean or covered, to an accuracy of several meV, by plotting the square root of the total yield of photoelectrons versus the photon energy when the photon energy is varied from values 0.5 eV below Φ to about 1 eV above the threshold. In a practical application of PEEM, since the grey scale intensity of the image is proportional to the photoelectron yield, the square root of the intensity value is shown to follow linearly the negative work function change. This means, high work function areas are imaged as dark, low work function change areas as bright in PEEM. By plotting the PEEM intensity versus time or temperature, one can *in situ* study the surface work function change during the reaction.

2.6.2 Instrumentation of PEEM

The PEEM is a parallel imaging instrument, and creates at any given moment a complete picture of the photoelectron distribution emitted from the imaged surface region [7]. The viewed area of the sample must therefore be illuminated homogeneously with appropriate UV-light, typically about 7 eV for work on Pt surfaces. The imaged area has a typical size between 40-600 μm in diameter. As an image intensifier a channel plate is utilized in front of the phosphorous screen.

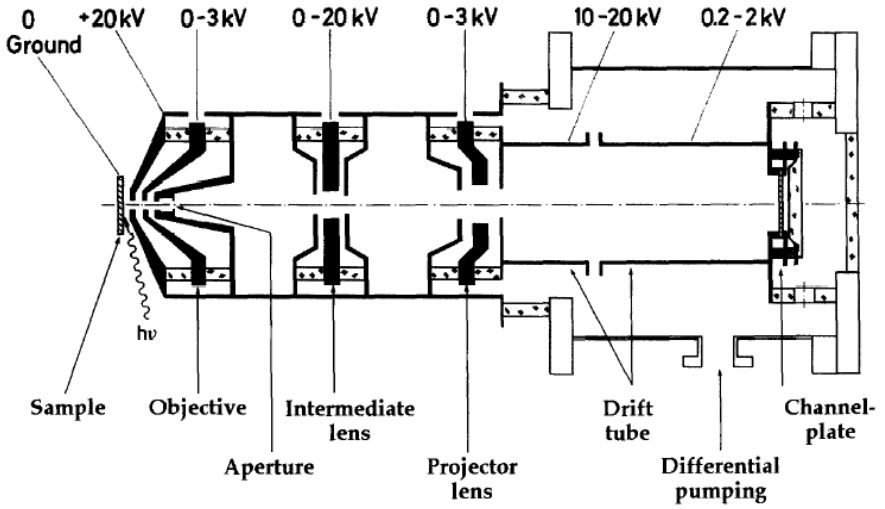

Figure 2.9. Schematic drawing of the photoemission electron microscope (PEEM), not to scale.

Normally the channel plate is restricting the operating total pressure in the electron optical column to less than 10^{-6} mbar. The PEEM is therefore differentially pumped, allowing a reactants total pressure up to 10^{-3} mbar in the chamber. To maintain three orders of magnitude pressure difference, an aperture of 300 μm diameter has to be incorporated at the focus of the objective lens. The PEEM is schematically reproduced in Fig. 2.9.

In principle, the resolution is inversely proportional to the accelerating field strength at the surface but proportional to the energy spread of the electrons. For the

PEEM illustrated in Fig 2.9 the resolution *r* is approximately:

$$r \approx d\Delta E / eU , \tag{2.16}$$

with d being the distance between the sample and the objective, ΔE being the distribution width of the initial electron energies and U the accelerating voltage. Using typical values of d = 4 mm, ΔE = 0.5 eV and U = 20 kV results in a theoretical resolution of *r* = 100 nm.

2.7 Temperature Programmed Techniques

The experimental setup of temperature programmed reaction spectroscopy, is shown in Fig. 2.10. A QMS is used to monitor the reaction on the surface as a function of temperature, and the surface is heated with a constant heating rate. Temperature programmed desorption and reaction spectroscopy are commonly used on qualitative basis. The interest is often confined to the total amount of reactants consumed or products evolved. Fragmentation patterns from the mass spectrometer data are used to identify molecules desorbing from the surface, for example, for mass 28, it could be N_2 or CO, so fragmentation of mass 14 (N) and 12 (C) also should be monitored during reaction.

In modern implementations of the technique the detector of choice is a small, quadrupole mass spectrometer (QMS) and the whole process is carried out under computer control with quasi-simultaneous monitoring of a large number of possible products. The data obtained from such an experiment consists of the intensity variation of each recorded mass fragment as a function of time or temperature. Typically the sample is very close to the QMS cone, and QMS is pumped differentially via turbo-pump.

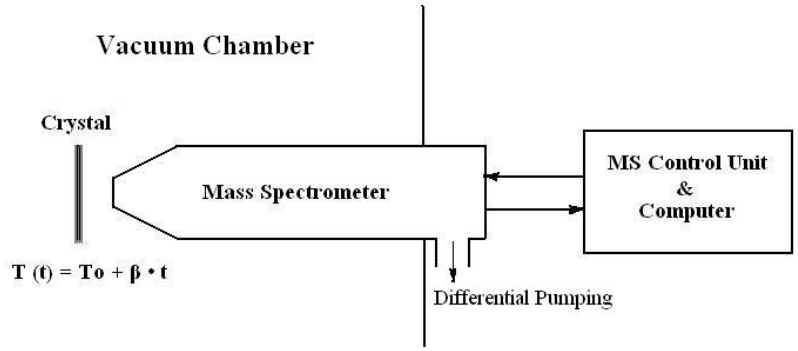

Figure 2.10. Scheme of the experimental setup for temperature-programmed techniques.

In TPRS a number of desorption products will normally be detected – this is where mass spectrometric detection and multiple ion monitoring really becomes essential. TPRS gives the most important information to describe the rate equation of the reaction, i.e., the way in which reaction rate depend on the temperature and the partial pressure of the gases. In this thesis, TPR experiments were used to determine the stationary reaction kinetics in different pressure ranges.

2.8 Scanning Electron Microscope (SEM)

The scanning electron microscope (SEM) is a type of electron microscope capable of producing high-resolution images of a sample surface. Due to the manner in which the image is created, SEM images have a characteristic three-dimensional appearance and are useful for judging the surface structure of the sample. X-rays, which are also produced by the interaction of electrons with the sample, may also be detected in an SEM equipped for energy dispersive X-ray spectroscopy (EDS). In this way, it possible to perform an element analysis of the sample surface region.

The lateral resolution of electron probe techniques, such as AES, SEM and EDS, is related to the size and distribution of the interaction volume between the incident electrons and the material, as shown in Fig. 2.11.

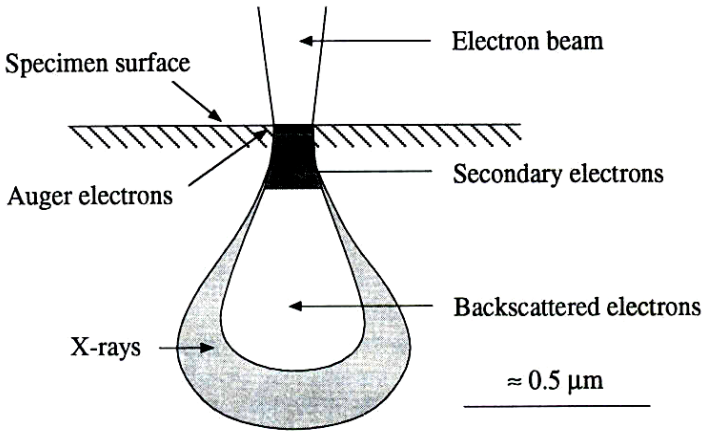

Figure 2.11. An electron beam impinging on a sample will create a pear shaped interaction volume [71].

When the primary electron beam interacts with the sample, the electrons lose energy by repeated scattering and absorption within a peardrop shaped volume of the specimen known as the interaction volume, which extends from less than 100 nm to around 5 μm into the surface. The size of the interaction volume depends on the electrons' landing energy, the atomic number of the specimen and the specimen's density. The energy exchange between the electron beam and the sample results in the emission of electrons and electromagnetic radiation, which can be detected to give a map of signal intensity coming from the sample, leading to the SEM image.

The beam electrons interact with atoms in the specimen. The signals resulting form these interaction escape from different depths within the sample. Secondary electrons, backscattered electrons and characteristic X-rays are the most widely utilized signal in a SEM.

Characteristic X-rays (sample depth is in the μm range) are generated by inelastic interactions of the probe electrons with specimen atom. By analysing the characteristic X-rays, the elements that constitute the specimen can be identified, and also quantitative calculation of their weight concentrations can be made. A widely used method of analysing characteristic X-rays is by the EDXS.

Chapter 3 Experimental Setup

3.1 Introduction

The general intention of the thesis work is to bridge the pressure gap and material gap in the study of ammonia oxidation on Pt catalysts. This means that, the studies of reaction under both ultrahigh vacuum conditions and intermediate pressure conditions are included in this thesis. Therefore a UHV system and a high-pressure reaction cell are combined in order to characterize the surface before and after the reaction in the intermediate pressure range. Different single crystal Pt surfaces and polycrystalline Pt are studied in order to investigate the structure sensitivity of the reaction. In this chapter, detailed descriptions of these experimental setup are given, some of the important operation methods of the instruments and experiments are presented as well.

3.2 The UHV System

Figure 3.1 shows a schematic drawing of the UHV system which was equipped with various scientific instruments: low energy electron diffraction (LEED), Auger electron spectroscope (AES) combined with LEED, quadrupole mass spectrometer (QMS), scanning tunneling microscopy. A standard ion gun was used for the sample cleaning via ion sputtering. A high precision UHV specimen manipulator supports

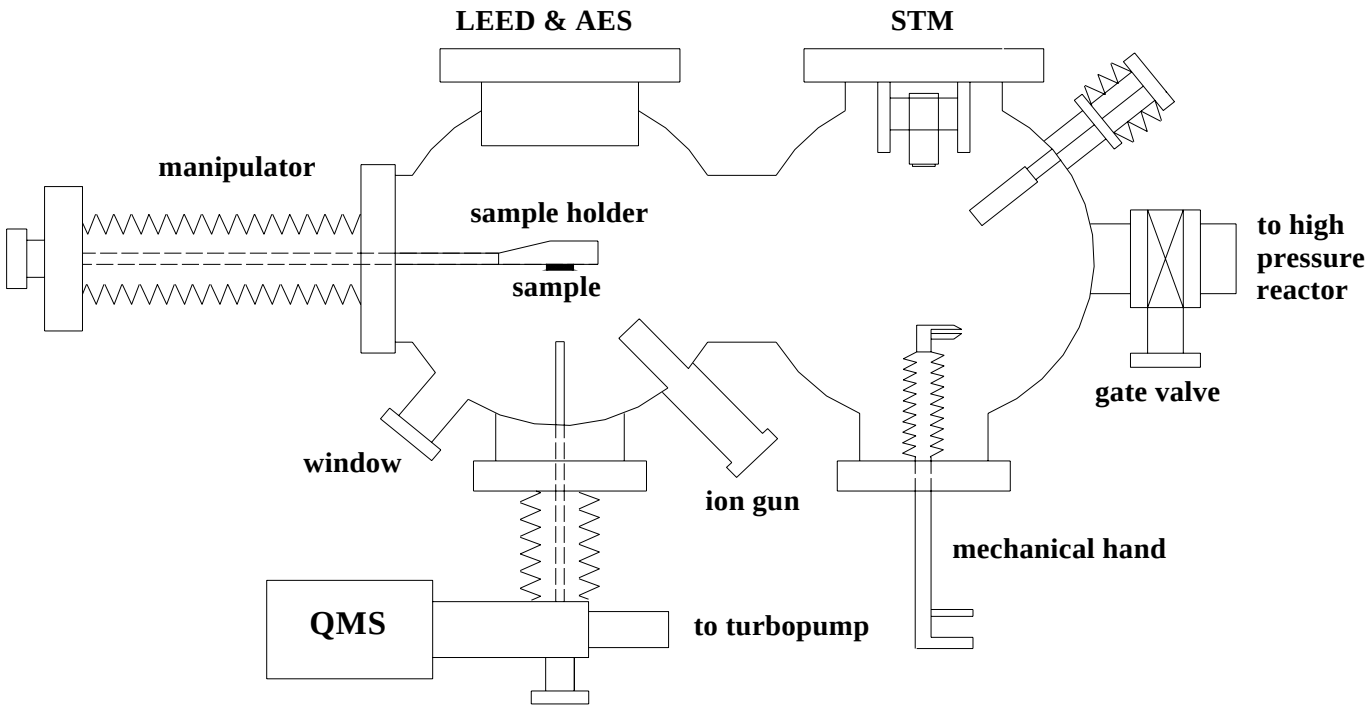

Fig. 3.1. Schematic drawing of the UHV system which was equipped with LEED & AES, QMS, STM.

sample movements in the chamber in all directions (x, y and z axis, rotation 360°). All the instruments were well calibrated to make sure the measurements are reliable and reproducible. The sample was heated indirectly by a filament behind the backside of the crystal either via radiation or via electron bombardment. Sample and sample holder are shown in Fig. 3.2.

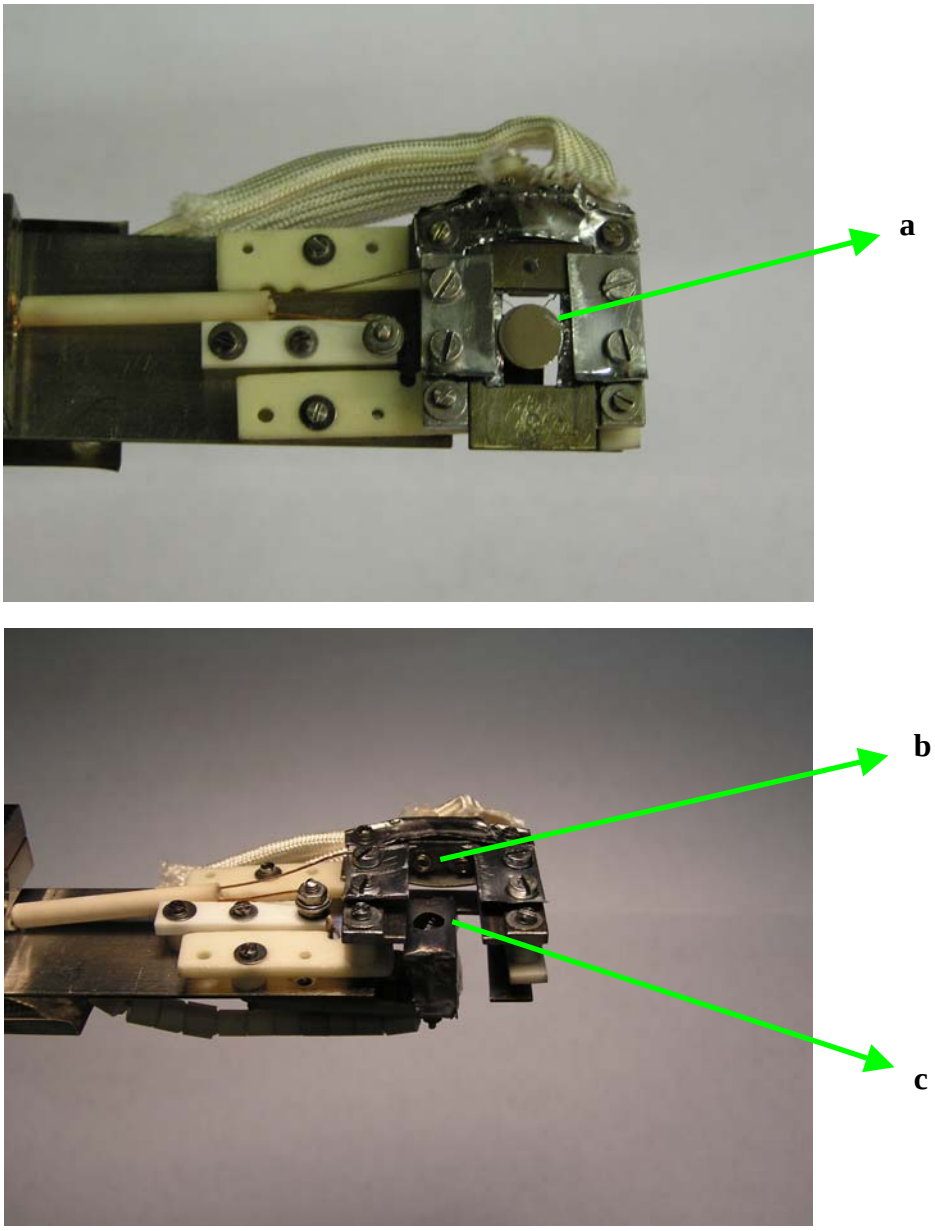

Figure 3.2. Sample holder in the STM UHV chamber, (a) Pt sample; (b) thermocouple connection; (c) heating filament in the shielding case.

During rate measurements the cone (opening 2 mm), which connected the differentially pumped QMS with the main chamber, was brought 1 mm in front of the surface. In this way reaction products from the backside of the sample and from filaments were excluded.

And Fig. 3.3 shows a schematic drawing of the other standard UHV system for the measurement of work function change. The chamber is equipped with an ion gun, a differential pumped quadrupole mass spectrometer (QMS), a photoelectron emission microscope (PEEM) and a Kelvin probe for work function measurements. And LEED and a retarding field analyzer for Auger electron spectroscopy (AES) are also in conjunction with this chamber to characterize the catalyst surface. The Pt crystal (2mm thick, D = 8 mm) is held by two Ta wires which also served for resistive heating. The temperature was monitored by means of a chronel-alumel thermocouple spot welded to the edge of the crystal.

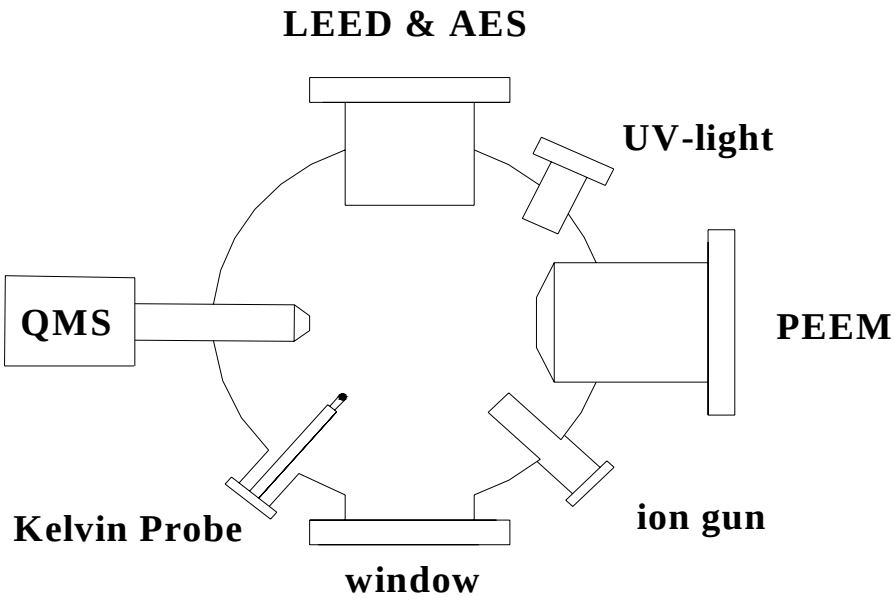

Figure 3.3. Schematic drawing of the UHV system which is equipped with LEED & AES, QMS, PEEM and Kelvin probe.

In PEEM the sample is illuminated with UV light from a deuterium discharge

lamp with maximum emission of 5.2-6.2 eV photon energy was focused onto the sample into a small spot ($\approx$ 2 mm^2). The emitted photoelectrons were collected by an electrostatic three-lens system, amplified by a channel plate and then imaged onto a phosphorous screen. The images were then recorded with a CCD camera and digitalized.

3.2.1 Ultrahigh Vacuum

The base pressure in both chambers was 2×10^{-10} mbar. Ultrahigh vacuum is necessary mainly because it provides the condition to work with a clean sample and since the analytical techniques rely on electrons as probes. To get such a low pressure condition (10^{-10} – 10^{-9} mbar), an initial vacuum (10^{-2} – 10^{-3} mbar) should be established prior to starting vacuum pump by roughing pumps. The pumps that are regularly used in the UHV regime are the turbomolecular pump, the ion pump and Ti sublimation pumps. QMS and PEEM are differentially pumped according to the requirement of their operations.

An important step in achieving UHV conditions in the main chamber is the bake-out process. When the inner walls of the UHV chamber are exposed to air, they become covered with a water film (H_2O sticks well due to its high dipole moment). On pumping down the chamber, these H_2O molecules would slowly desorb. In order to get rid of this water film the whole equipment has to be baked in vacuum for about 10 h at a temperature of 420 — 450 K. After the bake-out, all the filaments should be degassed to clean them from all impurities while the chamber is still hot.

3.3 Samples and Preparation

Five samples were used and mounted into the UHV system: stepped surfaces, Pt(533), Pt(443); kinked surface, Pt(865); planar surfaces, Pt(100); polycrystalline Pt foil.

3.3.1 Structural models and LEED patterns of clean surface

The surface structures of model catalysts used in this thesis are shown in Fig. 3.4.

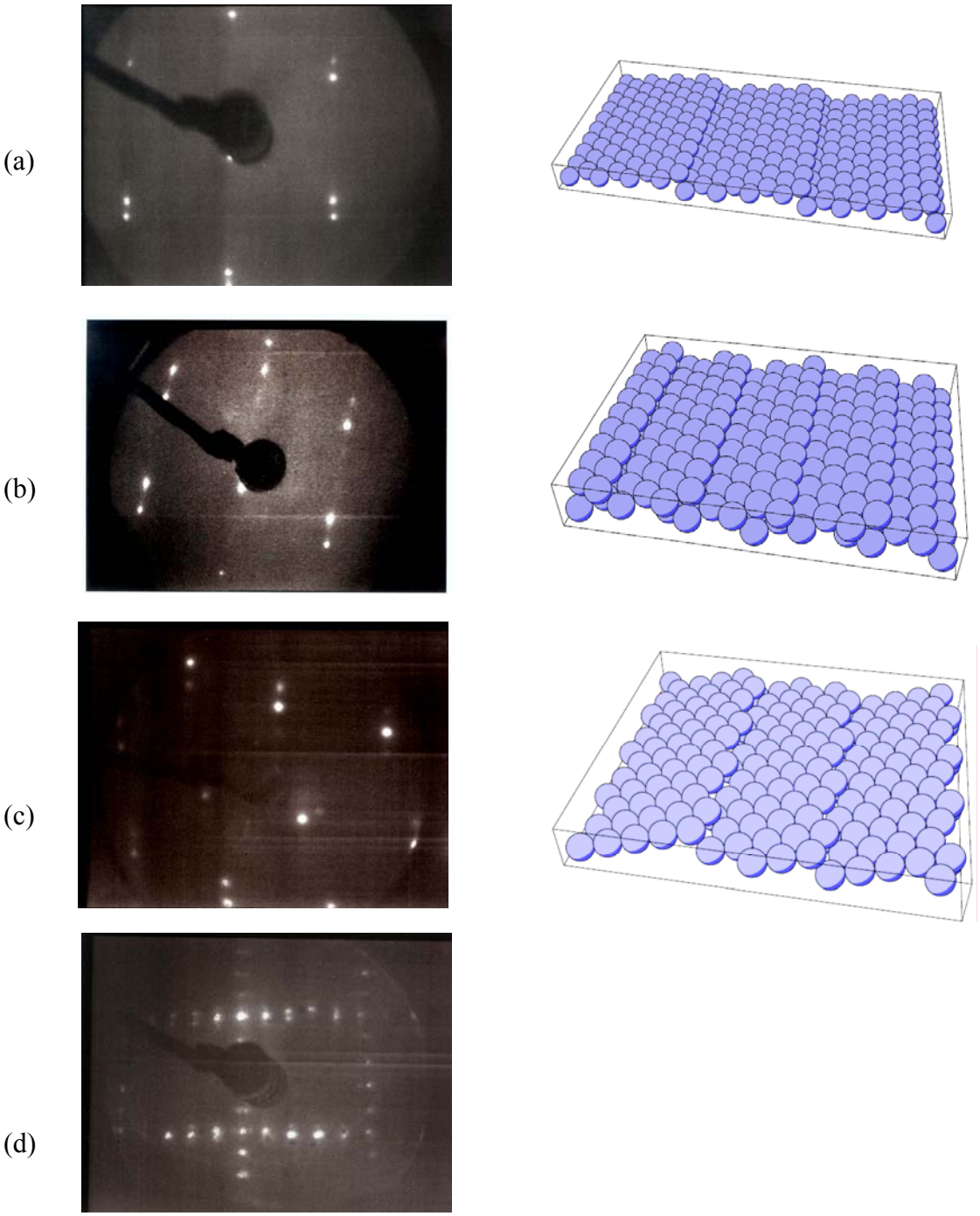

Figure 3.4. The LEED patterns and structure model of different Pt single crystal surface, (a) Pt(443), E= 100 eV; (b) Pt(533), E= 93 eV; (c) Pt(865), E= 110 eV; (d) Pt(100), E= 66 eV.

3.3.2 The standard procedure for cleaning surfaces

In the UHV chamber, the Pt surfaces were cleaned by repeated cycles of Ar ion bombardment, followed by annealing the sample, the details are shown as following:

(a) Sputter the surface for 15 min using Ar ion at room temperature, Ar ion energy is 1500 eV, p(Ar) = 2×10^{-5} mbar;

(b) Turn off Ar and ion gun, heat the sample to 1100 K with a rate of 3 K/s, hold the temperature of 1300 K for 15 s in UHV condition;

(c) Apply oxygen treatment to get rid of the main contamination: C. Hold the sample temperature on 650 K for 15 min in the oxygen environment, p(O_2) = 5×10^{-7} mbar;

(d) Anneal the sample to 1100 K, and hold it for 15 s after switching off oxygen.

3.4 Gas Calibration

The gas inlet system is connected to the UHV system by an all-metal valve. All gases are introduced via leak valves, and the gas grade purity of all gases we used are shown in table 3.1.

Gas	Grade
Ar	5.0
O_2	4.8
NH_3	5.0
NO	2.5
N_2	5.0

Table 3.1. The gas grade purity of all gases used in this study

Calibration gases (NH_3, O_2, N_2 and NO) are applied in order to relate the QMS signal to the partial pressure in the chamber.

Firstly, the relative gauge sensitivities for various gases should be considered. The sensitivity, S_g, supplied by gauge manufacturers, is valid only for the gas for which it is specified and the readout of the controller provides a direct pressure reading only for that specific gas. The standard gas, used by the entire industry for gauge specification, is nitrogen and, unless gas correction factors are applied, all readings are considered to be 'nitrogen-equivalent pressures'. So normally $S_{nitrogen}$ = 1, relative ionization gauge sensitivity factor, R_g, to convert nitrogen-equivalent readings into direct pressure readouts for gases, is equal to S_g. So nominal gas correction factors for gases used in this work are shown in the table 3.2.

Gas	**Sensitivity factor, S_g**
N_2	1.0
NO	1.2
NH_3	1.2
O_2	1.0

Table 3.2. Nominal gas correction factors

Nominal relative sensitivity factors cannot be relied upon for accurate measurements since they are known to vary significantly between seemingly identical gauges and even more for different gauge types, filament materials, and operating potentials. For general vacuum use, the discrepancy in the reported measurements is not greater than 10% for common gases.

Secondly, different gases were introduced into the chamber in the different pressure range, from 10^{-7} – 10^{-4} mbar. Then the mean value of the ratio of gas pressure to ion current of QMS could be obtained for the different gases. These factors are shown in the table 3.3. It should be mentioned that these factors would

vary with time because of a variation of emission of filament. Therefore, after a certain period calibration have to be done again.

Gas	Factor (mbar/mA)
N_2	3×10^4
NO	4.5×10^4

Table 3.3. The factors relating gas pressure to QMS ion current

3.5 Rate Measurement

3.5.1 Calculation of reaction rate

We should stress the fact that whenever we encounter the gas constant R, we deal with the unit "mol", while whenever we encounter Boltzmanns constant k we deal with the particle unit "atom" or "molecule". It is shown in the Equ. 3.1.

$$p \cdot V = n_{part} \cdot \frac{R}{N_A} \cdot T = n_{part} \cdot k \cdot T \,, \tag{3.1}$$

where V is the volume of the chamber, n_{part} is now the number of particles in V; Avogadros constant N_A.

Thermal desorption is important step in the process of surface reaction, according to Equ. 3.2,

$$dp / dt = \frac{A \cdot k \cdot T}{V} \cdot dn / dt \,, \tag{3.2}$$

where A denote the area of sample surface; p is partial pressure of gases.

In the pumped system, pressure change attributed to the pump speed could be described in the Equ. 3.3

$$dp_{pump} / dt = \frac{S \cdot p}{V} \,, \tag{3.3}$$

where S is the pumping speed of the chamber; p is partial pressure of gases.

For an equilibrium system, Equ. 3.2 and Equ. 3.3 should be equal. Accordingly,

$$\frac{A \cdot k \cdot T}{V} \cdot dn / dt = \frac{S \cdot p}{V}, \tag{3.4}$$

then the reaction rate of certain product dn/dt should be:

$$r = dn / dt = \frac{S \cdot p}{A \cdot k \cdot T}, \tag{3.5}$$

unit of r is molecule·cm^{-2}s^{-1}, gas temperature is assign to 300 K.

Since the pumping speed of the main chamber, S, is 210 L/min, the diameter of sample surface is 8 mm,

Finally r = 1.01 × 10^{22} p, (3.6)

where the unit of p is mbar, and the unit of r is molecule·cm^{-2}s^{-1}.

3.5.2 Reaction sticking coefficient

Sticking coefficient is the term used in surface physics to describe the ratio of the number of adsorbate atoms (or molecules) that do adsorb on a surface to the total number of atoms that impinge upon that surface during the same period of time.

In our experimental set-up the differentially pumped QMS is behind a cone whose tip is about 1 – 2 mm away from the sample surface. Due to this geometric arrangement to a good approximation only molecules reflected from the surface can enter the cone to be detected by the QMS: we can thus determine the reactive sticking coefficient s_{reac} *in situ* from the measured variation of the reactant partial pressures, i.e. of O_2 or NH_3. Denoting the signal of a gas without reaction by I_0 and during reaction with I we calculate the reactive sticking coefficient s_{reac} as

$$s_{reac} = \frac{I_0 - I}{I_0}, \tag{3.7}$$

where we take the signal at 300 K for I_0 assuming a negligible reaction rate at this temperature.

3.5.3 Order of reaction

The order of reaction with respect to a certain reactant is defined, in chemical kinetics, as the sum of all the exponents of the reactants involved in the rate equation. For our experiments, there are two reactants, NH_3 and O_2. It is difficult to measure the order of reaction rate.

$$r = k[A]^a[B]^b, \tag{3.8}$$

in order to find the order of reaction with respect to one of the reactants, a common solution is to keep the concentration of the reactant constant, e.g. $[B]_0$ is constant, then

$$r = k'[A]^a, \tag{3.9}$$

where $k' = k[B]_0$

$$\ln r = a \ln[A] + \ln k', \tag{3.10}$$

finally a plot of r and [A] gives a as the slope, then a is the order of reaction with respect to A.

3.6 High Pressure Reaction Cell

In order to investigate the reaction in an intermediate pressure range between 10^{-3} and 1 mbar, a high-pressure reactor was connected with the UHV system via a transfer system. A transfer rod moves the sample between two chambers that are separated by a UHV gate valve. After cleaning, the single crystal sample is transferred into the reaction chamber. The whole setup is shown in Fig. 3.5. In order to keep the gases pressure stable, mass flow controllers from MKS are used in the gas inlet system, the full scale range is 10 sccm of nitrogen. The pressure in the higer pressure chamber is measured by an MKS Baratron. The samples are heating by a lamp behind them, up to 840 K. A programmable temperature and process controller from Eurotherm is used to control the temperature.

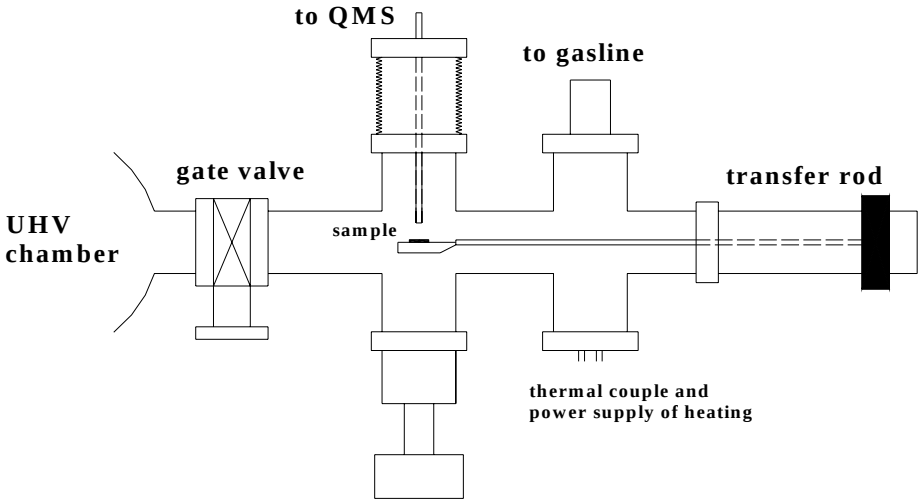

Figure 3.5. Schematic drawing of the high pressure reaction cell.

Chapter 4 The Steady-State Kinetics of Ammonia Oxidation over Pt

4.1 Introduction

The high temperature (T > 800 K) oxidation of ammonia with oxygen to NO on platinum in the so-called Ostwaldt process is one of the most important industrial chemical reactions. The catalyst of choice for this process is an alloy of Pt and Rh. At low temperature (T < 800 K) mainly N_2 and as to a smaller degree also N_2O are obtained, and N_2O appears as byproduct at pressures above 10^{-1} mbar. Under these conditions the reaction is used in environmental catalysis to remove excess NH_3, in the selective catalytic reduction (SCR) process of NO with NH_3, Pt can be used as a catalyst for the selective production of N_2 [20].

For the catalytic process to take place, apart from the actual chemical reaction, adsorption and desorption processes are of importance for the progress of the overall reaction. Diffusion processes in the gas phase are neglected since mass transport limitations play no role in a UHV system at low pressure ($p < 10^{-3}$ mbar).

A number of UHV studies on adsorption, desorption of pure oxygen or pure ammonia and decomposition of ammonia over Pt surface have been performed with a variety of surface sensitive techniques. Those studies focus on Pt(100) and on flat and stepped Pt(111) surface as model catalysts.

The adsorption of oxygen on a platinum surface plays an important role in ammonia oxidation and has been the subject of numerous studies. It has been found by Artsyukhovich et al. that at low coverages all the adsorbed molecules thermally dissociate upon heating, it follows that the minimum energy pathway leading to

thermal dissociation of adsorbed oxygen lies below the energetic barrier for thermal desorption [73]. Campbell et al. indicate that oxygen adsorption occurs through a weakly-held state, failure to stick is largely related to failure to accommodate in the molecular adsorption state [74].

The material and pressure gap has been a long standing challenge in the field of heterogeneous catalysis. In heterogeneous catalysis, the material gap refers to the discontinuity between well-defined model systems and industrially relevant catalyst. It has been established that catalyst surface structures play an important role in the catalytic reaction. Therefore, single crystal metal surfaces have been used as model systems to elucidate the role of surface defects and the mobility of reaction intermediates in catalytic reactivity and selectivity.

In this chapter, firstly we present a study of oxygen and ammonia on Pt(443) using a Kelvin probe in the conjunction with other techniques of QMS and LEED.

Secondly, in order to extend the studies on Pt(533) and Pt(443) which were carried out intensively by Scheibe et al. to other orientation, we also present a steady state kinetic study of ammonia oxidation over Pt(865), Pt(100), and Pt foil (polycrystalline). Those studies are conducted at pressures in the range of from 10^{-6} to 10^{-2} mbar. With these results we would try to build a connection between surface structure, and reaction conditions (e.g. feed composition, temperature) and catalytic activity and selectivity.

4.2 Oxygen and Ammonia Adsorption over Pt

4.2.1 NH_3 on Pt(443)

The motivation for studying the interaction of NH_3 with Pt surfaces lies in elucidating the role of NH_3 behavior in catalytic reactions. Ammonia is importance as a reactant or as a product in several reactions over transition metal catalysts,

particularly in ammonia oxidation over Pt. Ammonia adsorption and decomposition have been studied on different Pt surface. By means of density functional theory calculations Offermans et al. also investigated ammonia activation on Pt(111) in quantum chemical studies [10].

Atomic adsorbates usually tend to occupy surface sites with high chemical coordination. Molecular adsorbates are on those sites with a low coordination number.

Measurement of work function changes occurring upon adsorption is a valuable supplement to electron spectroscopy. Several methods can be used to measure work function changes, but the most advantageous method for our purpose here is the vibrating capacitor (Kelvin probe). It has a high sensitivity, and most importantly can be used in the presence of adsorbing gases [75].

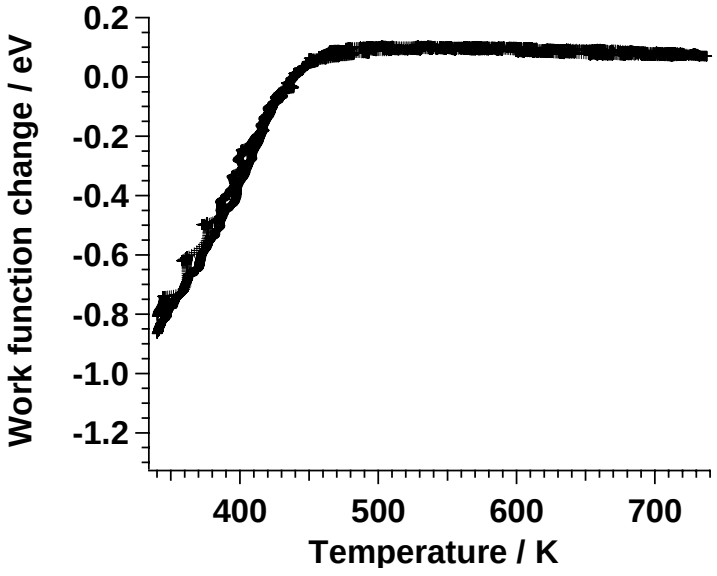

Figure 4.1. Work function change of Pt(443) during a heating/cooling cycle in a NH_3 environment, $p(NH_3) = 10^{-8}$ mbar, and the ramping speed is 0.5 K/s.

(a)

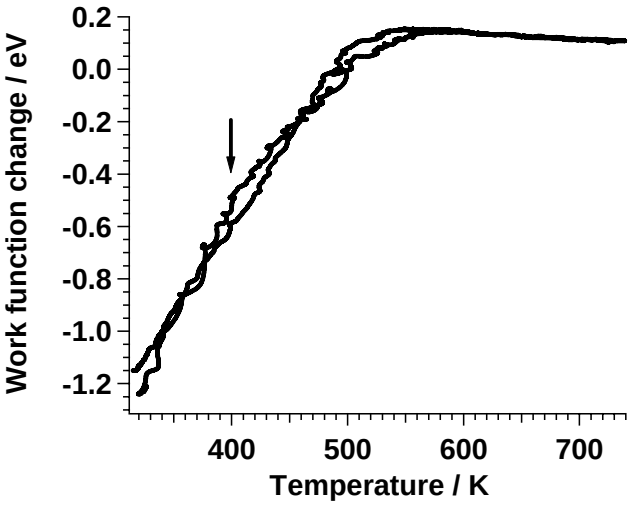

(b)

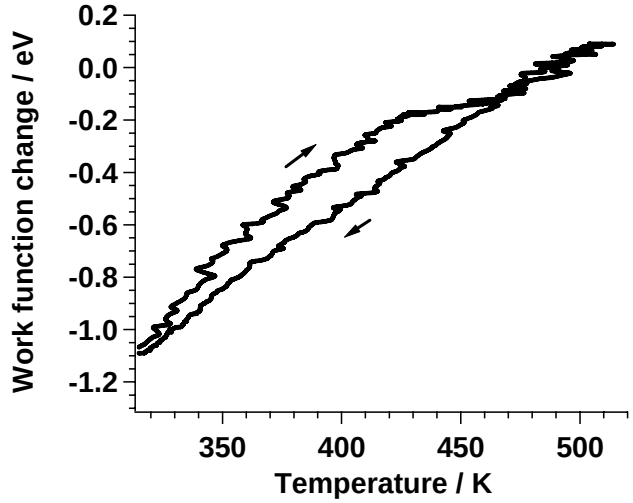

(c)

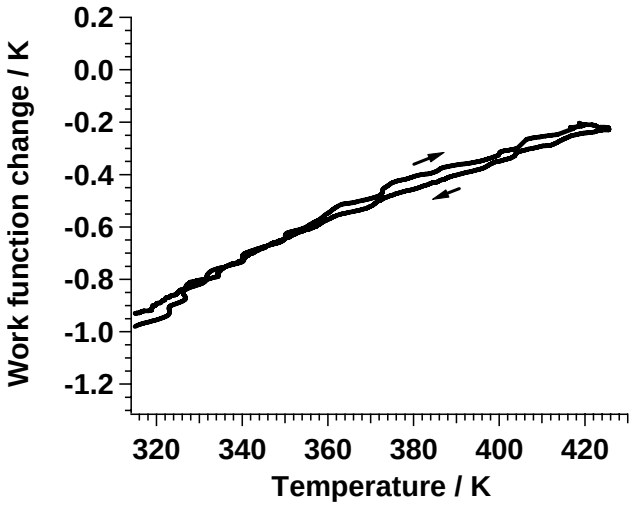

Figure 4.2. Work function change of Pt(443) during heating/cooling cycle in a NH_3 environment, $p(NH_3) = 2 \times 10^{-6}$ mbar, and the ramping speed is 0.5 K/s, heating to different maximum temperature. (a) ~800 K, (b) 500 K, (c) 420 K.

Figures 4.1 and 4.2a show work function changes as a function of surface temperature on Pt(443), the ammonia pressure are 10^{-8} and 2×10^{-6} mbar respectively. Under these pressures we got saturation ammonia covered surface from freshly cleaned surface at room temperature, which was indicated by work function change, then temperature cycling experiments were applied to get work function changes vs temperature via Kelvin probe.

Low work function values are found for the most open surfaces. The work function can also be lowered locally by adsorbed electropositive species (electron donator), like Alkali atom, NH_x (x = 1～3). Both figures show work function levels off when the temperature is high enough under different NH_3 pressure, 470 K under 10^{-8} mbar and 570 K under 10^{-6} mbar range. These results indicate that ammonia over a Pt surface desorbed completely above a certain temperature. If we set the work function on clean surface to zero, work function change due to ammonia adsorption according to Fig. 4.1 and Fig. 4.2a, are -1.0 eV and -1.3 eV respectively. Obviously the difference is due to the variation of ammonia coverage under different pressure. Compared to Pt(100), the work function change due to ammonia adsorption on Pt(100) is relatively smaller, which is around -0.6 eV [11]. This work function difference depends not only on ammonia coverage over the surface, but also on the interaction between ammonia molecular and Pt surface, because the induced dipole is due to the interaction with Pt, the resulting dipole is also influenced by the net charge transfer from NH_3 to Pt.

Figure 4.1 also shows work function change simultaneously during heating/ cooling process in a NH_3 environment. At $p(NH_3) = 10^{-8}$ mbar, there is no hysteresis between heating up and cooling down branch, at a ramping speed 0.5 K/s, the work function change is linear with the temperature up to 480 K. This indicates that ammonia coverage is a function of temperature, and that the adsorption is direct and non-activated on the Pt(443), this observation is consistent with the results of Pt(100) [11] and Pt(111) [41]. Fisher et al. studied the electronic structure of molecular

ammonia adsorbed on Pt(111) by work function measurement, they found that at low coverage ($\theta \leqslant 1/4$) the change of work function induced by the adsorption of ammonia on Pt(111) is linearly proportional to the ammonia coverage. For comparison, Fig 4.2a shows the overall work function change at 2×10^{-6} mbar, which exhibits a change in the slope of curve during the heating up branch, this change happens at around 400 K. Kelvin probes can access extremely low coverage with a sensitivity which is not available in TDS experiments. Since work function is sensitive to the electronic interaction on the surface, adsorption into a different type of site is often associated with a different charge transfer, the change is reflected in the work function too. The straightforward interpretation of the above observation would be: (i) a switch between different adsorption sites; initially ammonia would like to adsorbate at the top site, denoted α, oriented as an inverted umbrella as N bonds to surface. Part of ammonia molecular could adsorb on hollow sites due to the relatively high pressure and adsorption time; and (ii) possibly to the switch between ammonia adsorption in state α and β-NH_3, which also denotes a high coverage state, the β state is less tightly bound and appears to be hydrogen-bonded to the initial layer of ammonia. Jennison et al. calculated the adsorbate hydrogen bond strength of ammonia on Pt(111), and discovered that the H-bond on the surface is almost three times stronger and the bond length appreciably shorter compare to that of two molecules in the gas phase [40].

Figure 4.2b and Fig. 4.2c show the experimental results which followed the same temperature cycling experimental process as in Fig. 4.2a, except reaching a different temperature maximum, 500 K and 420 K respectively. Compared to Fig. 4.2a, the major difference appears to be the plateau at T_{max} = 500 K. There is broad hysteresis during this temperature cycling experiment, and the value of the work function in the cooling down branch is relatively lower, this observation indicates that possibly a partial decomposition of ammonia happened in a temperature range from 420 K to 500 K. When T_{max} is 740 K, the fragment of ammonia e.g. NH_x (x =

1～2), are all desorbed. Ammonia does not start to decompose below 420 K. Fig. 4.2b shows that the work function in the cooling branch is lower than that in heating branch, compared to figures 4.2a and 4.2c. In this sense we speculate that some fraction of ammonia fragments didn't desorb because of a high energy barrier. It is these fragments on the surface that are responsible for the decrease in surface work function. Some authors studied ammonia adsorption and decomposition over Pt, including polycrystalline, stepped surface and planar single crystal surface. Loeffler et al. and Guthrie both agreed that 'open' surfaces or low coordination surfaces are more reactive for the decomposition of ammonia to N_2 and H_2 than the flat (111) or (100) surface [27, 33, 38]. According to the intensely studies carried out by Gohndorne et al., the adsorption of ammonia on platinum is not structure sensitive since the vibrational spectrum of adsorbed ammonia and the basic structure of the TPD spectrum of ammonia is identical on all of the faces they examined. They also point out that there are some variations in the binding energy and sticking probability of ammonia depending on the surface orientation. These variations produce a large difference in the rate of ammonia decomposition over different surfaces. The rate of ammonia decomposition on Pt is mainly affected by residence time and sticking probability [39].

The surface structure of Pt(443) is studied by LEED during the temperature cycling experiments in an ammonia environment. Figure 4.3 show the LEED pattern at different conditions, the distance between the split spots which is corresponds to a terrace width has no change, no variation in LEED pattern was observed as a whole. The terrace width distribution doesn't change not only during adsorption at room temperature but also in T-cycling according to the LEED patterns. The step meandering at 300 K which was proved by STM dose not show up in LEED. Except a slight increase in the background intensity, only the FWHM (Full Width at Half Maximum) of spots increased and maximum intensity of spots dropped. These observations indicate that some disorder exists caused by ammonia adsorption on the

surface.

In the cooling branch of T-cycling, a (2×2) surface structure at around 400 K was observed, as shown in Fig. 4.3d. This indicates a transition from disordered to ordered surface structure. Since such a transition couldn't be observed in the heating branch, the absence of ordering demonstrates that the mobility of adsorbate over the Pt surface is rather low at low temperature and high NH_3 coverage.

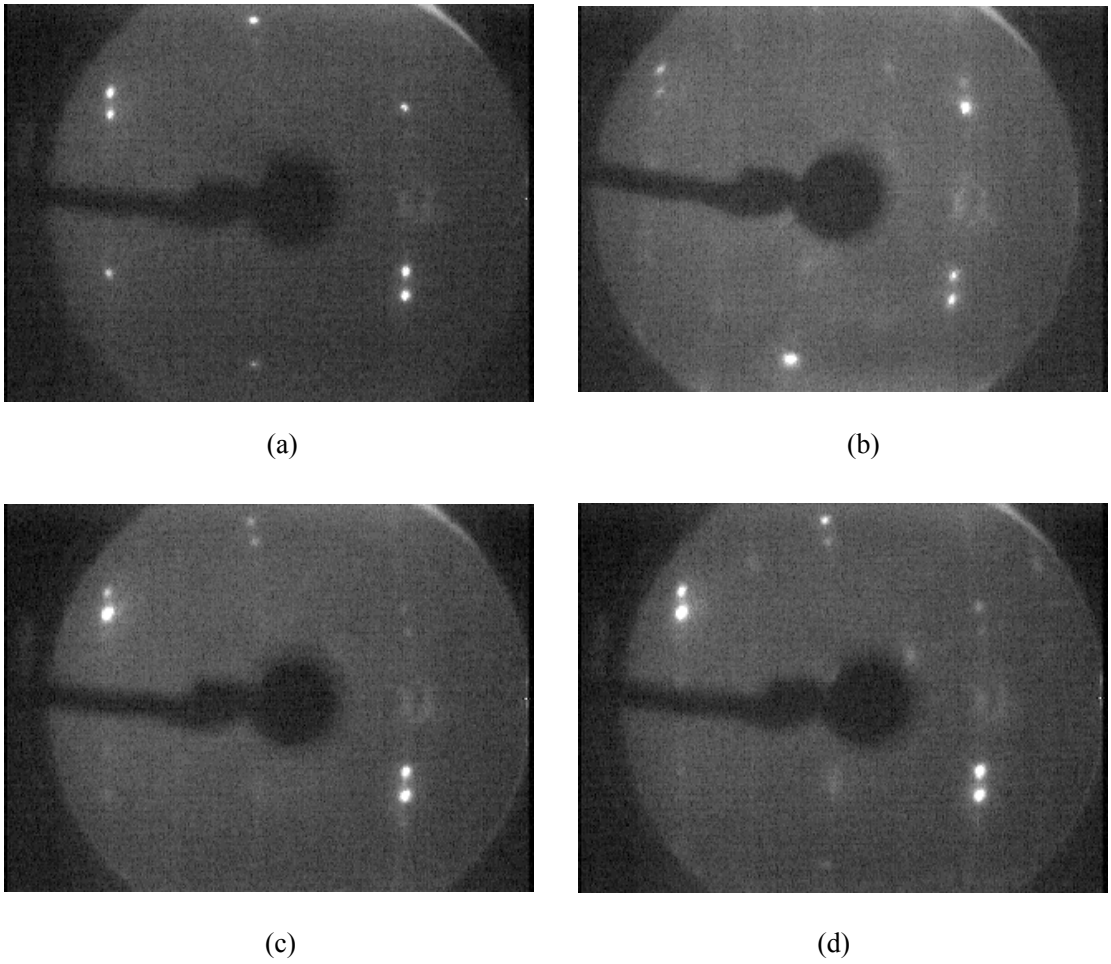

Figure 4.3. LEED pattern of Pt(443) at E = 90 eV under different conditions, (a) clean surface; (b) after ammonia adsorption at room temperature; (c) at 332 K after temperature cycling in ammonia, $p(NH_3) = 2 \times 10^{-6}$ mbar; (d) at ~ 400 K during cooling branch, a (2×2) structure formed.

4.2.2 Oxygen on Pt(443)

The stability of stepped metal surface in their clean state or when covered by adsorbate has been the subject of extensive studies. Many of these surfaces, in their clean state, appear to maintain their "ideal" structure over a large temperature range, i.e. low Miller index terraces separated by monatomic steps are stable. However, when heated in the presence of gases (O_2, CO) many the stepped surfaces lose their stability and reconstruct or facet [76]. Here we study work function variation and the reconstruction behaviors of Pt(443) during oxygen chemisorption using a Kelvin probe and LEED. The experiments are conducted in a range of temperature between 300 to 800 K with a oxygen partial pressure around 10^{-6} mbar. The adsorption of oxygen on platinum single crystal surfaces including planar [74, 75, 77-90] and stepped surfaces [91-96], have been the subject of numerous studies.

Figure 4.4a shows work function change as a function of temperature at p_{oxygen}= 10^{-6} mbar, and ramping speed is equal to 0.5 K/s. At room temperature the work function increase over Pt(443) due to oxygen adsorption is about 0.25 eV. Initially the work function increases with rising surface temperature, the maximum change reached is about 0.36 eV at 610 K, above 610 K the work function decreases due to increasing rate of O_2 desorption. Compared to the work function change induced by oxygen adsorption on Pt(443), the work function change on Pt(111) is about 0.15 eV with an oxygen coverage of 0.25 monolayers [85]. The work function increases monotonously with oxygen coverage. The results show that oxygen adsorption on Pt(443) is an activated process, which needs elevated temperatures to overcome the energy barrier. The line shape to work function show much complexity for oxygen over Pt(443) compare to ammonia.

Wang et al. studied oxygen adsorption and dissociation on Pt(335) with high-resolution electron energy loss spectroscopy (HREELS) and temperature programmed desorption [96]. Five adsorption state are found, atomic oxygen on terraces and steps, molecular oxygen on terraces and steps, and one metastable state

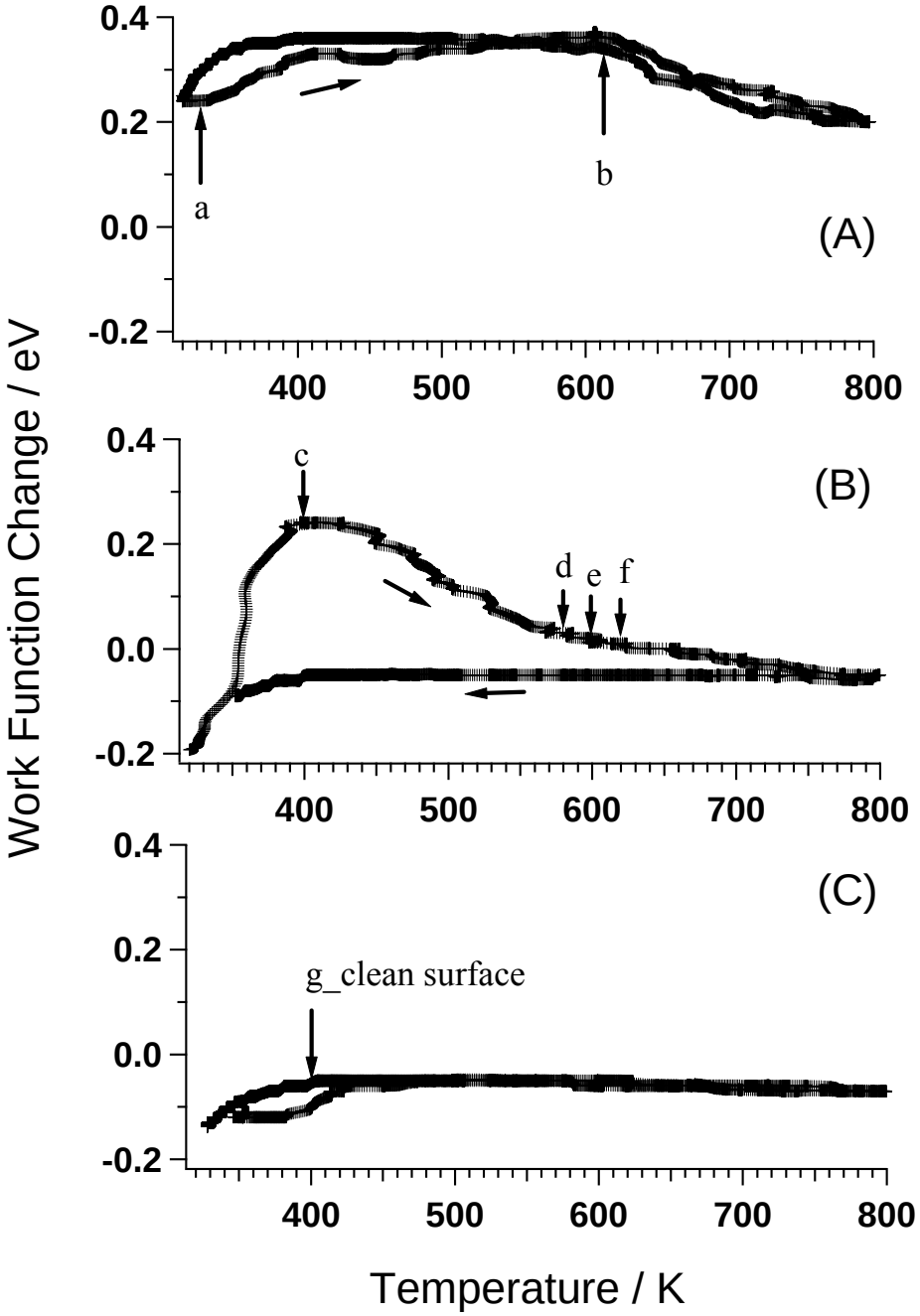

Figure 4.4. Work function change on Pt(443) during heating/cooling cycle, (A) in oxygen circumstance, $p(O_2) = 10^{-6}$ mbar, with a ramping rate 30 K/min; (B) turning off oxygen, background pressure is ~ 10^{-9} mbar, temperature cycling with the same ramping speed as (A); (C) right after (B), annealling the sample to 800 K.

for a molecular step species. Step species is bound to the exposed step edges.

Dissociation of O_2 occurs almost exclusively at the steps: at saturation coverage about 95% of the step O_2 species dissociates before desorbing, while 95% of the terrace O_2 desorbs directly without dissociation. Dissociation of the edge O_2 occurs in part directly and partially through a metastable state. In our case from work function measurements it is impossible to draw conclusions of what kind of species being present on the Pt(443) surface. At low coverage (<0.25 ML) oxygen adsorption into the atomic state proceeds probably through a molecular precursor state; and Campbell et al. suggested that at a coverage above 0.25 monolayers the dissociation step becomes activated on the (111) surface. Under these conditions dissociative adsorption probably proceeds via a route other than via direct dissociation [74]. That is the reason why either elevated temperature (and pressure) or atomic oxygen in the gas phase is required to achieve a high coverage.

We also investigate the surface structure via LEED when Pt(443) is exposed to oxygen. In the heating branch no LEED pattern change is observed except that the intensity of background abruptly becomes much stronger. We do observe a (2×2) structure at room temperature as shown in Fig. 4.5a, the formation of this (2×2) differs from ammonia adsorption over Pt(443), which also leads to a (2×2) pattern. Oxygen induced a step coalescence and a terrace broadening on the Pt(443) surface at around 610 K. This occurs only in the cooling down branch as shown in Fig. 4.5b, whereas no step coalescence can be observed during heating. The structure after step coalescence is stable at room temperature. This observation differs from the investigation by Lindauer et al. [92]. They found that the terrace broadening on Pt[6(111)×(100)] is accompanied by the appearance of the (2×2) layer. The heating of the sample, however, was conducted step by step which is more close to a static experiment at T-constant. Firstly the disagreement that the coalescence is only seen during cooling down, could be caused by kinetic effect. We heat up the sample by temperature-programmed controller, ramping 0.5 K/s. so it could be that atomic oxygen does not have enough time to equilibrate. Second, The distribution of oxygen

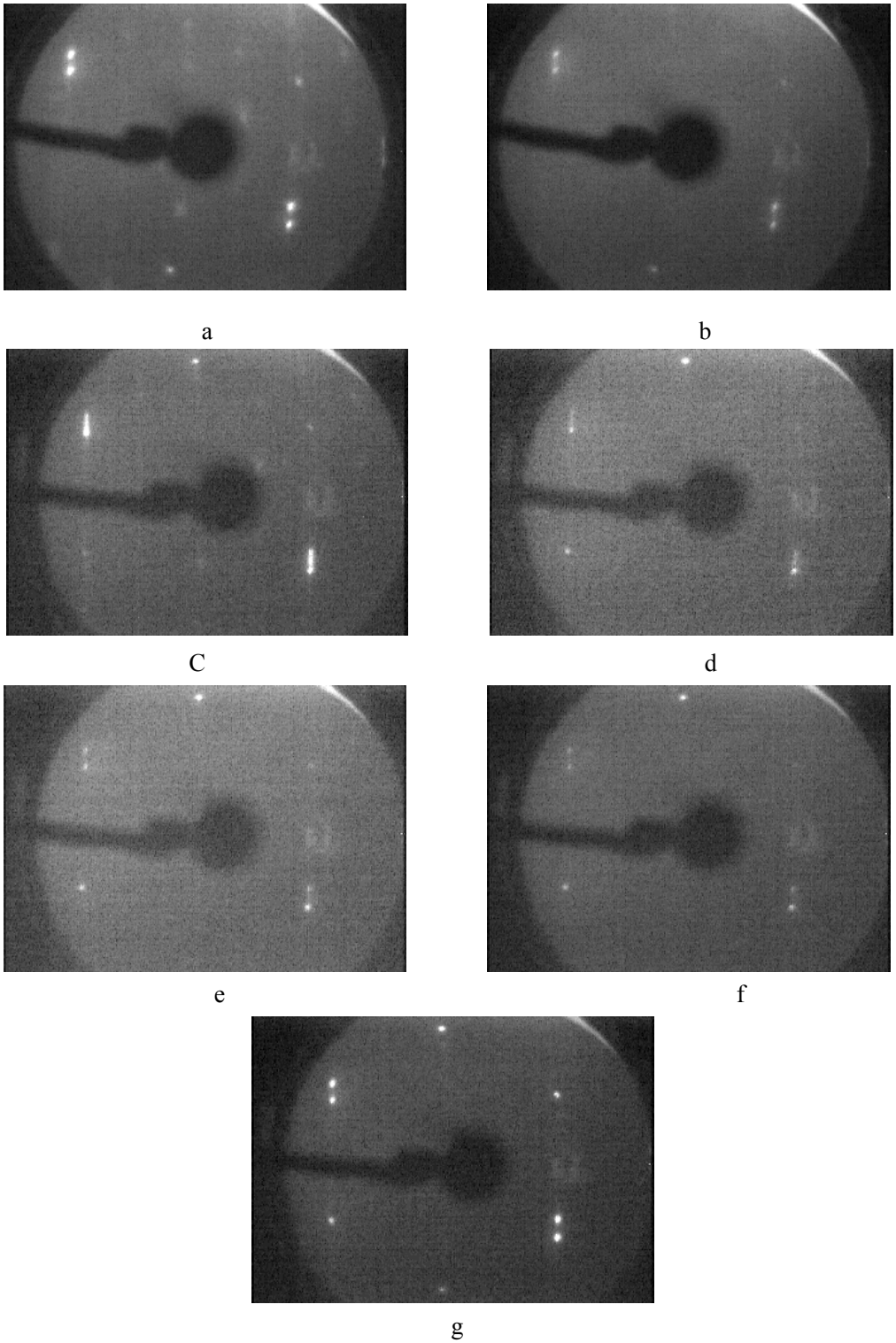

Figure 4.5. LEED pattern of Pt(443) at E = 90 eV under different condition, which are marked in corresponding to work function change profile in Fig. 4.4, (a) in oxygen at room temperature, a (2×2) structure is formed; (b) beginning of step coalescence only during cooling branch at around 610 K; (c) LEED pattern of step coalescence; (d), (e), (f), (g) are corresponding to conditions in Fig. 4.4.

at terraces site and oxygen at step sites could be difference in heating and cooling when the mobility is not high enough.

Once we got step coalescence followed by turning off oxygen until that pressure is below 10^{-9} mbar, the sample is annealed to 800 K to generate a clean surface. We investigate work function and structural change of Pt(443) via a Kelvin probe and LEED, the results are shown in Fig. 4.4b and 4.4c. The step coalescence vanished at around 600 K, we attribute this to oxygen desorption from terrace site. And during the cooling down branch, work function change levels off. These observations in previous work on O_2/Pt(111) system has been summarized. Briefly, three basic states exist for oxygen on this surface: one molecular (desorbing at around 170 K), one atomically chemisorbed above the surface (desorbing from 600 to 1100 K), another atomic, subsurface oxygen (desorbing above 1250 K).

LEED shows that a restructuring of the surface during temperature-programmed experiments takes place. Initially the work function increases during heating up until around 400 K. This increase is due to the desorption of residual gases. There is no change of LEED pattern until 400 K, as Fig. 4.5c shows. Commonly heating Pt causes desorption of oxygen first from the terrace sites, and then from the step sites [93]. Above around 600 K we can observe the disappearance of step coalescence, as shown in figures 4.5d, 4.5e and 4.5f. After reaching 800 K, the clean surface is restored, as shown in LEED Fig. 4.5g. No work function change during cooling down branch is seen.

The same thermal annealing procedure is applied to a mixture of ammonia and oxygen. The composition NH_3:O_2 is 1 to 10, i.e. oxygen is in excess with a oxygen pressure 10^{-6} mbar. No step coalescence was observed in this experiment. The steady-state O_{ad} concentration is expected to decrease when NH_3 is present due to the consumption of O_{ad} by NO and H_2O production during the oxidation reaction. We can assume that atomic oxygen does not accumulate enough to induce step coalescence. Therefore no change in the LEED pattern was observed. This

observation is different from ammonia oxidation on Pt(533) where oxygen induced a doubling of the step height, it is this different that is responsible for the broad hysteresis in the reaction rate on Pt(533) compared to Pt(443). We expect that this difference is due to the different step orientation on Pt(533) and Pt(443).

4.3 Stationary Reaction Kinetics

4.3.1 Temperature dependence and influence of reactant ratio

4.3.1.1 Pt(865)

A structural model of the single crystal surface Pt(865) which exhibits kinks is displayed in Fig 3.4c together with a characterization of the surface by LEED. Fig. 4.6 shows a TPR spectrum over Pt(865) obstained at a various mixing ratio $p(NH_3)$: $p(O_2)$ = 1:1, 1:3 or 1:10, respectively, from ammonia excess to oxygen rich, for $p(NH_3) = 5\times10^{-6}$ mbar. The TPR was recorded in a heating/cooling cycle with a ramping speed 15 K/min, starting always with freshly prepared surface. For the steady-state ammonia oxidation reaction, N_2 and H_2O were the major products at low temperature, whereas the selectivity toward NO and H_2O changed at higher temperatures. Under different feed composition, profiles of the reaction rates of the nitrogenous products (N_2 and NO) are similar, nitrous oxide (N_2O) wasn't observed under our experimental conditions, these observation are consistent with mechanistic and kinetic studies of ammonia oxidation on Pt in UHV. Only when the total pressure is above 10^{-1} mbar [25], nitrous oxide forms according to several other ammonia oxidation studies, the absence of N_2O at low pressure is believed to be part of effect of pressure gap.

The comparison of the reaction rate of nitrogenous products under different feed

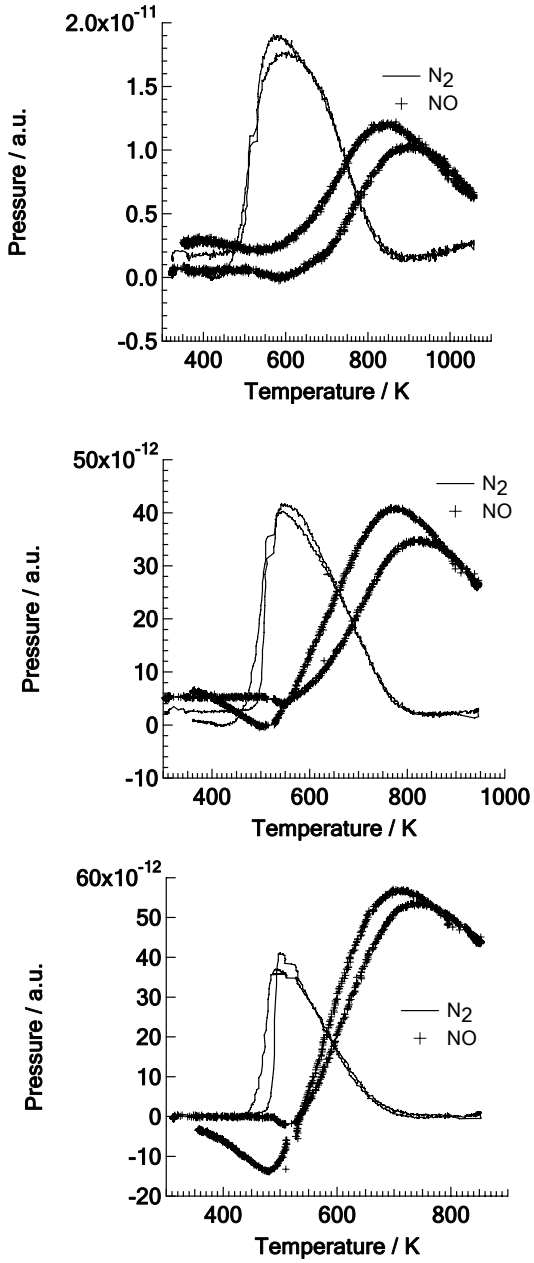

Figure 4.6. Temperature programmed reaction spectrum over Pt(865) at various mixing ratios of $p(NH_3):p(O_2)$, $p(NH_3)$ is fixed to 5×10^{-6} mbar, the ramping speed is 15 K/min. (a) 1:1; (b) 1:3; (c) 1:10.

composition shows that, firstly, the reaction rate depends on the ratio p_{NH_3}/p_{O_2}. The surface is more active when the oxygen partial pressure is increased. Compared to the ratio of 1:1, the reaction rate of N_2 is around 2 times higher, and that of NO being 6 times higher when the ratio is 1:10. Evidently the reaction rate of NO is

more sensitive to oxygen partial pressure than the N_2 production. Obviously, the distribution of products changes from N_2 to NO with increasing of oxygen partial pressure. According to Fig. 4.6 the temperature of the rate of maxima of N_2 and NO shift from 590 K to 500 K of N_2 and from 900 K to 720 K of NO, respectively. These temperature shifts also reflect the temperature at which the change in the N-selectivity occurred. The desorption of N_2 is fast because repulsive interactions from neighboring NO(a) and O(a) coverages reduce the N_2 desorption temperature. Therefore, the N_2 and NO formed in this reaction desorbs at a lower temperature with the increasing oxygen partial pressure of feed composition. Commonly, kinetic studies of ammonia oxidation show distribution of production are dominated by the surface composition during the reaction at different surface temperature. N_2(g) is formed when the surface is covered with an N-containing species and NO(g) is formed when O(a) is the majority surface species. The occurrence of this reaction is controlled by the NO desorption and the NO dissociation reaction. At low temperature, the coverage of N-containing species is relatively high, NO(a) can dissociate to N(a) and O(a). At high oxygen coverages and high temperature NO dissociation is impossible since the empty sites required for NO dissociation are blocked, under these conditions there exists a route to NO formation.

$p(O_2)/p(NH_3)$ / **Reaction rate (a. u.)**	**1:1**	**1:3**	**1:10**
N_2	15	40	40
NO	9	33	60

Table 4.1. Maximum reaction rate under different reactant composition on Pt(865). Here the unit of reaction rate are arbitrary unit, but the data are comparable since the results were acquired at the same condition. $p(NH_3) = 5 \times 10^{-6}$ mbar.

Table 4.1 shows the change of maximum reaction rate under different reactant

composition. And with the increasing of oxygen ratio of feed composition, N_2 reaction rate become to saturate, as comparison of 1:3 and 1:10, whereas NO reaction rate at the ratio of 1:10 is about double of that at the ratio of 1:3. In this sense, main product under oxygen excess reaction condition is NO.

Figure 4.7 shows the change of s_{reac} of oxygen during heating and cooling cycles. Increasing the O_2/NH_3 ratio didn't result in a change of the temperature at which the reaction starts, this temperature is around 480 K. These results suggest that the onset of ammonia oxidation is not only dominated by the oxygen partial pressure, but also by the N-species on the surface. The inhibition of the reaction by these N-species exists until a certain temperature. The inhibition is lifted roughly at the desorption temperature expected for ammonia and nitrogen. For comparison, oxygen desorbs at much higher temperature. The observation that the temperature of maximum oxygen consumption, i.e. highest s_{reac} shifts to high temperature with increasing mixing ratio O_2:NH_3 is coincident with the variation of production distribution from N_2 to NO. NO is the main product at high temperature. The selectivity of the reaction depends on the temperature, as well as on the mixing ratio of the reactants.

In Fig. 4.8, the reactive sticking coefficient, s_{reac}, of ammonia is shown as measured under different feed composition. We find that the peak of the reactive sticking coefficient shifts slightly to lower temperature with increasing oxygen partial pressure. The onset of the oxidation doesn't depend on the feed composition, it is always around 480 K. The hysteresis observed in s_{reac} of ammonia and in the formation of H_2O (shown in Fig. 4.9) was due to relative fast ramping rate compared to the desorption of ammonia and H_2O. Since a pronounced hysteresis is not observed in Figures 4.6 and 4.7, so it is quite likely that the hysteresis just result from a heating/cooling rate. Table 4.2 shows the maximum reactive sticking coefficient of ammonia and oxygen under different feed composition. The data show that s_{reac} of ammonia increases drastically with the increasing oxygen partial pressure,

up to 24% when the ratio (NH_3/O_2) is of 1:10. It is also easy to understand that s_{reac} of oxygen decrease when the feed composition changes from ammonia rich to oxygen in excess.

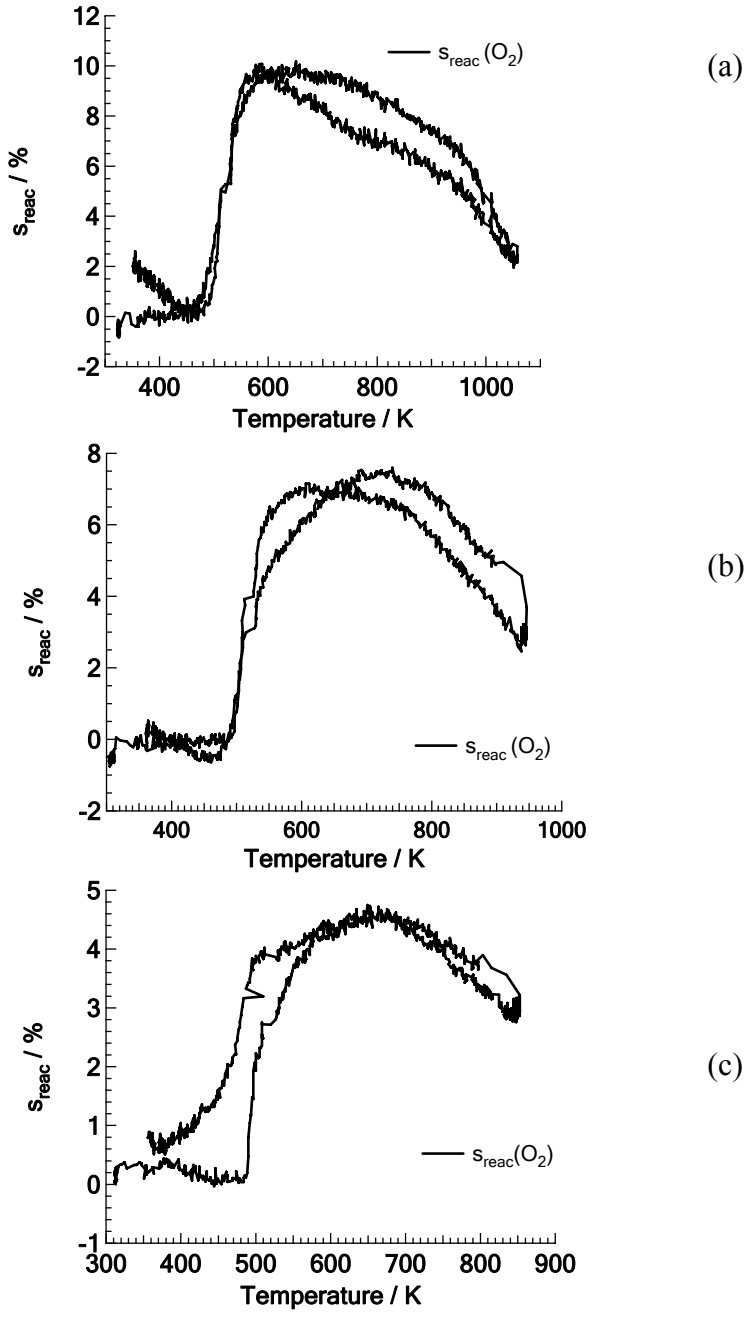

Figure 4.7. Variation of s_{reac} (O_2) on Pt(865) during temperature cycling at different feed composition of $p(NH_3)$: $p(O_2)$, and $p(NH_3)$ is fixed to 5×10^{-6} mbar, the ramping speed is 15 K/min. (a) 1:1; (b) 1:3; (c) 1:10.

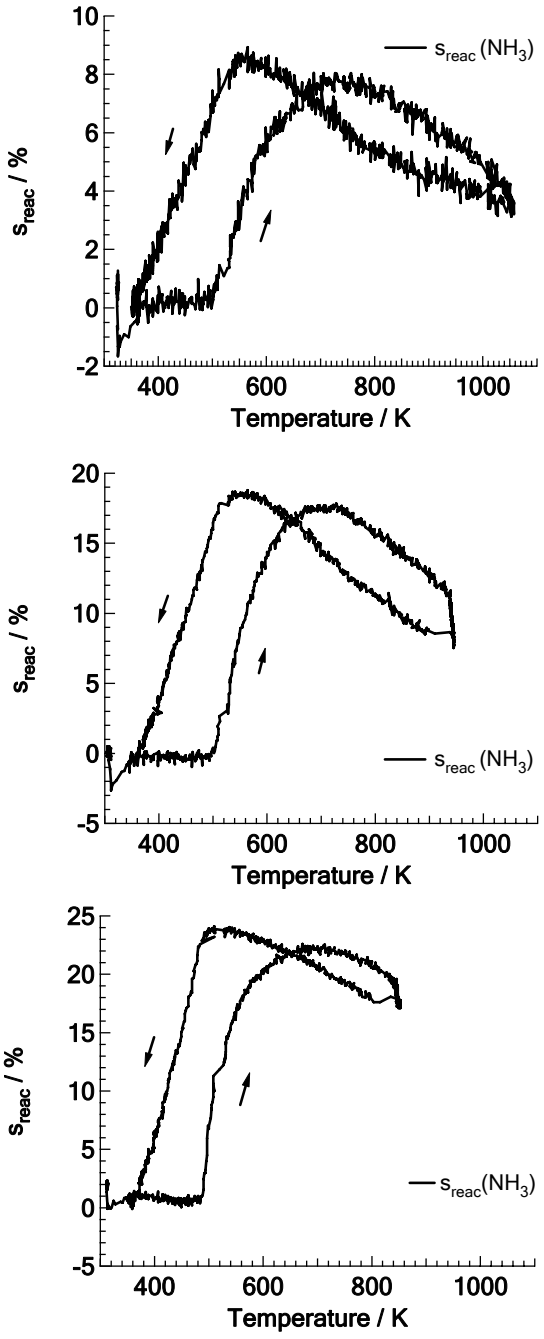

Figure 4.8. Variation of s_{reac} (NH_3) on Pt(865) during temperature cycling at different feed composition of $p(NH_3)$: $p(O_2)$, and $p(NH_3)$ is fixed to 5×10^{-6} mbar, the ramping speed is 15 K/min. (a) 1:1; (b) 1:3; (c) 1:10.

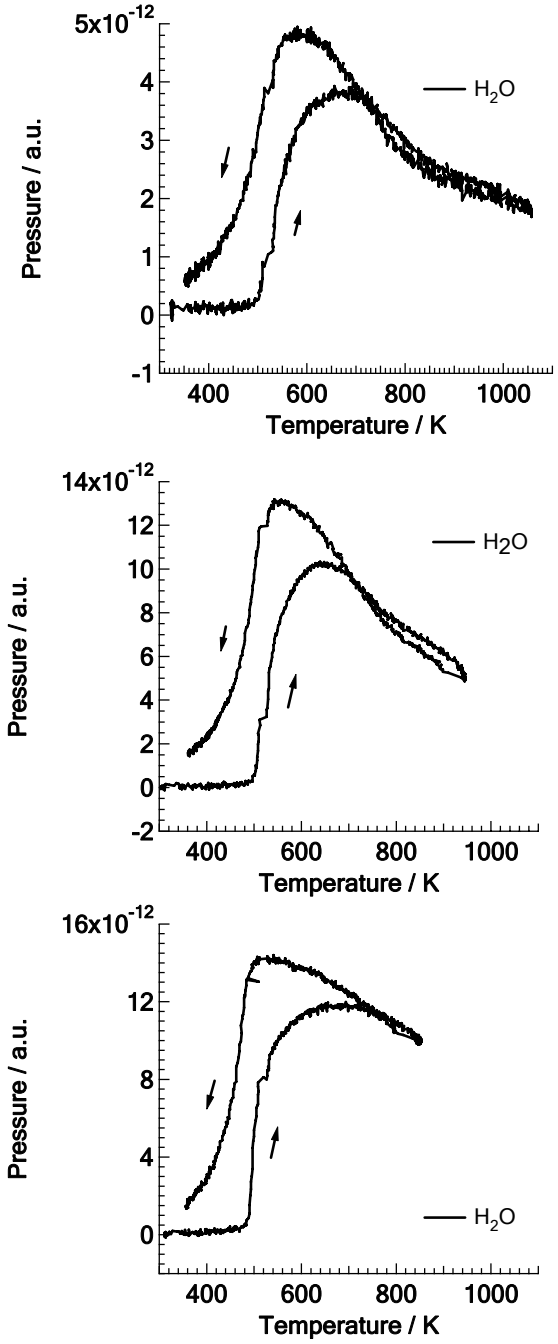

Figure 4.9. Variation of pressure of water production in ammonia oxidation on Pt(865) during temperature cycling at different feed composition of $p(NH_3)$: $p(O_2)$, and $p(NH_3)$ is fixed to 5×10^{-6} mbar, the ramping speed is 15 K/min. (a) 1:1; (b) 1:3; (c) 1:10.

$p(O_2)/p(NH_3)$	1:1	1:3	1:10
$s_{reac}(O_2)$	10 %	7.4 %	4.5 %
$s_{reac}(NH_3)$	8 %	18 %	24 %

Table 4.2. Maximum reactive sticking coefficient of ammonia and oxygen under different feed composition on Pt(865)

Figure 4.9 shows the formation rate of water as a function of temperature. Water(g) formed beyond 500 K, upon heating which is a little bit above the onset of reaction at 480 K. A sudden increase in the pressure was observed at this certain temperature for the products H_2O. The formation of H_2O(g) doesn't depend on the feed composition.

AES experiments were also carried out after heating and cooling cycles to check species were present on the surface. However, no significant build-up of N or O on the sample surface was found after evacuation of reactants. This result could be caused by clean-off reactions which come into play due to the relative long time required for AES measurements.

4.3.1.2 Pt(100)

In the same UHV chamber we used for the previous samples, we investigate ammonia oxidation on Pt(100) via TPR experiments. The ramping speed in the TPR experiments is 15 K/min. And $p(NH_3)$ is 5×10^{-6} mbar, the mixing ratio of ammonia to oxygen varies from 1:1, 1:3 to 1:10 respectively.

As shown in Fig. 4.10, the reaction ignites at around 370 K as the sample is heated, and the onset temperature of the reaction doesn't depend on the mixing ratio

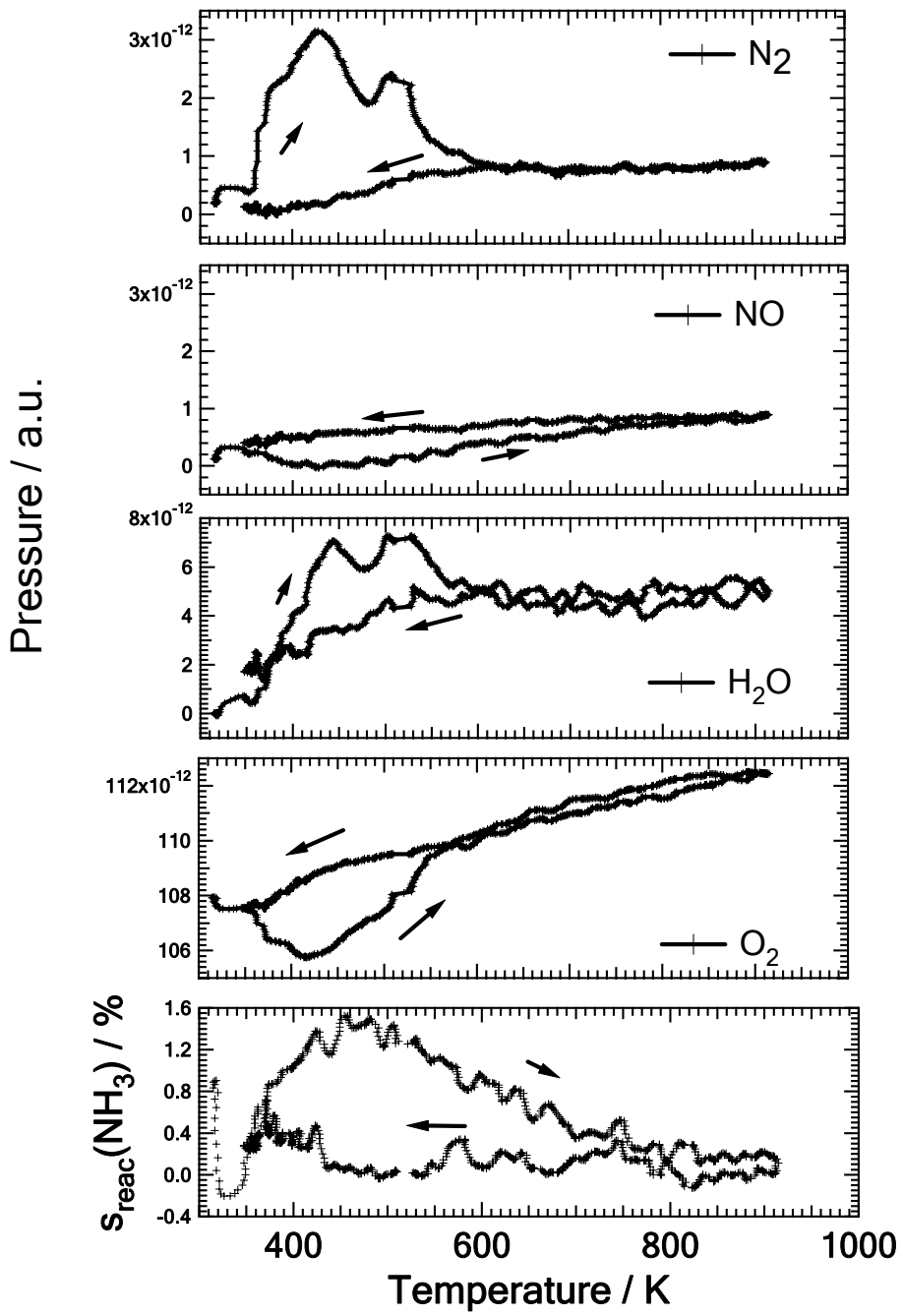

Figure 4.10. Variation of the product formation of N_2, NO and H_2O on Pt(100), of the partial pressure of the reactant O_2, the variation of reactive sticking coefficient of ammonia is also shown in this figure. The ammonia partial pressure was kept fixed at $p(NH_3) = 5 \times 10^{-6}$ mbar, the feed composition of $p(NH_3) : p(O_2)$ is 1:1. The ramping speed is 15 K/min.

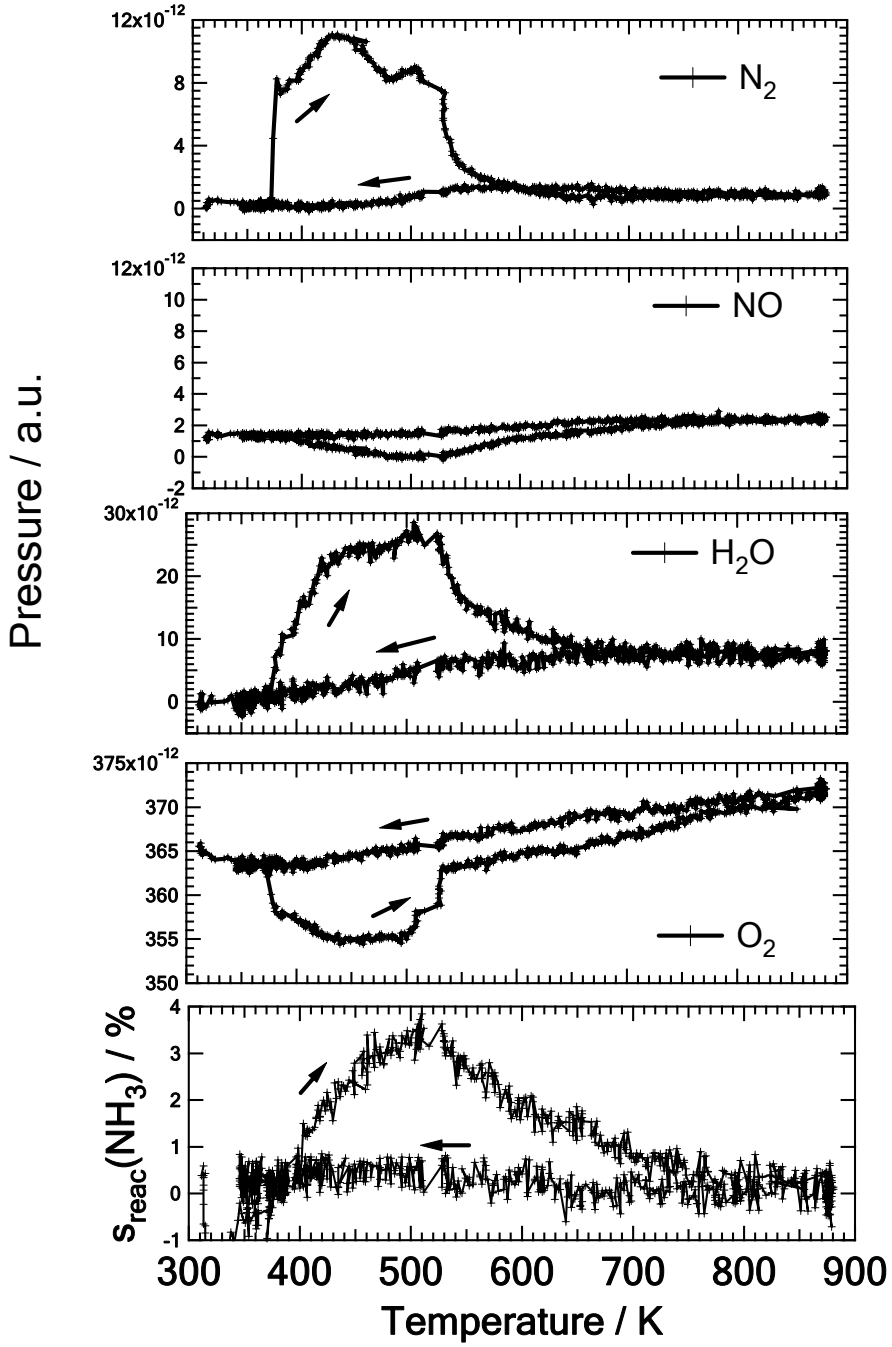

Figure 4.11. Variation of the product formation of N_2, NO and H_2O on Pt(100), of the partial pressure of the reactant O_2, the variation of reactive sticking coefficient of ammonia is also shown in this figure. The ammonia partial pressure was kept fixed at $p(NH_3) = 5 \times 10^{-6}$ mbar, the feed composition of $p(NH_3)$: $p(O_2)$ is 1:3. The ramping speed is 15 K/min.

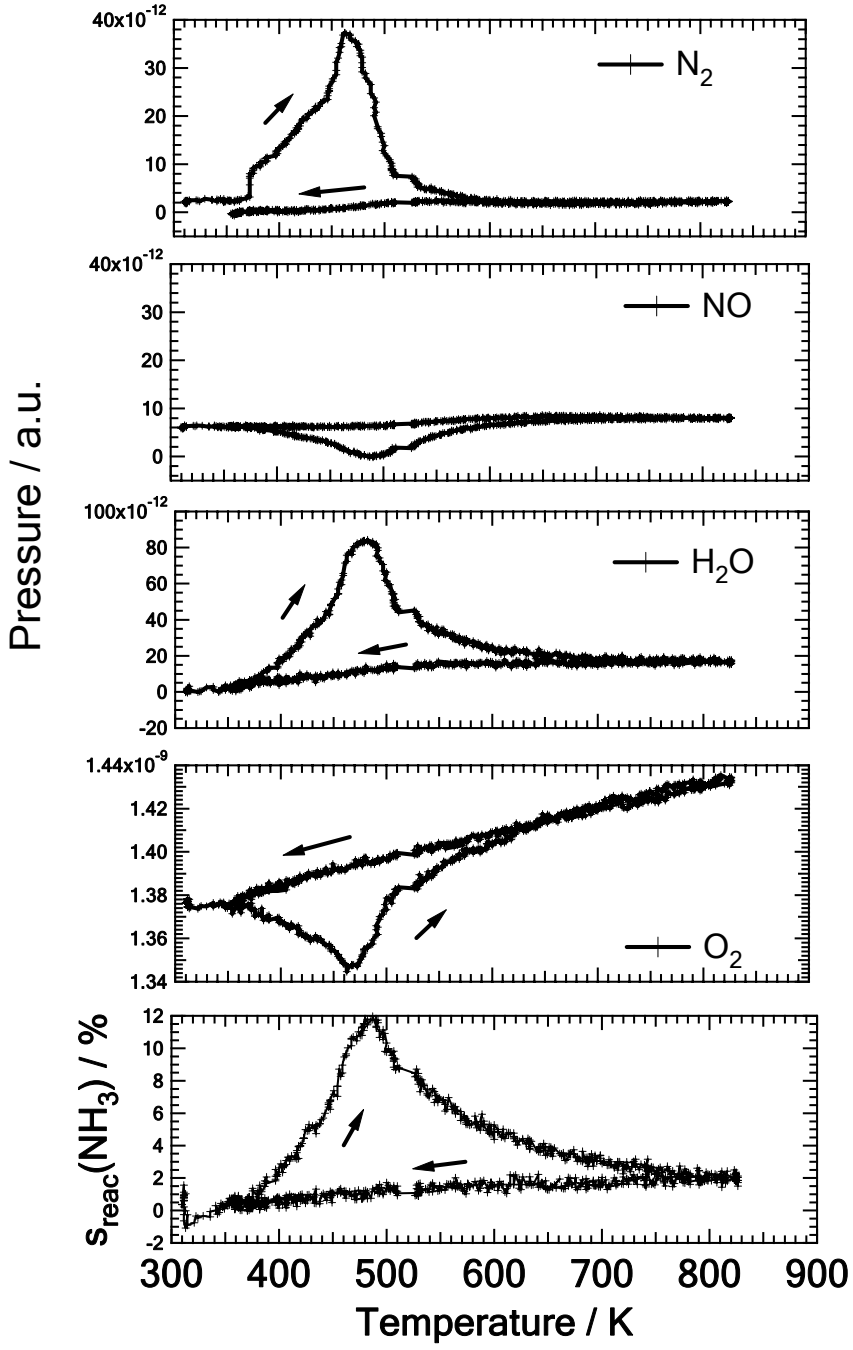

Figure 4.12. Variation of the product formation of N_2, NO and H_2O on Pt(100), of the partial pressure of the reactant O_2, the variation of reactive sticking coefficient of ammonia is also shown in this figure. The ammonia partial pressure was kept fixed at $p(NH_3) = 5 \times 10^{-6}$ mbar, the feed composition of $p(NH_3) : p(O_2)$ is 1:10. The ramping speed is 15 K/min.

of the reactants. Under a mixing ratio of 1:1 the rate of N_2 formation, after passing a

first peak at around 430 K, drops and then approaches a second high temperature peak at about 520 K. The H_2O production has similar profile of the reaction rate. During the cooling branch the reactivity is quite low. A pronounced hysteresis is thus present in the temperature cycling experiment. The hysteresis is reproduced in a second cycle, which means that it cannot be caused by irreversible changes of the catalyst surface but rather has to be caused by differences in the adsorbate coverages and surface structure.

The (100) plane of platinum is known to undergo a reconstruction from the bulk-like (1×1) surface to the "hex" reconstructed surface. The clean Pt(100) surface is stable in its well known hexagonal form and exhibits a complex LEED pattern which is commonly termed "hex" (T < 1100 K) or R0.7^o-hex (T > 1100 K), the LEED pattern of hex surface structure is shown in Fig. 3.4d. Griffiths et al. investigated the interaction of oxygen with Pt(100) [81]. They found two adsorption state, the oxygen coverages associated with saturation of the two phases are 0.44 and 0.63 monolayers, on the hex phase the oxygen coverage is less than 0.1 monolayers. Above 750 K, the stable surface structure is the hex phase in an oxygen atmosphere. This is in agreement with the observation that Pt(100) surface is inert for the ammonia reaction at high temperature. In the cooling branch ammonia cannot lift the reconstruction from the hex to the bulk-like (1×1) phase due to a too small heat of adsorption of ammonia [36]. Therefore the surface remains in the hex structure during cooling until O_2 adsorption lifts the hex reconstruction.

Figures 4.10, 4.11 and 4.12 display the variation of the formation of the products N_2, NO, and H_2O; and the consumption of the reactants (NH_3 and O_2) under different feed composition. As shown in Fig. 4.10, two peaks of formation rate of N_2 and H_2O are observed. The explanation could be that there are two routes for N_2 production. At low temperature (around 430 K) N_2 is formed by recombination of N(a), which is produced by stripping hydrogen from NH_3, involving O(a) and OH(a). At higher temperature (about 520 K) N_2 is formed from the dissociation of NO

followed by recombination of the N adatoms. With the transition from N_2 to NO formation occurs at a surface temperature when NO has a too short surface residence time to take part in secondary reactions, then NO starts to desorb substantially from the surface.

Except its practical applications in environmental chemistry and HNO_3 production, NO is also interesting from a purely scientific reasons. The dissociation energy of NO (628 kJ/mol) is much lower than that of the similar molecule, CO (1071 kJ/mol) [97, 98]. Therefore there is great probability of finding both, molecular and dissociated NO species on a surface. NO dissociation over Pt(100) was investigate by Ge et al. using the density functional theory [55]. They demonstrated that both, the presence of defects and the local geometry of the defects, are important in determining the reactivity of a surface. The dissociation of NO is characterized by a transition state, in which surface Pt atoms with a square arrangement, e.g. (100)-1×1, provide the preferential active site for NO dissociation. The square arrangement is favorable because this arrangement avoids that metal atoms are sharing N and O bonding at the transition state.

The TPRS obtained with variation of the oxygen partial pressure are displayed in figures 4.10, 4.11, and 4.12. After passing through two peaks in the N_2 rate the N_2 production starts to drop. Surface is almost inert when the temperature is above 600 K. With increasing oxygen partial pressure from 1:1 to 1:10, two peaks between 430 and 520 K combine to form one peak at ~470 K. The temperature of the N_2 rate maximum shifts to lower temperature, from 520 to 470 K, due to increase of oxygen partial pressure.

Note that the y-scale in each panel is proportional to the gas pressure. So despite arbitary units, they can be compared directly with the results from Pt(865) since all experiments were carried out in the same UHV system with the same defection. The comparison with N_2 production over Pt(865) in Fig. 4.6 reveals surprising facts. When p_{NH_3}/p_{O_2} is 1:1, the reaction rate of N_2 on Pt(865) is almost

5 times higher than that on Pt(100); but once the mixing ratio is 1:10, the reaction rate of N_2 on both surface is equivalent. On Pt(100) reaction rate of N_2 strongly depend on the oxygen partial pressure, basically this could be attributed to the surface phase transition induced by oxygen.

For NO production over Pt(100) it is not surprising that reaction rate of NO in TPRS is quite low since the transition from (1×1) to the hex phase happens when T > 600 K. As the oxygen sticking coefficient on hex structure is low, and since the oxygen coverage plays an important role in NO formation. The NO formation rate will be low too. A similar conclusion can be inferred from the variation of oxygen pressure in figures 4.10 – 4.12. Under different mixing ratios from ammonia rich to oxygen in excess, oxygen pressure firstly would pass through a minimum point in the temperature range of 400 and 500 K during heating. Then oxygen pressure keeps increasing towards higher temperature. This observation indicates that the maximum reactivity on Pt(100) exist in a range of 400 ~ 500 K, the surface is inert at T > 600 K. The surface resident time of oxygen becoming too short for reaction to occur would be possible factors responsible for this observation.

Figures 4.10, 4.11 and 4.12 also show a comparison of the reactive sticking coefficient of ammonia, $s_{reac}(NH_3)$, on Pt(100) for the different mixing ratios. The ammonia partial pressure was kept fixed at $p(NH_3) = 5 \times 10^{-6}$ mbar in all experiments. The data shown were obtained from the heating part of a heating/cooling cycle with a heating rate of 15 K/min. Apparently, the maximum $s_{reac}(NH_3)$ increases drastically with increasing oxygen partial pressure from 1.6% at a ratio of 1:1 to 13% at a ratio of 1:10 during heating. During cooling $s_{reac}(NH_3)$ is close to zero. Compared to $s_{reac}(NH_3)$ on Pt(865) in Fig. 4.8 under the same reaction condition (pressure, mixing ratio, heating/cooling rate), the maximum in $s_{reac}(NH_3)$ is much higher at Pt(865) varying from 8% to 24% with the composition changing from ammonia rich to oxygen excess. This indicates Pt(865) is more active at whole temperature range, but the selectivity towards N_2 is higher on Pt(100). Actually the

main difference between the two surfaces is the capability of NO formation at high temperature (> 600 K) which is better on Pt(865). The maximum in $s_{reac}(NH_3)$ on Pt(100) is in a temperature range between 450 and 500 K, whereas it is between 500 and 700 K on Pt(865).

4.3.1.3 Pt foil

The TPRS obtained in the 10^{-5} mbar range with different mixing ratios are displayed in Fig. 4.13. The feed composition are 1:1, 1:3 and 1:10, and the temperature ramping rate is 10 K/min. Note that the y-scale in each panel has been calibrated according to the total pressure. Figure 4.14 shows the reactive sticking coefficient, s_{reac}, of ammonia as measured from the variation of the feed composition are shown. After comparison of NO and NO_2 TPD data from Pt foil with TPD data from the Pt(111), Pt(100) and Pt(110) surface, Wickham et al. concluded that the surface of Pt foil mostly resembles a Pt(111) surface, with some contribution of (110) and (100) planes as well as steps and kinks [99].

No broad hysteresis could be found at different mixing ratios, but slight deactivations appear in TPRS as shown in Fig 4.13. These experiments were aimed at investigating the product selectivity and catalytic activity as a function of surface temperature and of gas phase composition. The rate maxima shift towards low temperature as the proportion of oxygen in the gas phase is increased from 1:1, 1:3 to 1:10 (p_{NH_3}/p_{O_2}). The temperature N_2 rate maximum reaction rate of N_2 decreased from 600 to 480 K, while that of NO decreased from 900 to around 680 K. This indicates that also on Pt foil, the adsorption of O_2 plays an important role. Above a certain higher temperature, the reaction rate start to drop. This drop is explained by the fact that O_{ad} starts to desorb (as O_2), resulting in a lower O_{ad} concentration, and thus lower reaction rate for all products.

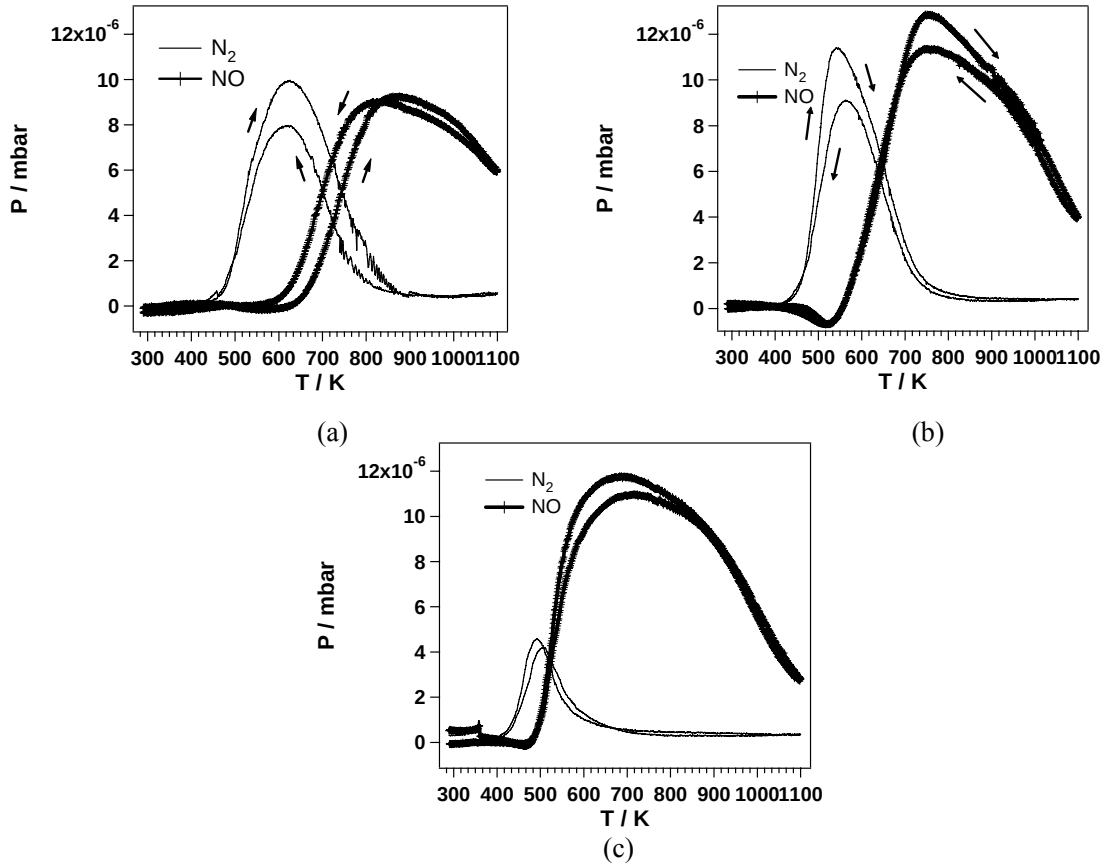

Figure 4.13. Temperature programmed reaction kinetics of ammonia oxidation on a Pt foil in the 10^{-5} mbar range, the ramping speed is 10 K/min, (a) total pressure is 3×10^{-5} mbar, the ratio of $p(NH_3)$: $p(O_2)$ is 1:1; (b) total pressure is 4×10^{-5} mbar, the ratio of 1:3; (c) total pressure is 5.5×10^{-5} mbar, the ratio is 1:10.

Here we compare the values of $r_{max}(NO)/r_{max}(N_2)$ in TPRS at different mixing ratios of the reactants. This ratio increases from 0.91, 1.14, to 2.7 on Pt foil with the increasing of oxygen partial pressure, i.e. the p_{NH_3}/p_{O_2} ratio variated from 1:1, 1:3 and 1:10. Compared to (100) surface, selectivity towards NO is much higher on the Pt foil. This observation is consistent with the previous studies on decomposition of NO on differently orientated single crystal surfaces. NO decomposition over Pt(111) exhibit low activity, as investigated by Gorte et al. Comparing NO adsorption and decomposition on Pt(111), Pt(110) and Pt(100), they found that the (100) surface binds NO more tightly than the (110) or (111) surface. The Pt(100) surface also produces the largest amount of NO dissociation, around 50% dissociates to yield N_2

and O_2. The other planes desorb without significant decomposition, the fraction of decomposed NO is less than 2% on the (111) surface [100].

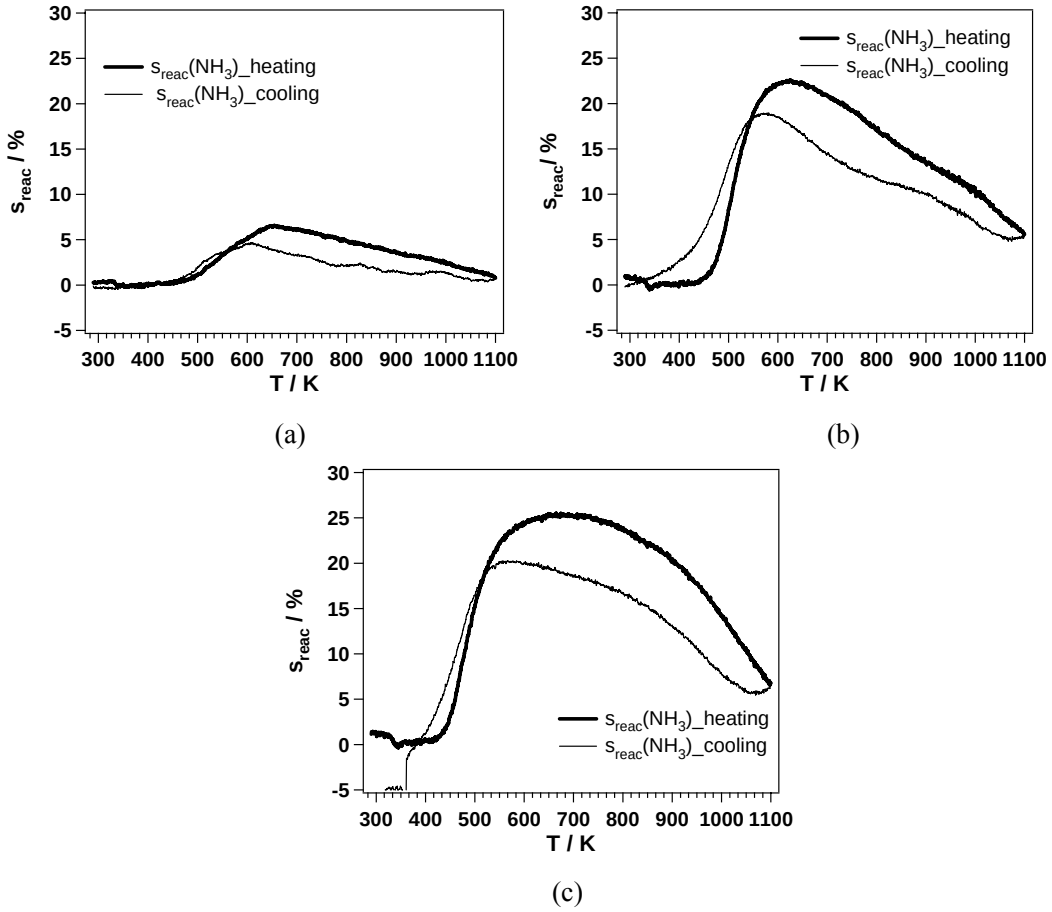

Figure 4.14. Variation of the reactive sticking coefficient of ammonia as a function of temperature on Pt foil in the 10^{-5} mbar range, the ramping speed is 10 K / min, (a) total pressure is 3×10^{-5} mbar, the ratio of $p(NH_3)$: $p(O_2)$ is 1:1; (b) total pressure is 4×10^{-5} mbar, the ratio is 1:3; (c) total pressure is 5.5×10^{-5} mbar, the ratio is 1:10.

The strong dependence of the activity of the Pt foil surface on the oxygen partial pressure is clearly shown in Fig. 4.14, which depicts the ammonia reactive sticking coefficient, s_{reac} at different reactant mixing ratios. The amount of the reactive sticking coefficient of ammonia provides a good measure of the reaction activity for three different ratios. With increasing oxygen partial pressure the ammonia sticking coefficient increased dramatically from 6.5%, 23% to 25%. s_{reac} of ammonia is thus about 4 times higher for the 1:10 ratio than for the 1:1 ratio. This clearly shows that

oxygen acts as a promoter for ammonia oxidation on a Pt surface. One additional observation is that the temperature at which the reaction starts decreased, from 470 K, 430 K to 415 K with increasing O_2/NH_3.

4.3.1.4 Pt(533) and Pt(443)

Ammonia oxidation over Pt(533) and Pt(443) have been intensively studied in UHV system by Scheibe et al. [12-14], the pressure range is 10^{-5} and 10^{-4} mbar range. In order to attempt to bridge the pressure gap to intermediate pressure range, we investigated ammonia oxidation on Pt(533) and Pt(443) in the pressure range of 10^{-3} and 10^{-2} mbar, these experiments were carried out in high pressure reactor (from 10^{-4} to 10^{-1} mbar).

Figures 4.15 and 4.16 show that investigation of reaction rate as a function of temperature with different feed composition over Pt(553) and Pt(443), and the total pressure is 10^{-3} mbar. The mixing ratio (NH_3/O_2) is of 1:1 and 1:3. The temperature range is from 400 K to 850 K, which was limited by the ability of the heating lamp. Therefore only the maximum peak of N_2 formation rate could be observed in TPRS. On Pt(533) quite large hysteresis effects are observed at 10^{-2} mbar, and as compared with (533) the hysteresis on Pt(443) are generally small. There is at least qualitative consensus from TPRS at intermediate pressure that N_2 rate curve still exhibits a dip as the observation from Scheibe et al. at 10^{-5} and 10^{-4} mbar range [14], which was attributed to the surface restructures. And this dip is relatively weak at intermediate pressure range compared to the TPRS in UHV. After passing through this dip the reaction rate of N_2 increased abruptly; the observation under different mixing ratio show that the NO product strongly depends on the feed composition. When the mixing ratio is 1:1, the NO formation rate is quite small on Pt(533) as we observed, whereas, if the feed composition is oxygen rich, e.g. 1:3, NO production was observed to increase dramatically, as shown in Fig. 4.15.

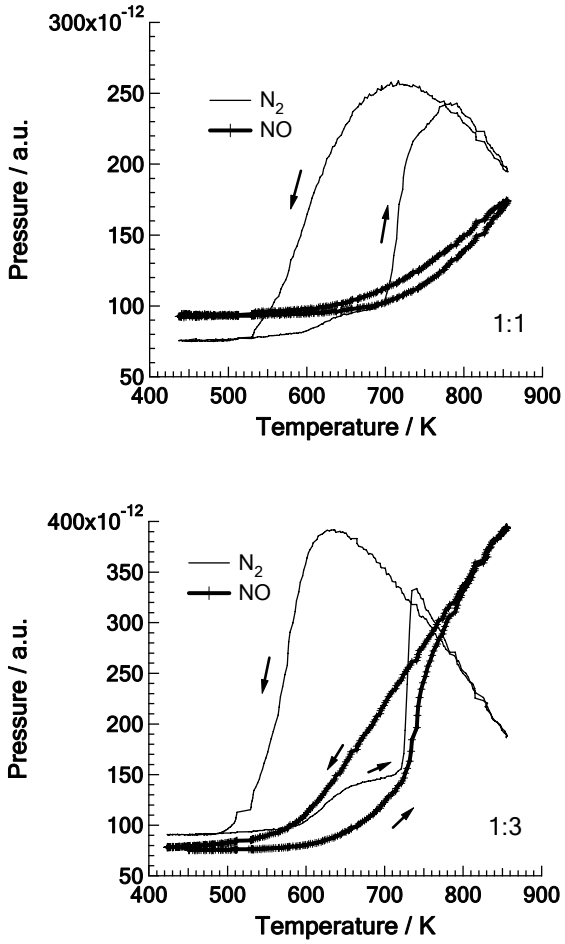

Figure 4.15. Variation of the reaction rate as a function of temperature with different feed composition over Pt(533), and the pressure range is 10^{-3} mbar, the ratio $p(O_2)$: $p(NH_3)$ is (a) 1:1, and (b) 1:3.

The observation of abrupt increasing of N_2 production indicates that an inhibition of the reaction could exist, and this effect is more likely due to the adsorption of N-containing species, which blocks the adsorption of oxygen on the surface. Compared to Pt(443) this inhibition is more pronounced on Pt(533), the major differences between Pt(533) and Pt(443) are the step density and the orientation of step. This also could be the reason why the selectivity towards NO on Pt(443) is relatively higher than that of Pt(533), as comparison between Fig. 4.15b and Fig. 4.16b. In temperature programmed desorption experiments it was shown that about

50% of the initially molecularly adsorbed NO decomposes on Pt(100), whereas Pt(111) and Pt(110) exhibit a rather low dissociation probability [100]. Since Pt(533) contains (100) steps where NO can dissociate, it is plausible that NO(g) production is more preferred on Pt(433) where NO can easily desorb without dissociation.

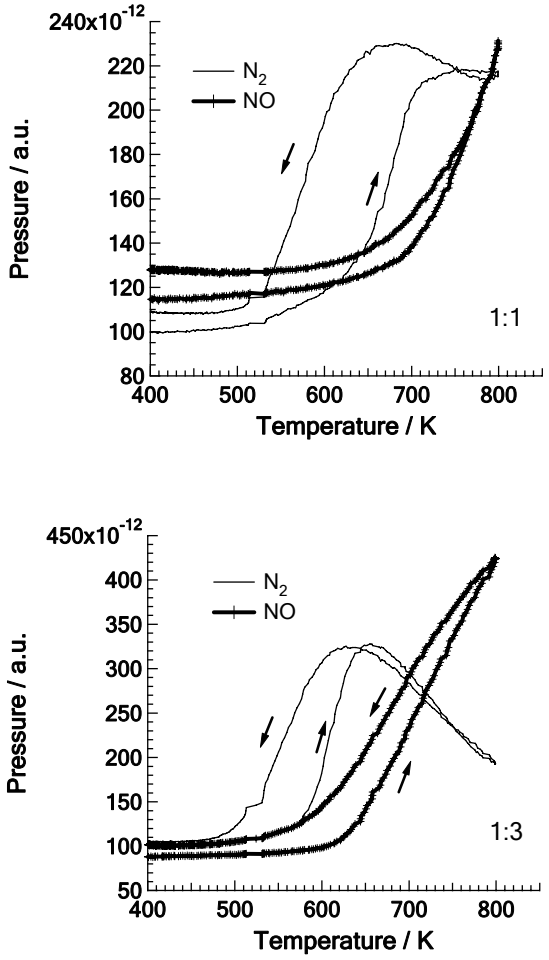

Figure 4.16. Variation of the reaction rate as a function of temperature with different feed composition over Pt(433), and the pressure range is 10^{-3} mbar, the ratio $p(O_2)$: $p(NH_3)$ is (a) 1:1, and (b) 1:3.

4.3.2 Partial Pressure Dependence

The dependence of the kinetics of NO and N_2 production on the oxygen or ammonia partial pressure at three temperatures, T = 550 K, 650 K and 800 K, were studied on Pt(865).

4.3.2.1 Oxygen

Figure 4.17 show the variation in product yield at a catalyst temperature of 550 K (around the peak of the N_2 production curve in TPR studies), 650 K and 800 K (around the peak of the NO production curve) with fixed oxygen pressure as a function of ammonia pressure. Ammonia pressure is 5×10^{-6} mbar, oxygen pressure increased stepwise from 5×10^{-7} to around 5×10^{-5} mbar, and the corresponding reaction orders of N_2 and NO with respect to oxygen obtained under steady state conditions, are shown in table 4.3.

First we discuss the results for Pt(865) in Fig. 4.17a. The data in Fig. 4.17a for 550 K show that at low temperature N_2 formation is the preferred reaction channel. With increasing oxygen partial pressure, N_2 formation increases abruptly, and till oxygen pressure is around 1.3×10^{-5} mbar N_2 formation starts to level off while no NO formation can be observed. Only when oxygen is much in excess, a small quantity of NO is formed. This observation is consistent with previous TPRS studies: NO(g) starts to form above 550 ~ 600 K. From the slope of the linear least squares fit to the data, the reaction order of N_2 with respect to oxygen before the leveling off of reaction rate is obtained as 1.24 ± 0.11. Obviously the positive order of reaction suggests that there is no inhibition of the reaction induced by oxygen partial pressure at 550 K.

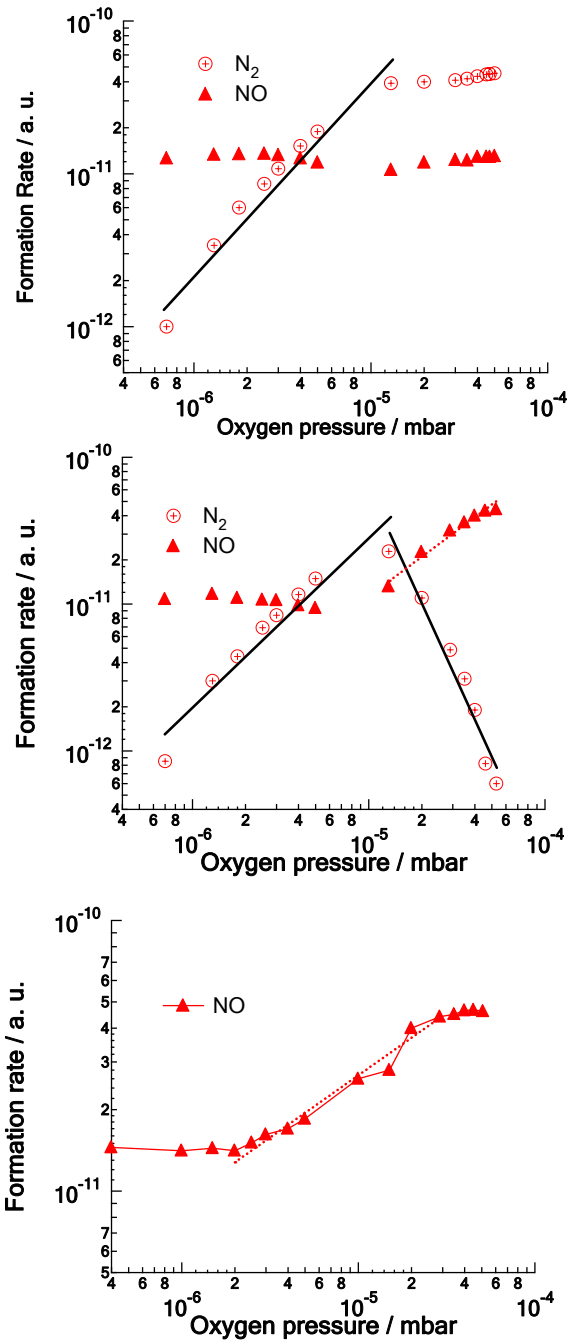

Figure 4.17. Dependence of the N_2 and NO formation rate on Pt(865) on oxygen partial pressure at different temperature over Pt(865), the ammonia pressure is fixed to 5×10^{-6} mbar, (a) 550 K, (b) 650 K, (c) 800 K.

The data in Fig. 4.17b for 650 K display a more complicate situation compared to the reaction at 550 K since NO starts to form under this reaction condition. We observe that with increasing oxygen partial pressure, N_2 production increases until

oxygen pressure is around 1.3×10^{-5} mbar, and the ratio of p_{O_2} / p_{NH_3} is about 2.6:1. After this crucial point NO product starts to form, while the rate of N_2 decreases. The straightforward interpretation of this observation is that the oxygen coverage increases with increasing oxygen partial pressure, the selectivity between NO and N_2 is determined by the oxygen coverage. With further increasing of oxygen coverage the formation rate of NO increases too, the rate of N_2 formation starts to drop immediately. When the mixing ratio p_{O_2} / p_{NH_3} is below 2.6, the reaction order of N_2 with respect to oxygen is 1.12 ± 0.13, the reaction order of NO with respect to oxygen is zero, apparently no NO formed; and after this crucial point the reaction order of N_2 with respect to oxygen is –2.61 ± 0.24, meanwhile the reaction order of NO with respect to oxygen is 0.87 ± 0.07. Therefore these observations demonstrate O adatom on the surface can inhibit the formation of N_2, in the mean time, NO production is favored if the oxygen coverage is above a critical value, this value on Pt(100) is around 0.2 monolayers (ML), which was reported by Bradley et al. [22].

The data in Fig. 4.17c for 800 K shows that NO is preferred at high temperature. No N_2 production can be found during this whole process. Formation of NO start when the ratio of p_{O_2} / p_{NH_3} is above 2:5, with oxygen partial pressure 2×10^{-6} mbar. When the ratio is around 6:1, the reaction rate of NO saturates. Before the saturation, the reaction order of NO with respect to oxygen is 0.43.

At 800 K, nitrogen-containing species have short resident time on the surface, so oxygen can adsorb uninhibitedly. We did not find a clue about ammonia dissociation via QMS under our experimental conditions. Even at very low oxygen partial pressure NO and N_2 production were not detected. With increasing oxygen partial pressure the oxygen coverage increases. Therefore NO is formed while NO dissociation is inhibited under high oxygen coverage, therefore gaseous NO is the main product of the reaction at 800 K.

Temperature / K	Reaction Order with respect to O_2	
	N_2 formation	NO formation
550	1.24 ± 0.11	0
650	1.12 ± 0.13	0
	-2.61 ± 0.24	0.87 ± 0.07 (1)
800	0	0.43 ± 0.03

Table 4.3. Reaction order for Pt(865) with respect to oxygen under different temperature, $p(NH_3) = 5 \times 10^{-6}$ mbar. (1) when $p(O_2) > 1.2 \times 10^{-5}$ mbar.

4.3.2.2 Ammonia

The dependence of the reaction kinetics of Pt(865) on the ammonia partial pressure are displayed in Fig. 4.18 for T = 550, T = 650 K and T = 800 K. The oxygen pressure is fixed to 5×10^{-6} mbar, the ammonia pressure variates from 5×10^{-7} mbar to 5×10^{-5} mbar. Experimentally, it is difficult to stabilize the pressure of ammonia in the UHV chamber, due to the adsorption at the walls, so we start the experiments from $p(NH_3) = 5 \times 10^{-5}$ mbar, then stepwise decrease ammonia pressure to 5×10^{-7} mbar. The corresponding reaction orders of N_2 and NO with respect to ammonia obtained under steady state conditions, are shown in table 4.4.

The data in Fig 4.18a for 550 K show that with increasing ammonia partial pressure the formation of N_2 increase steeply; the reaction order of N_2 with respect to ammonia is 1.33 ± 0.29. Then the rate starts to level off when the ammonia pressure is around 5×10^{-6} mbar, the mixing ratio is 1:1. As expected, there is no NO production to be observed at low temperature, N_2 is the dominant product at 550 K, even under the condition of excess oxygen.

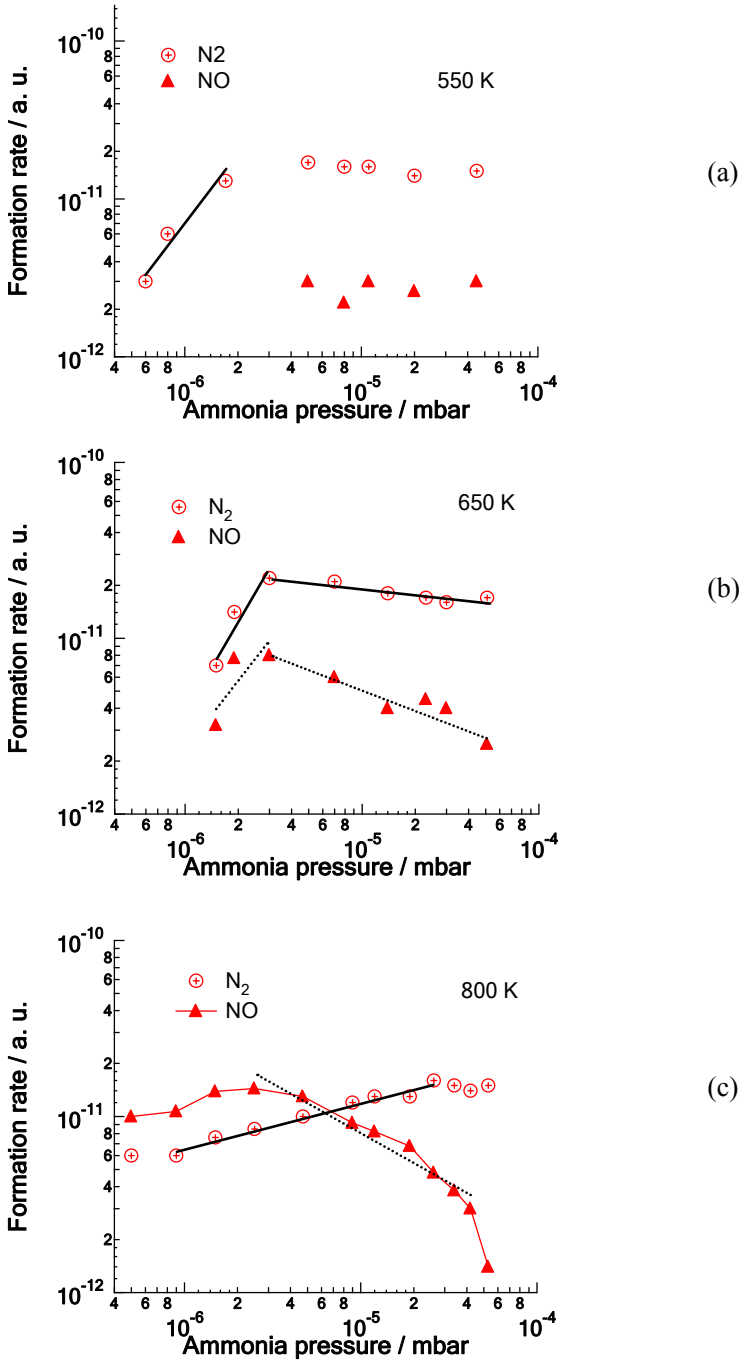

Figure 4.18. Dependence of the N_2 and NO formation rate on Pt(865) on ammonia partial pressure at different temperature over Pt(865). The oxygen pressure is fixed to 5×10^{-6} mbar, (a) 550 K, (b) 650 K, (c) 800 K

The data in Fig. 4.18b for 650 K demonstrate that initially increasing ammonia partial pressure promotes both reaction rate of N_2 and NO. Reaction order with

respect to ammonia is 1.56 ± 0.49, when $p(NH_3) > 3 \times 10^{-6}$ mbar, both reaction rate of N_2 and NO productions start to decrease slightly, this inhibition can be attributed to the blocking of adsorption sites by N-containing species. The selectivity change induced by variation of the ammonia partial pressure can be attributed to the change in surface coverage. From a mainly oxygen covered surface to a mainly N-containing species covered surface. The data in Fig. 4.18c for 800 K exhibit the reaction rate of N_2 and NO variate as a function of ammonia partial pressure. The data show that N_2 production increase weakly with ammonia partial pressure, yielding a reaction order of 0.26 ± 0.02. Above a ratio of 6:1 (NH_3/O_2) the reaction rate of N_2 starts to saturate. The NO rate as a function of ammonia partial pressure starts to drop abruptly while the ratio is above 1:2. The observation that the rate of NO drop with increasing ammonia partial pressure is in agreement with the observation by Gland et al.

Temperature / K	**Reaction Order with respect to NH_3**	
	N_2 formation	**NO formation**
550	1.33 ± 0.3	0
	0 (1)	
650	1.56 ± 0.50	1.15 ± 0.91
	-0.12 ± 0.02	-0.36 ± 0.06 (2)
800	0.26 ± 0.02	-0.56 ±0.06 (3)

Table 4.4. Reaction order for Pt(865) with respect to ammonia under different temperature, $p(O_2) = 5 \times 10^{-6}$ mbar. (1) when $p(NH_3) > 1.7 \times 10^{-6}$ mbar, $r(N_2)$ saturated. (2) when $p(NH_3) > 3 \times 10^{-6}$ mbar. (3) when $p(NH_3) > 2.5 \times 10^{-6}$ mbar

4.3.3 Work Function Measurement during Ammonia Oxidation

Work function changes in a surface reaction can be used to characterize adsorption states during a catalytic reaction. Work function measurements via a Kelvin probe sample an area of about 5 mm^2. In order to find out if pattern formation

occurs or oscillatory behaviour of ammonia oxidation on Pt(443) exists photoelectron emission microscopy (PEEM) was applied to follow surfaces processes with a spatial resolution of 1 μm.

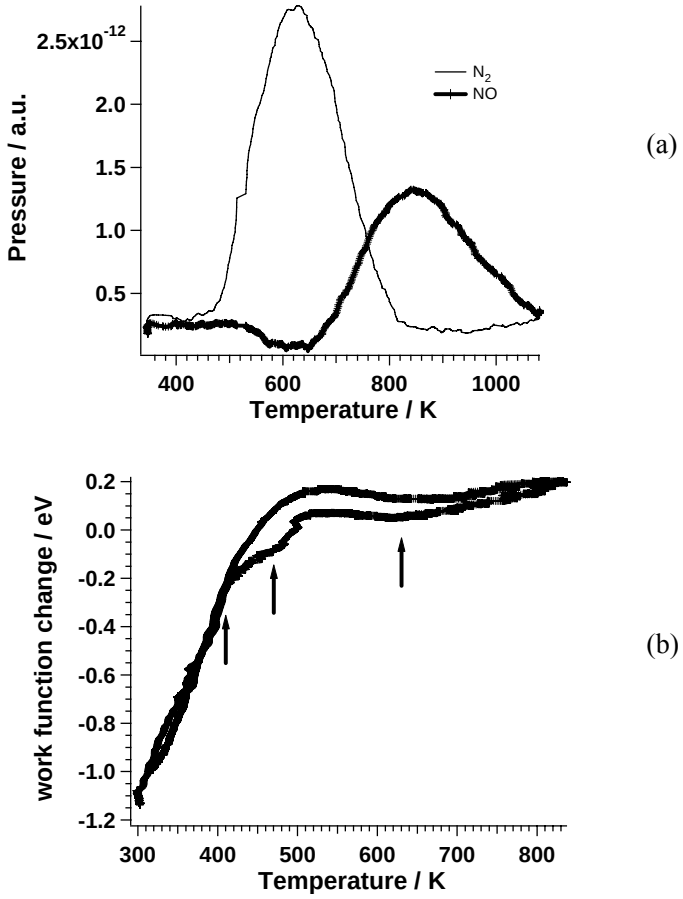

Figure 4.19. (a) Variation of N_2 and NO formation during temperature cycling experiment, the total pressure is 6×10^{-5} mbar, the ratio NH_3/O_2 is 1:1, the ramping rate is 15 K/min. (b) Measurement of work function change was carried out using a Kelvin probe under the same reaction condition as in (a).

Figure 4.19a displays the rate of N_2 and NO formation of Pt(865) during the catalytic reaction, simultaneously the work function change was investigated using a Kelvin probe, as shown in Fig. 4.19b. This TPR experiment was carried out under a pressure of 6×10^{-6} mbar, the feed composition is a 1:1, and the heating/cooling rate is 15 K/min. We see that the profile of work function change vs temperature is quite similar to the TPR experiments in an ammonia environment when the temperature is

below 500 K. With increasing surface temperature work function increases due to desorption of ammonia, and the slope of the curve decrease at around 400 K, which is similar to the work function change during heating/cooling cycle in NH_3 environment, as shown in Fig. 4.2. This indicate that the coadsorption of oxygen and ammonia on Pt(443) surface has little effect on ammonia adsorption on the surface. Since this reaction system has different intermediate species, it is hard to tell what the processes on the catalytic surface are in detail using only a Kelvin probe. The rate show that the reaction ignites at around 460 K. At this temperature, the slope of the curve increases as compared to the slope of the curve in the range below 460 K. This change in the slope is attributed to the consumption of ammonia by the reaction. The other important point is slightly around 630 K. Above 630 K, the work function increases, this might indicate a transition in the surface coverage from N-containing species to oxygen adatoms. Simultaneously, the selectivity of the reaction changes from preferred N_2 production to a domination of NO production.

In a series of experiments on ammonia oxidation over Pt(443) the total pressure, the feed composition and the heating/cooling rate was varied. PEEM showed no nonlinear behavior on Pt(443); during reaction, work function changes on the catalytic surface occur always homogeneous. Figure 4.20 shows PEEM image of Pt(443) surface under different conditions, including clean surface, surface fully covered by ammonia and coadsorption of ammonia and oxygen at 10^{-6} mbar range. With a feed composition of 1:1 (NH_3/O_2) the sample was heated up from 300 K to 800 K via a temperature programmed controller, the heating rate is 1 K/s. From a series of PEEM the mean gray value was plotted, as shown in Fig. 4.20d. We see that the surface work function strongly increases in a temperature range from 300 K to 480 K. From 480 K to 630 K, the rate of N_2 formation increases, while the work function only increased slowly with temperature continuing going up. And above 630 K, variation of work function is weak, which is assigned that catalyst surface has totally convert N-containing species covered surface to O_{ad} covered. This is

coincident with studies of rate measurement via QMS and work function studies using Kelvin probe.

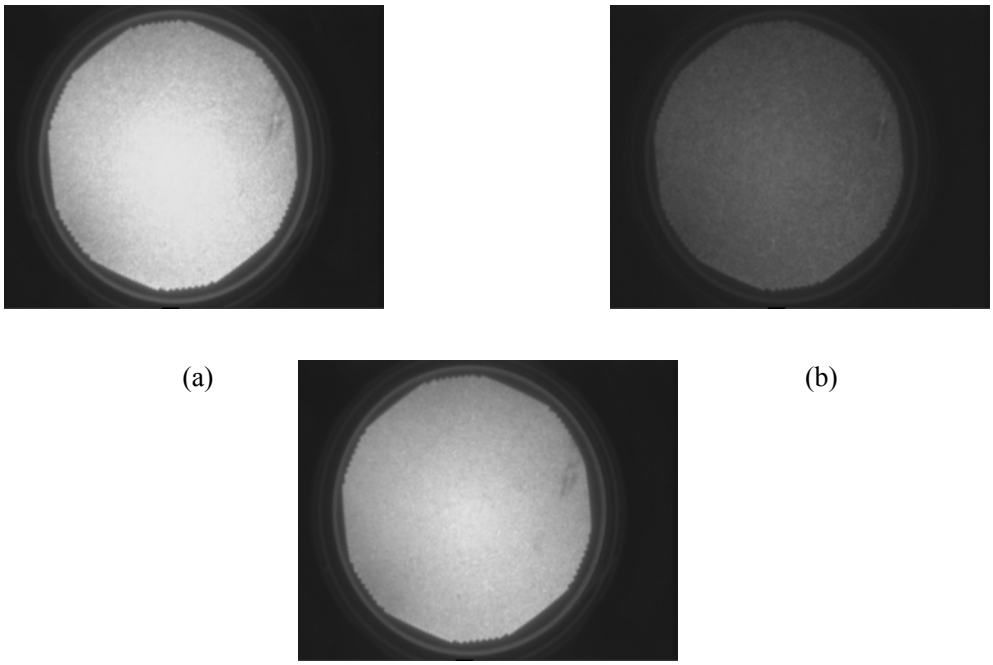

(a) (b)

(c)

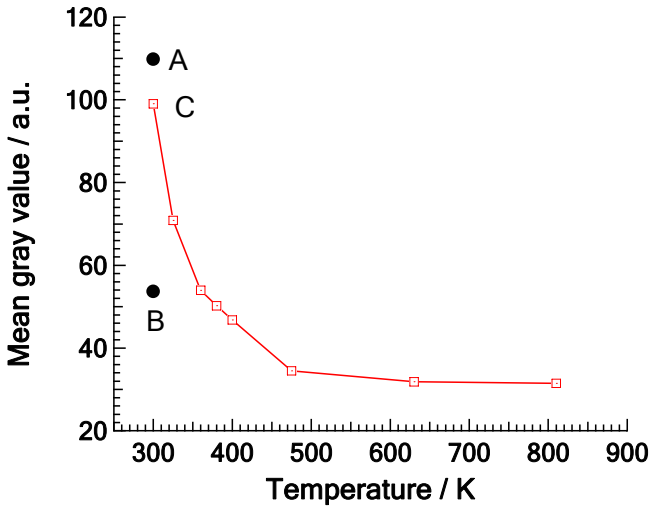

(d)

Figure 4.20. PEEM images of Pt(443) under different conditions, (a) ammonia covered surface at $p(NH_3) = 3 \times 10^{-6}$ mbar, (b) clean Pt(443) surface, (c) coadsorption of ammonia and oxygen, $p(NH_3) = 3 \times 10^{-6}$ mbar, and the ratio NH_3/O_2 is 1:1, (d) the condition of point A, B and C correspond to figure a, b and c, the other point denote mean gray value of PEEM images during reaction, which start from point B. The heating rate is 1 K/s. The diameter of imaged area is 600 μm.

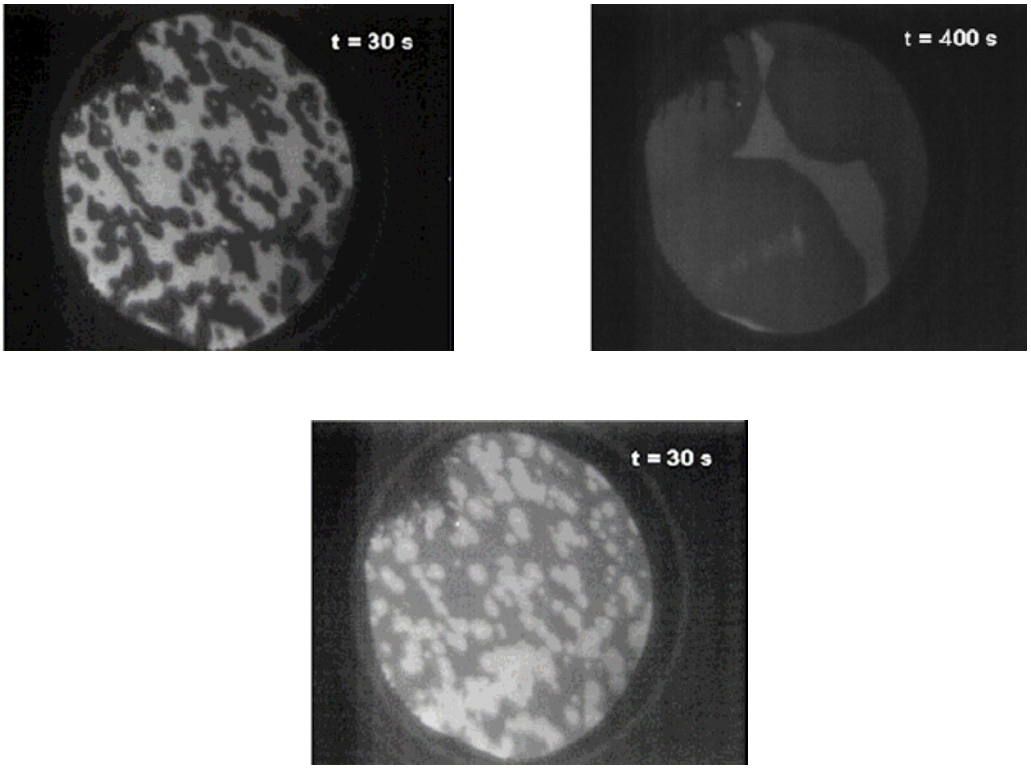

Figure 4.21 PEEM images showing the fronts-like transitions during heating up a Pt(100) crystal in a NH_3/O_2 atmosphere with pressure ratio $NH_3:O_2$ = 1:8 and $p(NH_3) = 3 \times 10^{-6}$ mbar. Heating rate is 0.5 K/s. The diameter of imaged area is 600 μm. For more detail, see [11].

While three kind of reaction front and one homogeneous transition during ammonia oxidation were observed on Pt(100) using PEEM under a certain reaction condition, which are displayed in Fig. 4.21. And these nonlinear behaviors strongly depend on the reaction condition, e.g. mixing ratio and heating rate. As shown above in Fig. 4.20, no reaction fronts have so far been observed in ammonia oxidation with oxygen on Pt(443). Accordingly, it is believed that the phase transition between 1×1 and hex structure is actually essential for the transitions via fronts observed.

4.4 Reaction Mechanism

From the above described findings of the stationary reaction kinetics and

different adsorbate coverages and how they relate to the surface reactivity and selectivity we can get numerous information concerning the reaction mechanism of ammonia oxidation over Pt under low pressure conditions.

The prominent feature of the reaction mechanism in this system is the dissociative adsorption of oxygen and NO dissociation on Pt surface. The PEEM / Kelvin probe / LEED / QMS measurement conducted here clearly indicate that the decomposition of ammonia without the presence of oxygen is quite weak reaction rate, only a small amount of N-containing species could be detected according to work function measurements via Kelvin probe on Pt(443). So the first step of this reaction is ammonia adsorption and dissociative adsorption of oxygen:

$NH_3(g) \longrightarrow NH_3(ads)$ (R1)

$O_2(g) \longrightarrow 2O(ads)$ (R2)

Then ammonia molecules could be stripped of hydrogen by oxygen adatoms to form NH_2(ads), NH(ads), N(ads), OH(ads) and H_2O(ads):

$NH_3(ads) + O(ads) \longrightarrow NH_2(ads) + OH(ads)$ (R3)

$NH_2(ads) + O(ads) \longrightarrow NH(ads) + OH(ads)$ (R4)

$NH(ads) + O(ads) \longrightarrow N(ads) + OH(ads)$ (R5)

$N(ads) + O(ads) \longrightarrow NO(ads)$ (R6)

$OH(ads) + H(ads) \longrightarrow H_2O(ads)$ (R7)

According to DFT calculation by Offerman et al., OH_{ads} also activates the dehydrogenation of all $NH_{x,ads}$ species [10]. So the following reactions cannot be rule out:

$NH_3(ads) + OH(ads) \longrightarrow NH_2(ads) + H_2O(ads)$ (R8)

$NH_2(ads) + OH(ads) \longrightarrow NH(ads) + H_2O(ads)$ (R9)

$NH(ads) + OH(ads) \longrightarrow N(ads) + H_2O(ads)$ (R10)

Bradley, Hopkinson and King performed an exhaustive molecular beam study of the reaction, the mechanism deduced suggest that there two routes for N_2 production [22, 61]:

At low temperature, below 350 K, N(ads) from (R5) and (R12) combine to form N_2(ads), then desorb as gaseous N_2 from the surface, and release the adsorption site:

$$N(ads) + N(ads) \longrightarrow N_2(g) + 2* \quad (R11)$$

At higher temperature, NO(ads) dissociates to form N(ads) and O(ads), then N(ads) combine and desorb to form N_2(g):

$$NO(ads) \longrightarrow N(ads) + O(ads) \quad (R12)$$

Actually at higher temperature, another possible route could not be ruled out, which is the secondary reaction of NH_x and NO, which also can form N_2 production:

$$NH_x(ads) + NO(ads) \longrightarrow N_2(ads) + OH_x(ads) \quad (R13)$$

All the possible route for N_2 production are accompanied by the formation of H_2O, this is consistent with our TPRS studies presented before.

For NO formation, there are one routes, as (R6) shown the combination of N(ads) and O(ads) form NO(ads).

In our experiments (10^{-6} ~ 10^{-2} mbar), no formation of gaseous N_2O was observed. N_2O production was observed when the total pressure is above 10^{-1} mbar. Two reaction routes for N_2O can be formulated [16]:

$$NO(ads) + NO(ads) \longrightarrow N_2O(ads) \quad (R14)$$

$$NO(ads) + NH_x(ads) \longrightarrow N_2O(ads) + xH(ads) \quad (R15)$$

This N_2O formation could represents the pressure gap between technical catalysis and traditional surface science.

The present results cannot discriminate between the various mechanisms. An XPS study on Pt(533) carried out by Guenther et al. showed that at temperatures below 670 K the surface is covered mainly by the N-containing intermediates NH_x(ads) (x = 0~3) whereas above this temperature chemisorbed oxygen dominates [101]. So the oxygen coverage plays a crucial role for the selectivity of this system.

According to our TPRS data for different orientations, we find that single crystal surfaces with (100) structural unit are more active, for example (533) or (100). Since NO exhibits a high dissociation activity on Pt(100), this observation indicates that

the dissociation of NO also is critical factor in ammonia oxidation.

4.5 Summary and Conclusion

In this study we investigated the elementary steps occurring during ammonia oxidation on a Pt surface. Including The steady state kinetics of ammonia oxidation have been studied over several Pt surface, Pt(100), Pt(533), Pt(443), Pt(865) and polycrystalline under low pressure (10^{-6} to 10^{-4} mbar) condition and in an intermediate pressure from 10^{-3} to 10^{-2} mbar.

During ammonia oxidation on Pt(443) a step coalescence were not observed. The reason is probably that oxygen adatoms are reacted away immediately by the hydrogen stripping of ammonia, so that the oxygen coverage remains too low to induce a restructuring of the surface.

In principle, all those results on single crystal surfaces agree that the reaction between NH_3 and O_2 leads to N_2 and H_2O formation at low temperature, but selectivity of reaction switch to NO and H_2O as dominant production at higher temperature. The temperature at which the selectivity switches depends strongly on the feed composition and the surface structure. According to our studies, the selectivity towards N_2 is relatively high on surfaces with (100) structural elements, e.g. (533) and (100). Surface with (111) structural elements have a higher selectivity towards NO, e.g. (443). Similar behavior appeared on a Pt foil which is believed to be consist mainly of (111) surface. All of these phenomena can be assigned to the high dissociative ability of NO on Pt(100).

On Pt(865), at low temperature (~550 K) no NO production occurs; and the selectivity is towards N_2 at ~ 650 K, selectivity switches to NO if oxygen is in excess. Excess ammonia inhibits the reaction to some extent, which is attributed to the blocking of adsorption sites by N-containing species.

The spatiotemporal dynamics of ammonia oxidation on Pt(100) and Pt(443) have

been studied by photoelectron emission microscopy (PEEM) in the UHV system. Reaction fronts and spatially homogeneous transition were observed on Pt(100). Since the reaction proceeds spatially homogeneously over Pt(443), these results indicate that nonlinear phenomena of reaction rate on Pt(100) could be assigned to the phase transition from active 1×1 to inactive hex phase.

Chapter 5 Structure Sensitive Reaction – Ammonia Oxidation on Pt

5.1 Introduction

The catalytic oxidation of ammonia over platinum is a key step, both in the industrial manufacturing of nitric acid and in environmental chemistry where ammonia is removed in the so-called selective catalytic reduction (SCR process) [20]. Theoretical studies as well as experimental data show that ammonia decomposition on platinum is activated through direct interaction of ammonia with chemisorbed oxygen or OH species [10, 22, 61]. Single crystal studies have been performed with Pt(100) [22, 61], Pt(111) [21, 63] and with stepped Pt(111) orientations [13, 14, 27, 38]. Already in the very early studies of Gland et al. it was concluded that the reactivity of Pt samples in catalytic ammonia oxidation is determined by the density of steps [26]. Since two elementary steps of the reaction mechanism, dissociative oxygen chemisorption [81, 91, 93, 94, 96, 102] and NO decomposition [56, 100, 103, 104] are highly structure sensitive on Pt, ammonia oxidation should be structure sensitive too.

In this chapter we compare the activity of Pt(533), Pt(443), Pt(865), Pt(100), and a Pt foil in ammonia oxidation up into the 10^{-2} mbar range. Their kinetics of the surfaces Pt(533) and Pt(443) have been studied quite in detail up to 10^{-4} mbar before [13, 14]. The Pt(865) surface or 11(111)×2(5 1 –1) [105] in microfacet notation is a kinked surface. The Pt(100) surface is exhibits an adsorbate-induced surface phase transition between a catalytically active bulk-like (1×1) termination and a quasi-hexagonal reconstruction of the topmost layer (“hex”) which is practically inert.

Catalytic processes on transition metal surfaces were divided into two classes of processes by Boudart [106]: structure insensitive and structure sensitive reaction, respectively. For structure sensitive reactions the surface structure and the restructuring induced by reaction both play important role. Catalytic reactions are known to modify the surface of a catalyst, which often associated with an activation and deactivation process. And such modification may also lead to real morphological changes. Surface restructuring was observed to occur on three different time scales: Chemisorption induces restructuring (10^{-6} sec), surface reconstruction (10^{-2}-10^{2} sec) and surface atom transport controlled restructuring (10^{2}-10^{4} sec) [64].

The structure sensitivity of ammonia oxidation contains a dynamic aspect which is that the substrate structure is modified by the reaction. This is certainly true for all catalytic reactions but the effect is particularly strong for ammonia oxidation on Pt where a visible roughening of Pt/Rh gauzes used in the Ostwald process already occurs during the first minutes of operation. Phenomenological studies with Pt spheres at high pressure [107] and single crystal investigations with Pt(533) and Pt(443) in the 10^{-5} and 10^{-4} mbar range have been conducted focusing on reaction-induced restructuring. On Pt(533) a reversible doubling of the step height occurs [12] and on Pt(443) already in pure ammonia the initially straight step edges start to meander [14]. The reversible restructuring of Pt(533) shows up in a hysteresis of the N_2 and NO production rates upon cycling the temperature. The obvious questions are which orientations exhibit restructuring orientation, and how the restructuring depends on the total pressure? Furthermore, one would like to know whether the restructuring is associated with an activation/deactivation and with selectivity changes.

The purpose of the work reported here is to determine to what extent the reaction of ammonia oxidation is structure sensitive. In addition, in this study we use hysteresis measurements and LEED to follow how reaction-induced restructuring changes as we increase the pressure from 10^{-4} mbar to 10^{-2} mbar. As will be shown

the total pressure has a drastic influence leading to quite unexpected results.

5.2 Structure Sensitivity of the Reaction Rate

In Fig. 5.1 we compare the activity of two stepped Pt (111) surfaces, Pt(533) and Pt(443), with that of a kinked surface, Pt(865), with Pt(100), and with a Pt foil. The samples were subjected to heating/cooling cycles in an NH_3/O_2 atmosphere with a 1:1 ratio of the partial pressures at a total pressure of 1×10^{-5}mbar. The same scaling of the Y-axis has been used for all samples so that the curves can be compared directly. Structural models of the single crystal orientations are displayed in Figures shown in chapter 3. The relatively small hysteresis we observe on Pt(443) and on Pt(533) can be attributed to transients caused by a heating/cooling rate of 0.5 K/s which is still too large to ensure true steady state conditions. The larger hysteresis we see on Pt(865), Pt(100), and the Pt foil are true hysteresis we assign to reversible structural changes of the Pt substrate. A broad hysteresis connected to reaction induced structural changes has also been observed with Pt(533) but only at a total pressure beyond 1×10^{-5} mbar. Therefore we do not see such a hysteresis here.

Qualitatively the rate curves of all samples are similar. N_2 formation is the dominant reaction pathway at low temperature whereas at high temperature NO production prevails. If we take the maximum in N_2 production as a measure of the catalytic activity we obtain the following sequence in catalytic activity: Pt foil : Pt(533) : Pt(865) : Pt(443) : Pt(100) = 6 : 4 : 4 : 2 : 1 . We also note that with exception of Pt(100) the N_2 rate maxima shift to lower temperature with increasing catalytic activity of the sample.

A hysteresis in the activity can arise (i) due to reversible structural changes or an activation/deactivation by oxide formation and reduction (ii) due to the inhibitory effect of adsorbates on the adsorption of reactants or (iii) through the formation and removal of surface contaminants. Realistic mathematical models of ammonia

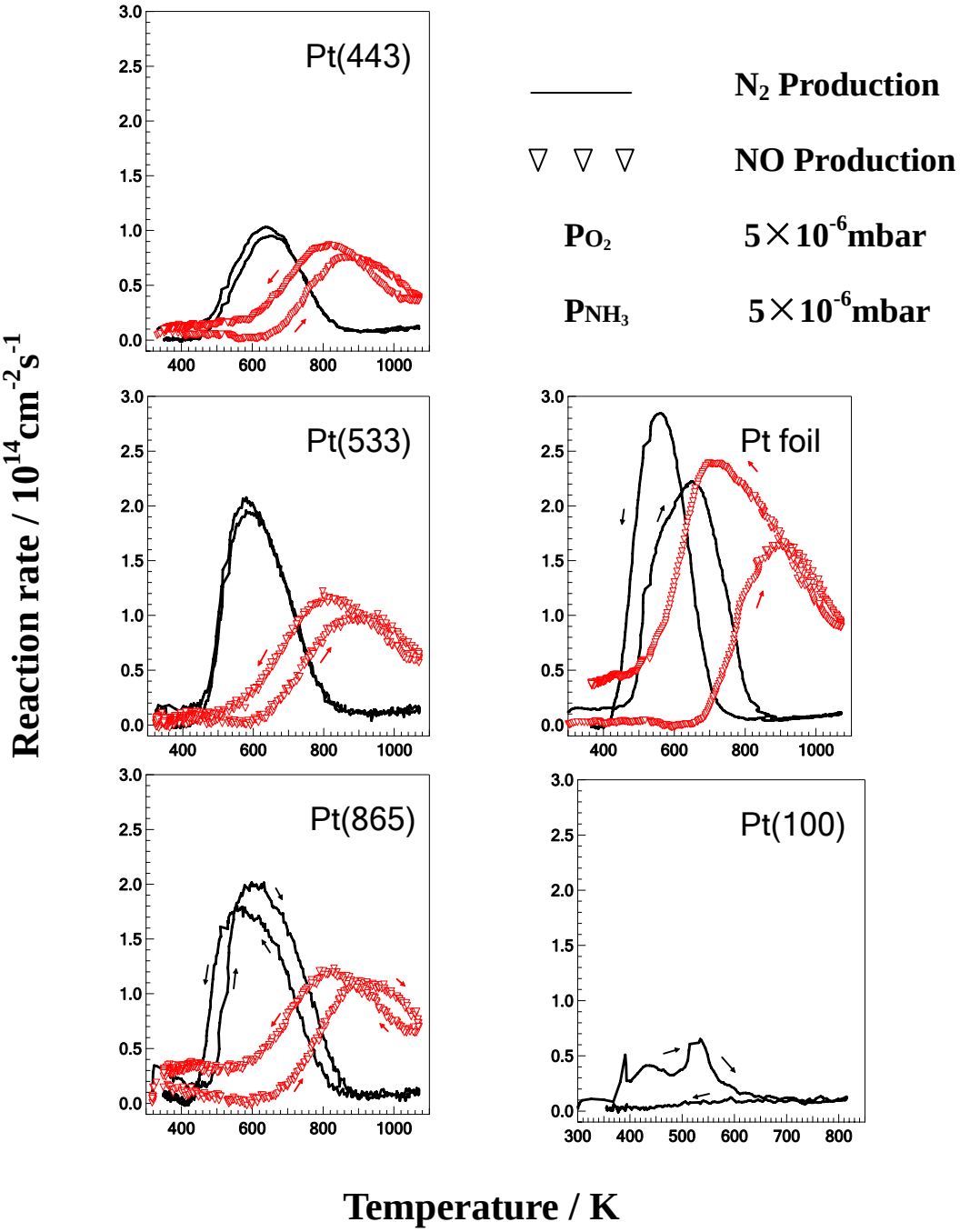

Figure 5. 1. Comparison of the catalytic activity of Pt(533), Pt(443), Pt(865), Pt(100), and a Pt foil in the 10^{-5} mbar range, and 1:1 mixing ratio of the gases. The ramping speed in T-cycling experiments was 30 K/min. Due to the relatively high ramping rate the hystereses with exception of Pt(100) are mainly caused by transients.

oxidation on Pt did not reveal any kinetic multistability which makes (ii) rather

unlikely [10]. *In situ* XPS measurements of Pt(533)/NH_3 + O_2 showed that up to 1 mbar no Pt oxide forms [101]. Reversible restructuring and a potential influence of surface contaminants remain therefore as possible causes for the hysteresis. For Pt(100) the hysteresis in the reaction rates is clearly associated with the (1×1) ⇔ hex phase transition. The low rate branch is connected with inactive hex reconstructed surface whereas the high rate branch belongs to the active (1×1) termination of the substrate.

As will be shown below LEED data taken after completion of the measurements reveal a very drastic restructuring of the Pt(865) surface. This indicates that structural changes take place in the heating/cooling cycles. For the Pt foil we have no means of detecting structural changes but since the texture of the foil contains grains with (100) and (111) orientations that have been shown to undergo restructuring, the large hysteresis we observe there should have the same origin.

For characterizing the surface *in situ* we can measure the reactive sticking coefficient of oxygen. Due to the geometric arrangement of the QMS that is shielded behind a cone, only molecules reflected from the surface can enter the cone to be detected. We obtain the reactive sticking coefficient S_{reac} following the variation of the partial pressures of the reactants, i.e. of O_2 or NH_3. Denoting the signal of a gas without reaction by I_0 and during reaction with I we calculate the reactive sticking coefficient $S_{reac} = \frac{I_0 - I}{I_0}$. In this case the reaction rate at 300 K was assumed to be negligible so that the partial pressures at 300 K should represent I_0.

The variation of the reactive sticking coefficient (S_{reac}) of oxygen during the temperature cycling experiments is reproduced in Fig. 5.2 for the Pt foil, Pt(865) and Pt(100). The variation of S_{reac} reflects in general rather well the behavior of the reaction rates during the T-cycling experiments displayed in Fig. 1. For Pt(100), for example, the low reactivity of the cooling branch is due to the low oxygen sticking coefficient on the hex phase which according to the literature is as low 10^{-3} for a

structurally nearly perfect hex phase. During heating up S_{reac} does not reach the value S_{oxygen} = 0.2 reported for oxygen adsorption on Pt(100)-(1×1) [22]but only goes up to 0.03. The discrepancy might indicate that the hex phase has not been lifted completely during cooling down so that a significant portion of the surface remains in the inactive hex state all the time.

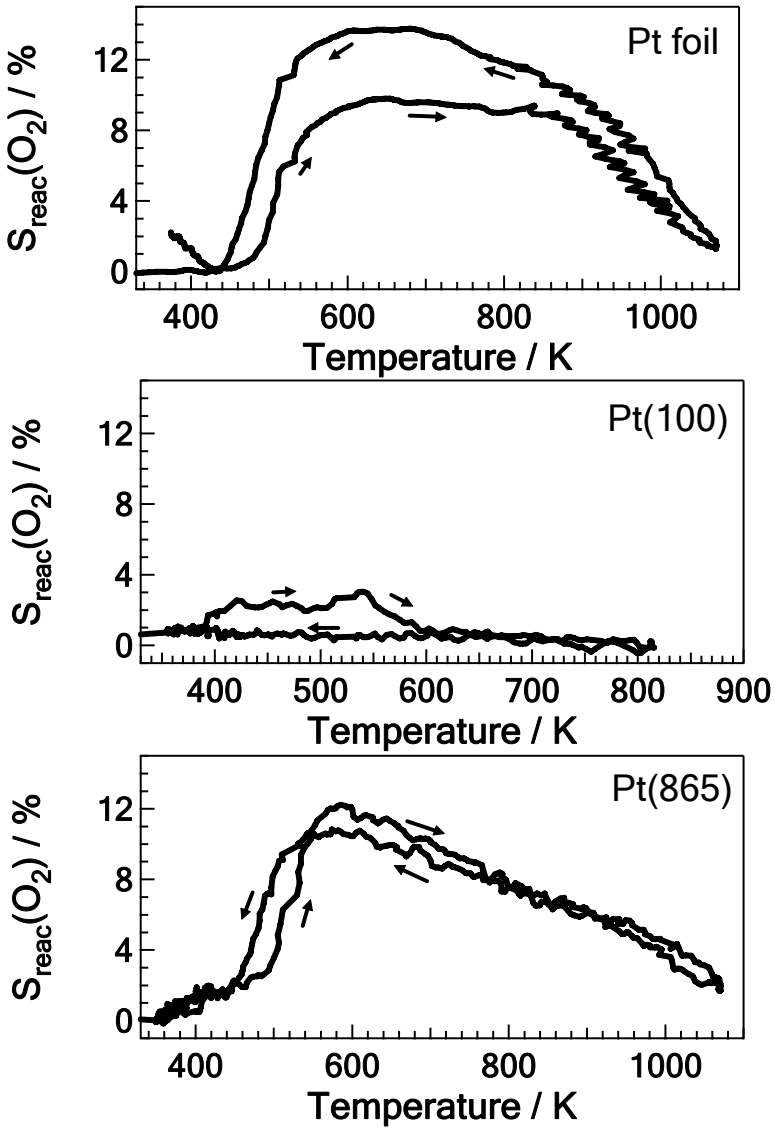

Figure 5.2. Variation of oxygen reactive sticking coefficient (S_{reac}) during temperature cycling experiment on Pt foil, Pt(865) and Pt(100). The total pressure is in the 10^{-5} mbar range, and a 1:1 mixing ratio of the feed composition is used. The ramping speed in the T-cycling experiments was 30 K/min.

In contrast to Pt(100) on the Pt foil the activity is increased by heating up as

evidenced by higher rate maxima for N_2 and NO and a higher S_{reac} in Fig. 5.1 and 5.2, respectively. Remarkably, between roughly 600 and 800 K the selectivity changes drastically from preferential N_2 formation on heating up to NO as main product during cooling down. The increase in the overall activity after heating is reflected by the increase in S_{reac} in Fig. 5.2. The comparison of the Pt foil with Pt(865) shows that on these two samples S_{reac} reaches about 0.14 and 0.12 respectively.

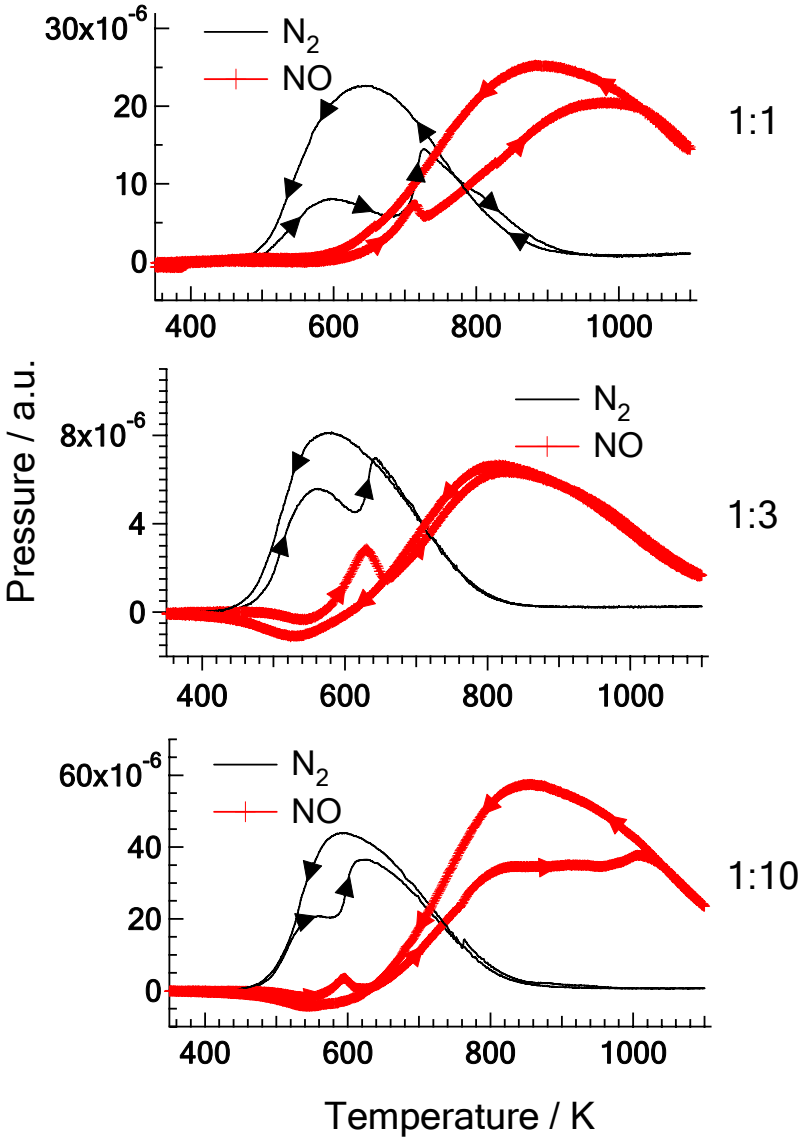

Figure 5.3. Temperature cycling during ammonia oxidation on Pt(533) with different mixing ratio, $p(NH_3)/p(O_2)$. The ramping speed is 10 K/min. The total pressure is around 10^{-4} mbar.

Even for the same orientation the structure sensitivity of the reaction may show

up differently due to a different amount of restructuring under different reaction condition. We investigated the influence of the feed composition on kinetics of N_2 and NO production in the 10^{-5} mbar range. Fig. 5.3 display the results for Pt(533) obtained for 1:1, 1:3 and 1:10 ratio NH_3/O_2 of the reactants and with identical ramping speed. It was demonstrated that the doubling of the step height under reaction conditions is associated with a change in the selectivity from N_2 towards NO formation [12]. We also find that the small dip of NO reaction rate around 600 – 700 K which represents the formation of double steps shifts to lower temperature with increasing oxygen partial pressure. The temperature is about 700 K when the feed composition (NH_3/O_2) is of 1:1, and when this ratio is 1:3 or 1:10, the temperature shifts to 630 K or 590 K, respectively.

Since the availability of oxygen controls the selectivity towards NO an increase in the oxygen sticking coefficient could explain the observed change in selectivity. With oxygen being in excess, anyhow, there is no need to restructure the surface in order to increase the oxygen sticking coefficient. So it is plausible that the hysteresis become weaker with increasing ratio O_2/NH_3. For comparison, the data in Fig. 5.4a show that upon heating S_{reac} increases sharply at 700 K which is roughly the temperature where we expect the doubling of the step height to occur. S_{reac} however also remains high during the cooling branch, but as shown in earlier LEED measurements, during cooling down the steps of the catalyst surface remain single-atomic [12]. This demonstrates that besides the step structure also the adsorbate coverages determine S_{reac} through their blocking effect for adsorption. In addition, also local structural changes that are not detectable in LEED pattern might play a role. Measurements of S_{reac} with different rations NH_3:O_2 show that the hysteresis becomes smaller the more oxygen is in excess. For a 10-fold excess of O_2 the hysteresis practically vanishes.

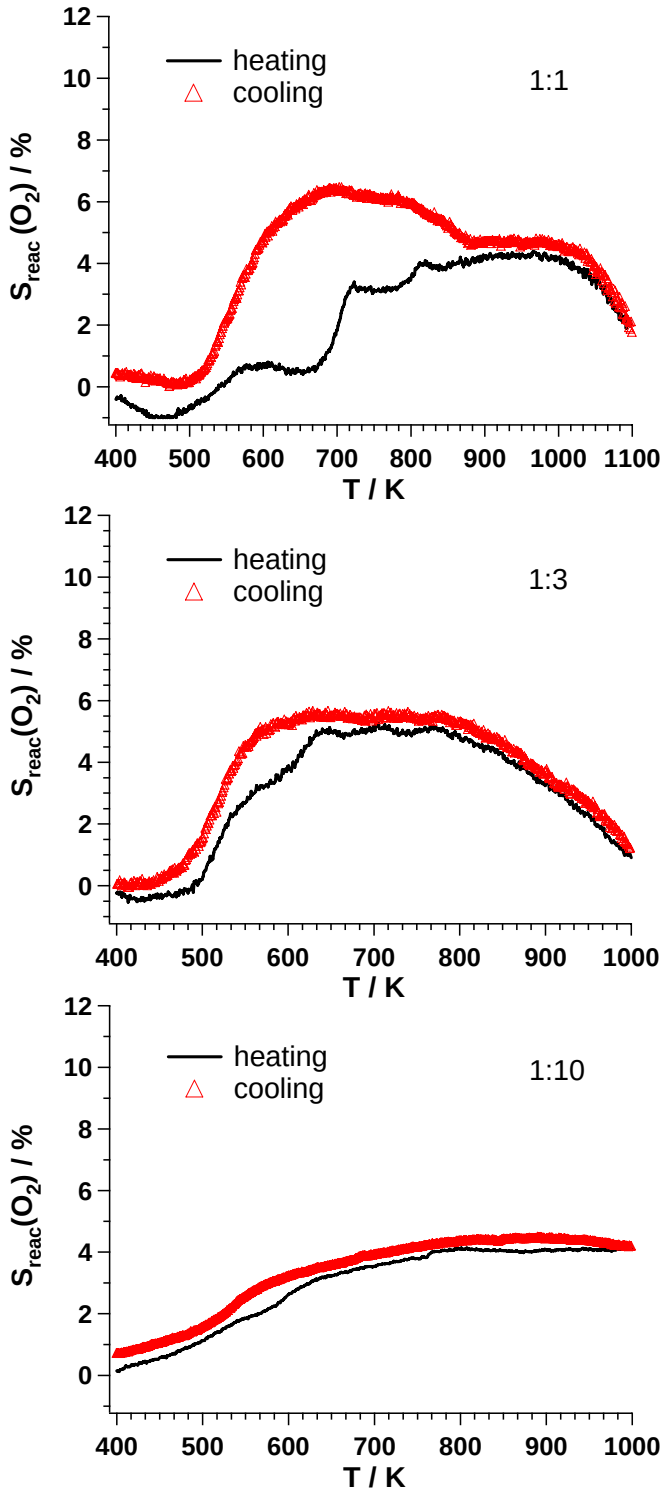

Figure 5.4. Reactive sticking coefficient of oxygen during ammonia oxidation on Pt(533) under different feed composition, from 1:1 to 1:10 (NH_3:O_2). The ramping speed is 10 K/min. The total pressure is at around 10^{-4} mbar.

5.3 Influence of Total Pressure

We studied the influence of the total pressure on the kinetics of N_2 and NO production in the 10^{-5}-10^{-2} mbar range. Figures 5.5 and 5.6 display the results for Pt(533) and Pt(443) obtained for a 1:1 ratio NH_3/O_2 of the reactants with identical ramping speed. In all experiments we started with a freshly prepared surface after Ar-ion sputtering, oxygen treatment and annealing to 1100K. Experiments with a pressure above 10^{-3} mbar were carried out in the high-pressure chamber, and with a pressure below 10^{-3} mbar in the main chamber.

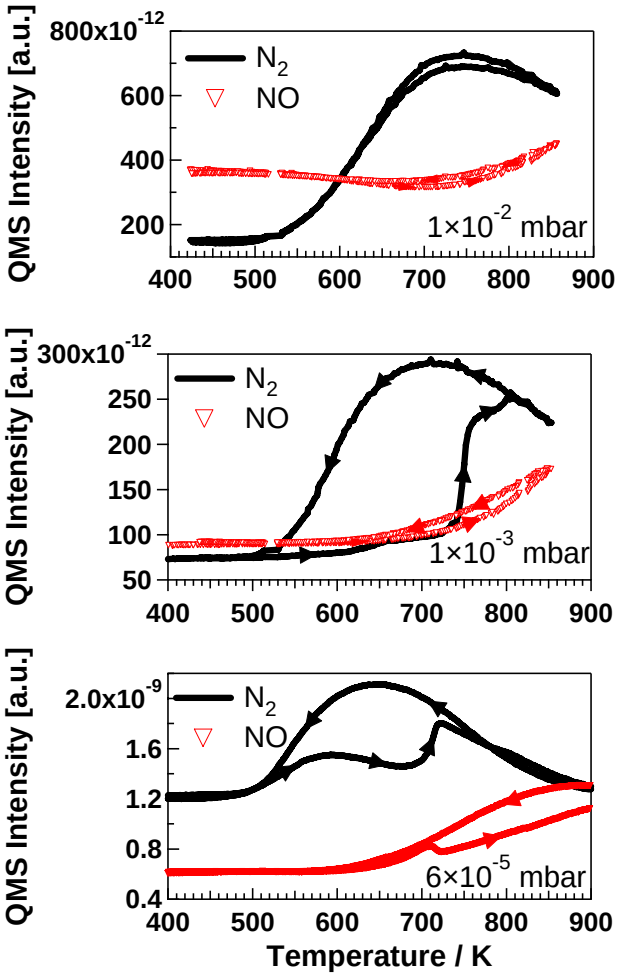

Figure 5.5. Effect of the total pressure on the kinetics of N_2 and NO production on Pt(533) in the 10^{-5}-10^{-2} mbar range under a feed composition 1:1 and a ramping speed is 0.5 K/s.

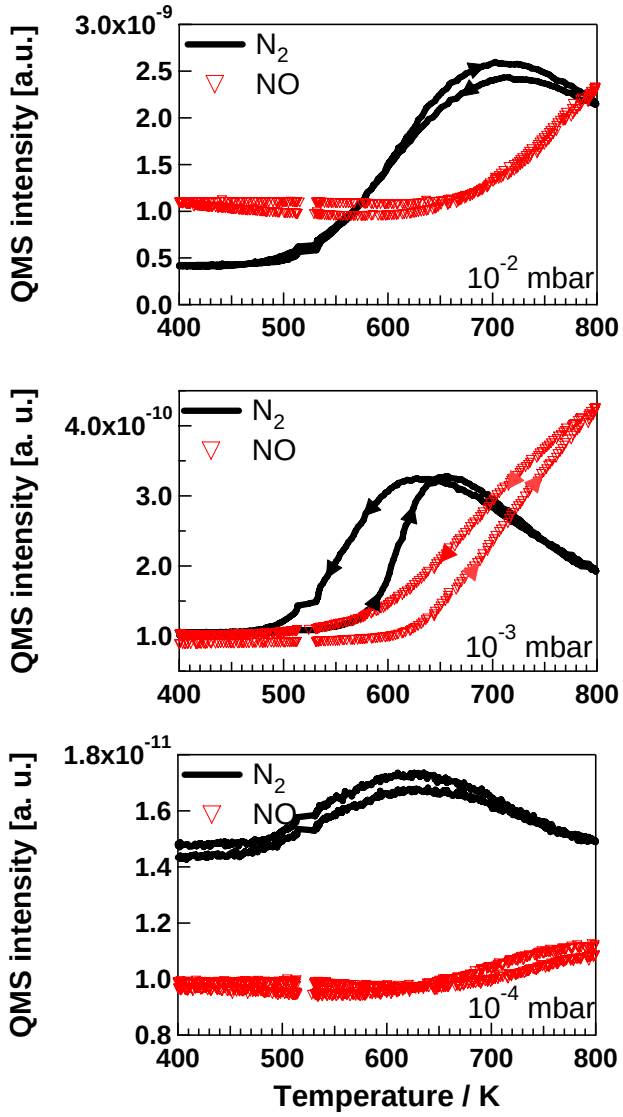

Figure 5.6. Effect of the total pressure on the kinetics of N_2 and NO production on Pt(443) in the 10^{-5}-10^{-2} mbar range under a feed composition 1:1 and a ramping speed is 30 K/min.

On Pt(443) practically no hysteresis is seen at 10^{-5} mbar and at 10^{-4} mbar but increasing the total pressure to 1×10^{-3} mbar causes the appearance of a substantial hysteresis as evidenced by Fig. 5.6. After a further rise to 1×10^{-2} mbar the hysteresis vanishes again similar to the behavior of Pt(533). The hysteresis of Pt(533) and Pt(433) are all counterclockwise, i. e. heating up leads to an activation of the

catalyst.

The preceding measurements show an unexpected result: a non-monotonic variation of the hysteretic behavior with pressure for both orientations, Pt(533) and Pt(443). At low pressure ($p < 10^{-5}$ mbar) no hysteresis occurs, at intermediate pressure a very pronounced hysteresis is observed and at high pressure (10^{-2} mbar) the hysteresis vanishes again. The two orientations Pt(533) and Pt(443) differ in so far as on Pt(443) the low p-range without hysteresis extends into the 10^{-4} mbar range whereas on Pt(533) this range ends at roughly 1×10^{-5} mbar.

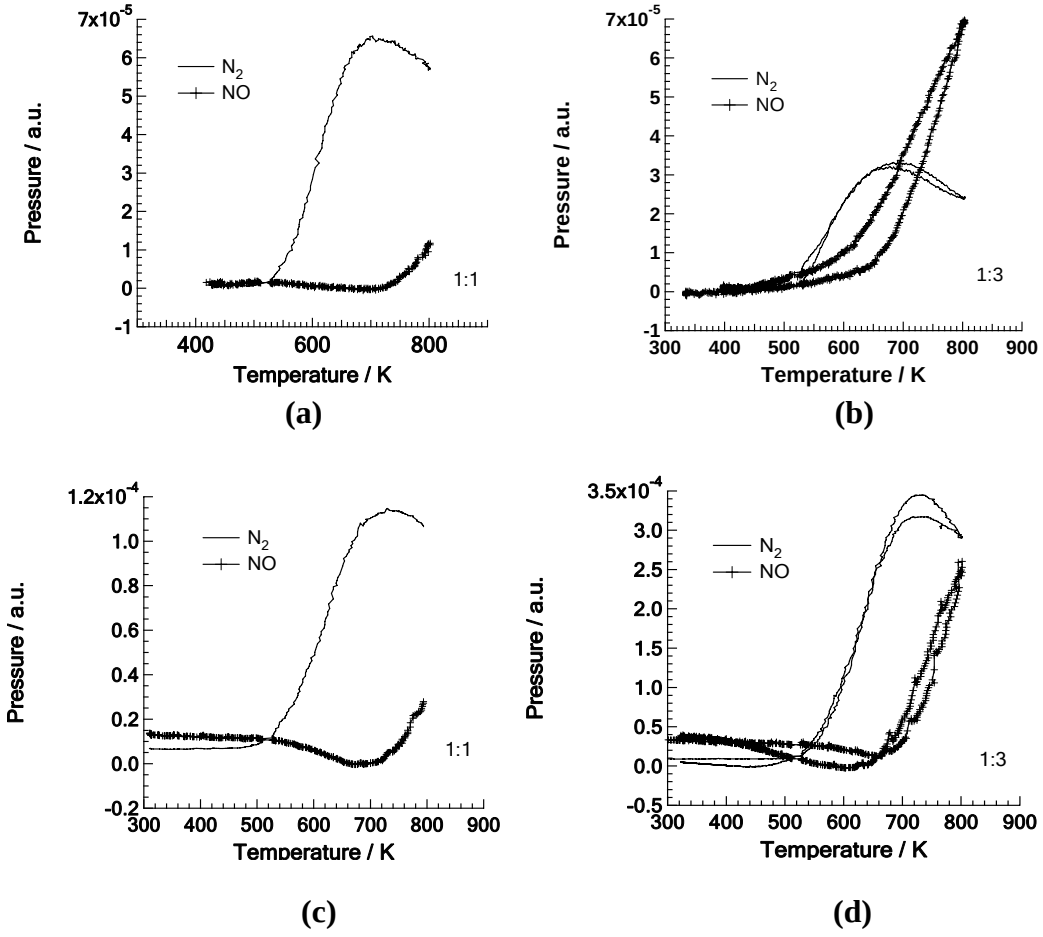

Figure 5.7. TPR spectra of ammonia oxidation over Pt(865) are displayed. These studies were carried out in the intermediate pressure range. Panel (a) and (b) were carried out at 10^{-3} mbar; panel (c) and (d) at 10^{-2} mbar. And the mixing ratios of $p(NH_3)/p(O_2)$ are 1:1 and 1:3 respectively. The ramping speed is 30 K/min.

In Fig. 5.7 TPR spectra of ammonia oxidation over Pt(865) are displayed. These studies were carried out in the intermediate pressure, at from 10^{-3} to 10^{-2} mbar range at mixing ratios of $p(NH_3)/p(O_2)$ of 1:1 and 1:3, respectively. At 10^{-3} mbar range with increasing oxygen partial pressure the peak of N_2 formation shifts to lower temperature from 700 K to 670 K, and the formation rate of NO increases drastically in the temperature range we studied. The NO rate at 1:3 is almost sevenfold increased compared to the rate under a feed composition of 1:1. At 10^{-2} mbar the formation rate of N_2 and NO both increase with rising oxygen pressure, in particular, for NO production, the increase is around 10 fold. This result indicates that oxygen coverage on Pt(865) plays an important role in the formation of NO. This observation is consistent with the performance of Pt catalysts in UHV system and with the behaviour of industrial Pt catalysts. After comparison with different total pressure under the same mixing ratio we find that the temperature for the maximum rate of N_2 shifts to higher temperature with increasing total pressure. Basically no hysteresis appeared in all these temperature cycling processes.

For comparison, we also performed similar TPR experiments with Pt(100) at the intermediate pressure range from 10^{-3} to 10^{-2} mbar. To some extent quite different pressure effects on the reaction rate and selectivity of ammonia oxidation were observed on Pt(100). Fig. 5.8 shows the TPR spectrum of ammonia oxidation on Pt(100) with different mixing ratios under two different total pressure ranges. The observations on Pt(100) are largely different from the results on Pt(865). Pronounced hysteresis could be observed due to the well-known phase transition between the hex (quasi-hexagonal reconstruction) and the bulk like (1×1) structure. Figures 5.8a and 5.8b show the variation of the products (N_2 and NO) as a function of temperature. With increasing oxygen partial pressure, the surface becomes more active; the onset of the formation of both products, N_2 and NO, shifts to low temperature. The formation rate of N_2 increased by a factor of around 5 with rising oxygen pressure; the yielding of NO is much higher than the previous studied at low pressure in the

UHV system. Since the oxygen coverage controls the selectivity in the ammonia oxidation, we can safely postulate that oxygen adsorption was strongly dependent both on the effective pressure of oxygen at the surface and on the temperature of the Pt sample. In our previous studies on Pt(100) at 10^{-5} mbar, only a small quantity of NO product was observed, which was attributed to the hexagonal structure with a low oxygen sticking coefficient.

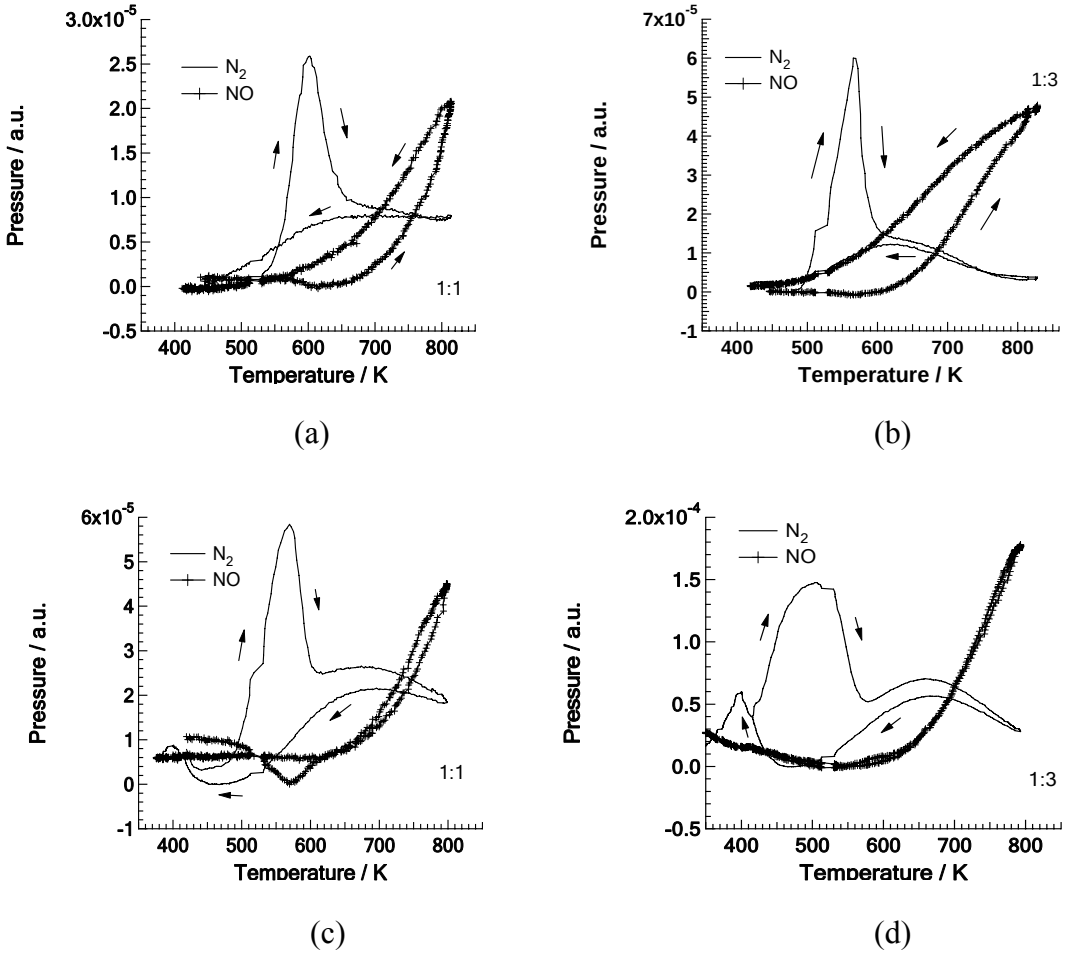

Figure 5.8. TPR spectra of ammonia oxidation over Pt(100) are displayed. These studies were carried out in the intermediate pressure: Panel (a) and (b) were carried out at 10^{-3} mbar; panel (c) and (d) at 10^{-2} mbar. The mixing ratios of $p(NH_3)/p(O_2)$ are 1:1 and 1:3 respectively. The ramping speed is 30 K/min.

Figures 5.8c and 5.8d show the TPR spectrum for Pt(100) in 10^{-2} mbar range. As far as these temperature cycling experiments are concerned, we did six consecutive heating/cooling ramps. So irreversible changes of the surface by oxidation, for

example, can be ruled out. Three peaks of the formation of N_2 can be observed, at 400 K, 560~500 K and 650 ~ 690 K, respectively, the temperatures depend on the mixing ratio. The peak of N_2 at 400 K we ascribe to the combination of N_{ad} which originates from NH_3 stripped of hydrogen. No temperature shift appears with increasing oxygen partial pressure. The other two peaks can only tentatively attribute two possible causes: (ⅰ) the 1×1 to hex phase transition, and (ⅱ) the different adsorption sites of oxygen on Pt(100), in particular, the existence of a high coverage β_1-state. Since the surface density of Pt atoms differ in the 1×1 and in the hex phase. The phase transition involves the mass transport of about 20% of the surface Pt atoms [108]. This mass transport necessarily creates structural defects and since these defects presumably have a high catalytic activity, the peak at around 400 K could be due to the hex to 1×1 phase transition. Oxygen adsorption on Pt(100) was studied by Barteau et al. using LEED and thermal desorption spectroscopy. The TD spectrum for oxygen showed two peaks, referred to as β_1 and β_2 (low and high temperature, respectively). The β_1 peak which is associated with the highest coverages desorbed with so-called autocatalytic kinetics, in that the rate accelerated with decreasing β_1 coverage till the depletion of this kind of coverage. The β_2 state was found to desorb with first-order kinetics [89]. Accordingly, it should be possible to achieve a high oxygen coverage in our experiment where we operate in the intermediate pressure range at 10^{-2} mbar. Therefore, we can speculate that with the increase of total pressure it is the change of oxygen coverage that resulted in the variation of the product formation profile.

Due to the heating limitation in the high-pressure cell, only the maximum in the rate of N_2 could be observed, but not in NO. Figure 5.9 display the variation of maximum rate of N_2 as a function of total pressure over different orientation surfaces, including Pt(533), (443) and (865), with a mixing ratio of ammonia and oxygen of 1:1. The reaction rates of N_2 production over Pt(533) and Pt(865) are close to each other in the investigated pressure range. Compared to Pt(533) the rate of N_2

formation on Pt(443) is weaker, a fact attributed to the step density and the orientation of the step, since they have the same (111) terraces. Actually Pt(865) and Pt(443) have similar step density, but the difference lies in the kink which only exists on Pt(865). The low coordinated kink site could represent a very active site. We also found that when the total pressure is around 10^{-2} mbar, the difference in the reaction rates of the three surfaces tends to decrease. A straightforward explanation would be that with increasing total pressure, mass transportation limitations of the reactants start to play a role. But at 10^{-2} mbar mass transport through the gas phase should still be fast enough. And the other possibility is that surface restructuring eliminates the differences in reactivity between the various orientations. Serious restructuring was observed on both Pt(533) and Pt(865), while Pt(443) is relatively stable compared to the other two surfaces.

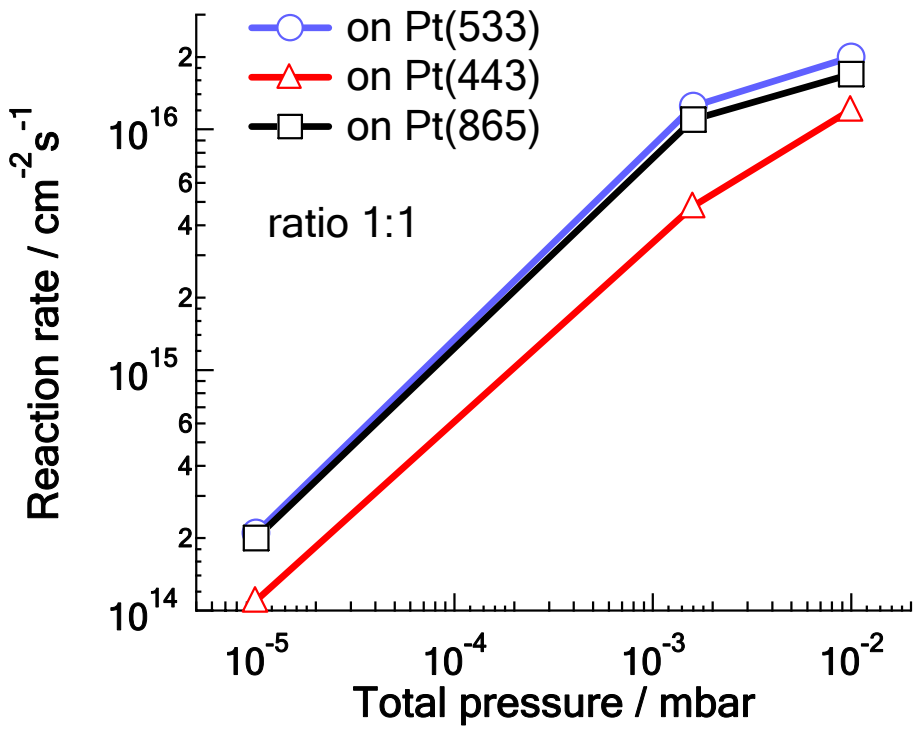

Figure 5.9. Variation of maximum rate of N_2 production as a function of total pressure over different Pt orientations, including Pt(533), (443) and (865), the same reaction conditions are applied, and the mixing ratio of ammonia and oxygen is 1:1.

It was rather unexpected phenomena that the degree of order on the restructured surfaces of Pt(533) and Pt(443) depends in a non-monotonous way on the total pressure. We performed a series of experiments on Pt(533) in order to rule out the effect of contamination on the surface which could be introduced by the reactant gases. First ammonia oxidation was carried out at 10^{-2} mbar, consecutively the total pressure was switched to 10^{-3} mbar, and then the reaction was performed on the same sample. These results are displayed in Fig. 5.10. Figure 5.10a show the profile of reaction rate on N_2 and NO at 10^{-2} mbar range, and (b) show the results at 10^{-3} mbar acquired using the same sample right after the experiments in Fig. 5.10a. We find that a hysteresis still appears only at 10^{-3} mbar. One possibility to explain the non-monotonous variation of hysteresis behavior is by postulating that different restructuring processes under different reaction conditions, e.g. different total pressure. Even though the results were reproducible, an experimental artifact cannot be entirely ruled out. However we are unware of any experimental problems that would produce this effect.

With increasing total pressure in general the risk of a surface contamination rises for two reasons. The partial pressure of contaminants in the gas phase rises and the higher chemical potential of the reactants enhances the segregation of bulk contaminants to the surface. One might suspect that contamination effects are responsible for the pressure dependent vanishing of the hysteresis but so far Auger electron spectroscopy provided no indication of surface contaminants. Moreover, the segregation of Si that leads to SiO_2 formation would cause an irreversible reduction of catalytic activity, which is not what we see. On the other hand, since we cannot completely rule out a potential influence of contaminants, this possibility should still be taken into account.

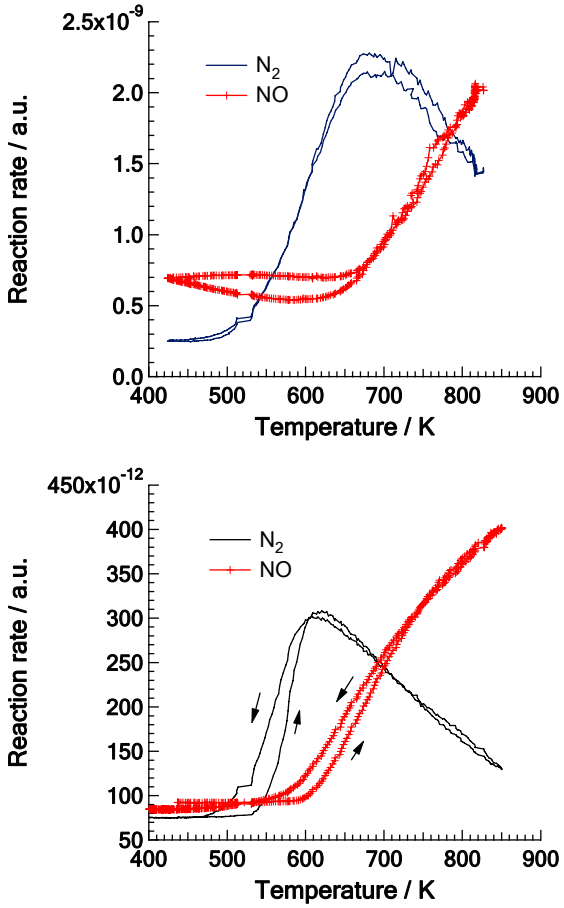

Figure 5.10. Panel (a) shows the profile of reaction rate on N_2 and NO on Pt(533) at 10^{-2} mbar, and (b) shows the results acquired using the same sample right after the experiments in panel (a). The feed composition is 1:1, and the ramping speed is 30 K/min.

5.4 Stability of surface structure

In a dynamical model of a catalytic surface, the surface atoms are constantly changing their equilibrium positions in response to the changing chemical environment. Changing the crystallographic arrangement of the substrate atoms does induce a significant modification of the adsorbate bonding which may in return affect the chemical reactivity [65]. The non-rigid surface undergoes rapid adsorbate -induced restructuring on the time scale of chemisorption, or slower restructuring on

the time scale of catalytic surface reactions. The latter involves diffusion-controlled faceting, or solid-state reactions. In ammonia oxidation substantial efforts were undertaken by Schmidt et al. to systematize the morphological changes but no microscopic understanding of the restructuring has been obtained and the driving force as well as the connection to activity and selectivity changes remains unknown [109, 110]. Especially at high temperature and high pressure reaction conditions drastic restructuring happens. The morphological changes of the Pt catalyst in the Ostwald process have been ascribed to the formation of a volatile Pt oxide, PtO or PtO_2, which results in loss of Pt gauze [109, 111, 112]. Here we studied the surface modification in adsorption experiments and restructuring under mild reaction conditions using LEED and SEM, respectively.

5.4.1 Adsorption on Pt(443)

We studied the adsorption of ammonia and oxygen over Pt(443), and investigated the variation of terrace width distribution in different environments. In the presence of ammonia, Pt(443) was stable, there is really no change in the terrace width was detectable on the basis of the splitting point of LEED beams. Scheibe et al, however, observed via STM that step meandering took place in the presence of ammonia at room temperature [12, 14]. Apparently these change of microstructure do not affect the distribution of terrace width as a whole. This result is in contrast to the observation of step coalescence during oxygen adsorption on Pt(443).

Using LEED we also studied the variation of step height in the presence of a single reactant over Pt(443). For Pt(443) the (111) layer spacing could be calculated from the lattice constants, resulting in a value of ~ 0.226 nm (monoatomic step height). The step height is determined by the method described in previous chapter. Table 5.1 shows the numerical values of voltages where the split spots coalescence into single bright spot of the (0,0) beam. As shown in the table the mean value of the

step height and its standard deviation were calculated. From these successive values of the energies we obtain the step height. The step height of a surface with step coalescence induced by oxygen adsorption is exactly the same as that of a clean Pt(443) surface. In particular, no doubling of step height was observed.

s in Equ. 2.10	Clean Pt(443) Surface		Over oxygen Covered Pt(443) Surface	
	Beam energy (eV)	d (nm)	Beam energy (eV)	d (nm)
2	37.8	0.1992	37.7	0.1995
3	73.2	0.2147	66.8	0.2247
4	116.4	0.2270	116	0.2274
5	177.2	0.2300	177	0.2301
6	220.3	0.2475	217	0.2494
Mean value of d (nm)	0.2237 ± 0.007		0.2262 ± 0.007	

Table 5.1. Step height analysis before and after oxygen adsorption on Pt(443) at 700 K. Given are the voltages where a single bright spot of the (0,0) beam appears.

s in Equ. 2.10	Pt(443) heated up and cooled down in ammonia at p= 2×10^{-6} mbar					
	Before heating		800 K		After cooling to 300 K	
	energy (eV)	d	energy (eV)	d	energy (eV)	d
2	31.3	0.2189	37.7	0.1994	32.6	0.2145
3	79.4	0.2061	74.4	0.2130	79.3	0.2063
4	128.8	0.2158	112.4	0.2310	130.1	0.2148
5	178	0.2295	170.7	0.2343	177	0.2301
Mean value of d (nm)	0.2176±0.004		0.2194±0.007		0.2164±0.004	

Table 5.2 Step height analysis of Pt(443) under different conditions, ammonia adsorption at room temperature, at 800 K in ammonia, and after temperature cycling, $p(NH_3) = 2 \times 10^{-6}$ mbar. Given are the voltages where a single bright spot of the (0,0) beam appears.

We also studied the effect of ammonia on the step height of Pt(443). In table 5.2 the step height analysis is shown for Pt(443) before and after temperature cycling in a NH_3 environment, including heating to 800 K. No evidence indicates a variation of step height. And no faceting phenomena could be found under all condition we investigated here. All results show that the terrace width distribution of Pt(443) is relatively stable in ammonia, no change of terrace width and step height could be observed.

5.4.2 Under Reaction Condition

5.4.2.1 LEED Studies

With LEED the surface structure of Pt(533), Pt(443), and Pt(865) was examined after exposure to reaction conditions. The beam profiles of the split (0,0)-beam after the hysteresis measurements in the 10^{-2} mbar range are displayed in Fig. 5.11. These spot profiles were plotted along spot the direction of splitting. The X-scale is in units of the reciprocal lattice in spot splitting direction. On all three surfaces the beam intensity strongly decreased in comparison to the initial value. On Pt(865) the ordering after the reaction was so poor that the LEED spots were hardly discernible from the background. The splitting of the spot is no longer visible and instead a very small peak appears at the middle position of the original spot splitting. On Pt(533) we observe a widening of the spot splitting by roughly 20%. On Pt(443) the spot splitting remained unchanged but the FWHM of the spots increased and the maximum intensity dropped by 50%, which means a surface disordered to some extent compared to a freshly prepared surface. Apparently the average terrace width on Pt(443) has not been changed by the reaction in contrast to Pt(533) where the average terrace width decreased. This indicates that Pt(443) is more stable than Pt(533), the stability of Pt(865) is the lowest of these three orientation. The different

surface energy and the different activity of three crystal planes result in a different extent of restructuring, i.e. a different stability during reaction conditions [113].

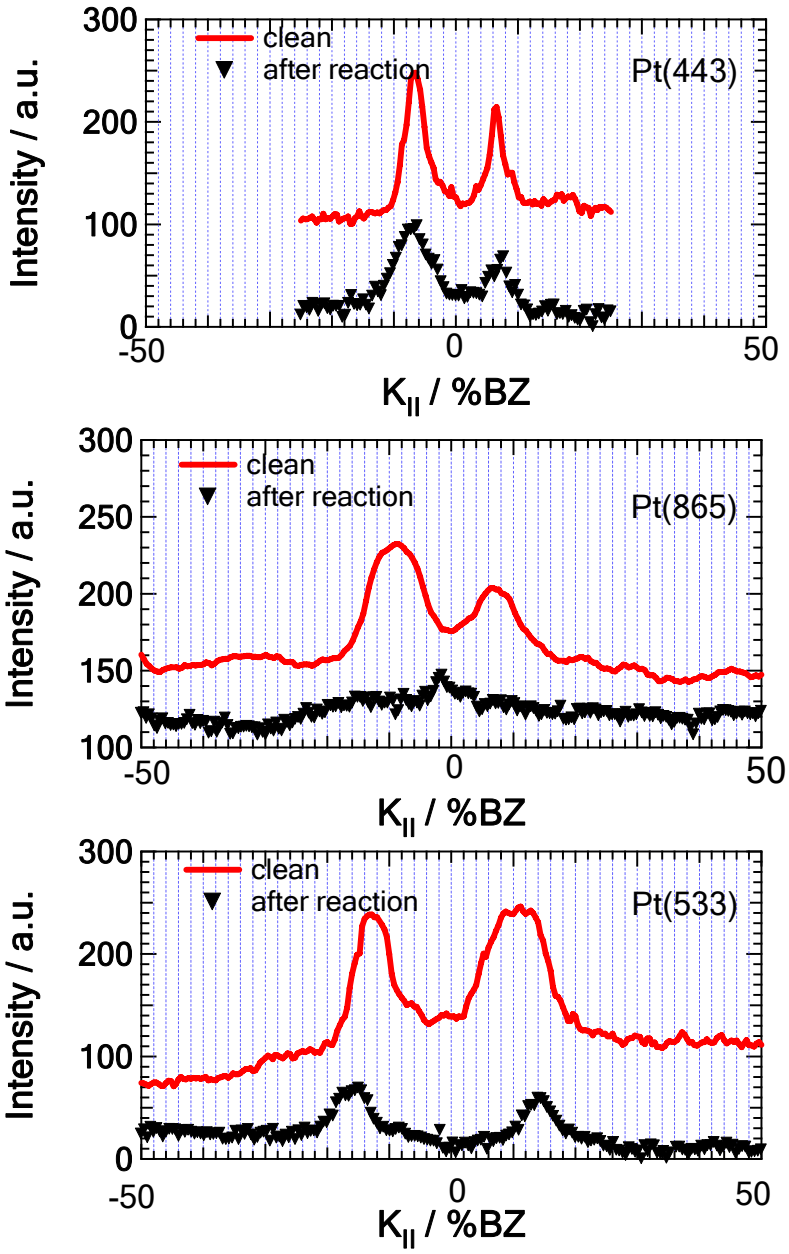

Figure 5.11. LEED spot profile analysis showing reaction-induced restructuring in the 10^{-2} mbar range. The beam profile of the (0,0)-beam was taken between the (0,-1/2) and (0,1/2) beams which is the direction of spot split. The sample was exposed to NH_3/O_2 at 10^{-2} mbar during temperature cycling from 300 to 800 K for 150 min.

5.4.2.2 SEM Studies

The data shown in Fig. 5.11 and table 5.3 indicate that kinked surfaces have a low structural stability under reaction conditions followed by stepped surfaces. The Pt(100) surface exhibits the highest stability under reaction conditions. This is consistent with the results of Schmidt et al. who studied small single crystal spheres of Pt in a NH_3/O_2 atmosphere and found that after exposure to reaction conditions only the (111) and (100) orientations survive [107].

(a) **(b)**

Figure 5.12. SEM micrographs of the clean Pt(865) surface in panel (a), the sample after exposure to reaction conditions in panel (b), the temperature cycling reaction from 300 K to 800 K was carried out at 10^{-2} mbar range for 5 h. The size of the imaged area is 240 × 180 μm^2.

Under relatively mild reaction condition of an UHV experiment the microscopic structural changes are not associated with variations in the macroscopic surface topography. Mass transportation on the catalyst surface is not visible on a macroscopic scale. Faceting and the growth of smaller crystals from the surface were not observed by SEM [25]. Here the surface morphology of Pt(865) was studied by SEM after temperature cycling experiments of ammonia oxidation in the high pressure cell. The total pressure is 2×10^{-2} mbar. After reaction the sample was transferred to the UHV system equipped with LEED, we found drastic restructuring

as evidence from a disordered structure. The SEM micrographs of clean Pt(865) (Fig. 5.12a)and the sample after reaction (Fig. 5.12b) are presented. Occasionally some melting dots could be observed, which can't be restored only by cleaning cycle (sputtering and annealing sample), as shown in Fig. 5.12a. Initially, these dots were ascribed to the manufacturing procedure of the crystal. And the remainder of the surface is quite even. Whereas, except those melting dots we also found the formation of some shallow ditches, as shown in Fig. 5.12b. Those ditches indicate that a significant mass transport on the surface is involved in the reaction process. This mass transport can be restored by a number of cleaning cycles. Element analysis of post-reaction sample surface was carried out by SEM which is equipped with energy dispersive detectors (EDX). Only Pt element could be observed in the whole area we investigated, as shown in Fig. 5.13. Since the depth of the detection is several μm (whereas the escape depth of second electron is just in the nm range), so we can safely conclude that no significant amount of oxygen can penetrate into the bulk during ammonia oxidation, even in the intermediate pressure range (10^{-2} mbar).

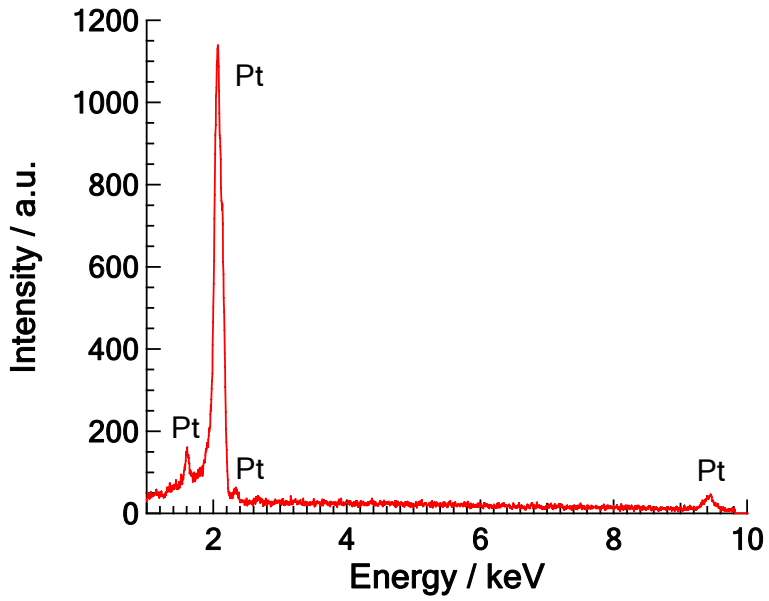

Figure 5.13. Elemental analysis on the whole area we observed, the probed area is about 240 × 180 μm^2 using energy dispersive detectors (EDX) in a SEM instrument. Only Pt element could be observed.

5.5 Overview of Hysteresis and LEED Pattern Change after Reaction

Table 5.3 displays an overview of hysteresis and restructuring of different Pt orientations surface under different reaction conditions. Previous LEED and STM investigations of Pt(533)/NH_3 + O_2 conducted in the 10^{-5} and 10^{-4} mbar range have shown that the rate hysteresis is connected with reversible structural changes, i. e. a reversible doubling of the step height [12]. In the pressure range investigated here no *in situ* methods were available to monitor structural changes during the rate hysteresis. The fact that according to Table 5.3 at 10^{-3} mbar large hysteresis on Pt(533) and Pt(443) are connected with a disordered surface seems not to be consistent with the previous statement. However, the LEED data in Table 5.3 only show the state of the surface after completion of the experiment. This leaves the possibility that during the T-cycles an ordered surface may exist in a certain parameter range. A second point is that the absence of long range order does not exclude that some short range order still exists and that certain local configurations of Pt atoms might be associated with different reactivities.

One rather unexpected phenomenon was the non-monotonic variation of the hysteretic behavior and surface ordering with total pressure we observe with Pt(533) and Pt(443) (Table 5.3). In principle, one could envision a surface which is roughened by the reaction at some intermediate pressure, but which orders again as the dynamics of the reaction beyond a certain threshold become large enough to overcome certain kinetic barriers preventing ordering. At the present stage, this is pure speculation and experiments extending beyond 10^{-2} mbar are required in order to substantiate this.

Pressure range	Pt(533)		Pt(443)		Pt(865)		Pt(100)	
	Hysteresis in reaction rate	**Surface ordering / LEED**	**Hysteresis in reaction rate**	**Surface ordering / LEED**	**Hysteresis in reaction rate**	**Surface ordering / LEED**	**Hysteresis in reaction rate**	**Surface ordering / LEED**
10^{-4} mbar	yes	Ordered (1×1)	no	Ordered (1×1)	yes	Ordered (1×1)	yes	Ordered (1×1)
10^{-3} mbar	yes	disordered	yes	disordered	no	disordered	yes	Ordered (1×1)
10^{-2} mbar	no	Ordered (1×1)	no	Ordered (1×1)	no	*	yes	Ordered (1×1)

Table 5.3. Overview of hysteresis and restructuring of different Pt orientations surface under different reaction conditions. * indicate that split spot turns into a diffuse broad single spot with low intensity.

5.6 Summary and Conclusion

Ammonia oxidations over different Pt surfaces, from single crystals to polycrystalline Pt, have been studied in the 10^{-5} to 10^{-2} mbar range. The main result is that surface structure has a strong effect on the reaction rate and selectivity. In addition, the reaction rate changes are associated with structural modifications of the surface induced by the reaction. Rough surfaces have higher reaction rate, the reactive sticking coefficient of oxygen over a Pt foil reaches 0.14. Compared with other single crystal surfaces, the reaction rate over Pt foil is the highest, then the activity decreased in the order Pt(865), Pt(533), Pt(443), and Pt(100).

On Pt(443) no LEED detectable substrate changes and no rate hysteresis occurred below 10^{-3} mbar. But above 10^{-3} mbar a substantial hysteresis effect were seen. The restructuring which tends to increase with rising total pressure was found to depend in a non-monotonic way on the total pressure. So on both orientations, Pt(533) and Pt(443), a hysteresis was present at 10^{-3} mbar, but vanished again at 10^{-2} mbar. LEED showed a disordered surface at 10^{-3} mbar.

The hysteresis of the reaction rate observed in T-cycling experiments is also a function of feed composition and surface structure. Under reaction conditions, low-index surface planes have a higher stability than high-index surface planes.

For Pt(100) we find that the total pressure has a strong effect on the reactivity and selectivity. In view of the very low oxygen sticking coefficient of the hex reconstructed surface where oxygen sticking coefficient, $s(O_2)$, is around $10^{-4} – 10^{-3}$, this result is not very surprising.

Chapter 6 Summary

Generally, the task to bridge the gaps between fundamental research and applied heterogeneous catalysis is one of the major challenges in catalysis science. As a part of this effort, in this work, ammonia oxidation over various model Pt catalysis has been studied, following the strategy of systematically increasing the total pressure and varying the crystallographic orientations, the reaction kinetics have been measured. The aim was to find out the dominant surface species, the influence of surface structure, and the effect of restructuring induced by reaction and adsorption.

First of all, the molecular adsorption and dissociative adsorption of ammonia and oxygen on Pt(443) were studied via QMS, Kelvin probe and LEED. With oxygen adsorption steps coalesce. This structure is stable at room temperature in UHV. During ammonia oxidation process on Pt(443) such step coalescence was not observed probably due to oxygen adatoms being reacted away immediately by the hydrogen from ammonia.

The steady state kinetics of ammonia oxidation over Pt surfaces have been studied under low pressure (10^{-6} to 10^{-4} mbar) and intermediate pressure (10^{-3} to 10^{-2} mbar) range. All single crystal results with different orientations agree that the steady state reaction between NH_3 and O_2 leads to N_2 and H_2O formation at low temperature, but the selectivity switch to NO and H_2O as dominant production at higher temperature. The exact temperature at which the selectivity change occurs depends strongly on the feed composition and the surface structure.

On Pt(865), at low temperature (~550 K) no NO production occurs; and the selectivity is towards N_2 at ~ 650 K, selectivity switches to NO if oxygen is in excess. Excess ammonia inhibits the reaction to some extent, which is attributed to the blocking of adsorption sites by N-containing species.

Ammonia oxidation over different Pt crystal surfaces, from single crystals to polycrystalline Pt, has been studied in the 10^{-5} to 10^{-2} mbar range. Surface structure has a strong effect on the reaction rate and on the selectivity. The reaction is associated with structural modification of surfaces. High-index planes have higher reaction rate than low-index planes, the reactive sticking coefficient of oxygen over Pt foil reaches 0.14, compared with other single crystal surfaces, the reaction rate over Pt foil is the highest one, then the activity decreased in the order Pt(865), Pt(533), Pt(443), and Pt(100).

On Pt(443) no LEED detectable substrate changes and no rate hysteresis occurred below 10^{-3} mbar. But above 10^{-3} mbar a substantial hysteresis effect were seen. The restructuring which tends to increase with rising total pressure was found to depend in a non-monotonic way on the total pressure. So on both orientations, Pt(533) and Pt(443), a hysteresis was present at 10^{-3} mbar, but vanished again at 10^{-2} mbar. LEED showed a disordered surface at 10^{-3} mbar.

The occurrence of a hysteresis in the reaction rate is also a function of the feed composition and of the surface structure. Under reaction conditions, low-index surfaces have higher stability than high-index surface planes.

In a high-pressure reaction cell that is connected to a UHV system, the kinetics of ammonia oxidation over Pt surfaces has been studied in 10^{-3} – 10^{-2} mbar range. The temperature of reaction rate maximum shifts to higher temperature with increasing total pressure. The reactivity of Pt(100) strongly depends on the total pressure. A wide hysteresis occurs due to an adsorbate-induced phase transition, from an inactive hexagonal structure to an active bulk-like (1×1) structure.

The spatiotemporal dynamics of ammonia oxidation on Pt(100) and Pt(443) have been studied by PEEM in the UHV system. Reaction fronts and spatially homogeneous transition were observed on Pt(100). Since the reaction proceeds spatially homogeneously over Pt(443), these results indicate that nonlinear phenomena of reaction rate on Pt(100) could be assigned to the phase transition from

active 1×1 to inactive hex phase.

Reference

1. Hagen, J., *Industrial Catalysis: A Practical Approach*. 2006, Weinheim: Wiley-VCH.
2. Freund, H.-J., et al., *Models in Heterogeneous Catalysis: Surface Science Quo Vadis?* Phys. Stat. Sol. (a), 2001. **187**(1): p. 257-274.
3. Somorjai, G.A., *Molecular concepts of heterogeneous catalysis.* Journal of Molecular Structure: THEOCHEM, 1998. **424**(1-2): p. 101-117.
4. Somorjai, G.A., *Directions of theoretical and experimental investigations into the mechanisms of heterogeneous catalysis.* Catal. Lett., 1991. **9**(2): p. 311-328.
5. Hutchings, G.J., *Promotion in heterogeneous Catalysis: a topic requiring a new approach.* Catal. Lett., 2001. **75**(1-2): p. 2001.
6. Jacobs, P.W. and G.A. Somorjai, *Conversion of heterogeneous catalysis from art to science: the surface science of heterogeneous catalysis.* Journal of Molecular Catalysis A: Chemical, 1998. **131**(1-3): p. 5-18.
7. Rotermund, H.H., *Imaging of dynamic processes on surfaces by light.* Surf. Sci. Rep., 1997. **29**: p. 267.
8. Dellwig, T., et al., *Bridging the Pressure and Materials Gaps: High Pressure Sum Frequency Generation Study on Supported Pd Nanoparticles.* Physical Review Letters, 2000. **85**(4): p. 776-779.
9. Somorjai, G.A., et al., *The evolution of model catalytic systems; studies of structure, bonding and dynamics from single crystal metal surfaces to nanoparticles, and from low pressure (<10(–3) Torr) to high pressure (>10(–3) Torr) to liquid interfaces.* Physical Chemistry Chemical Physics, 2007. **9**(27): p. 3500-3513.
10. Offermans, W.K., A.P.J. Jansen, and R.A.v. Santen, *Ammonia activation on platinum (111): A density functional theory study.* Surf. Sci, 2006. **600**(9): p. 1714-1734.
11. Rafti, M., et al., *Homogeneous and front-induced surface transformations during catalytic oxidation of ammonia over Pt(100).* Chemical Physics Letters, 2007. **446**(4-6): p. 323-328.
12. Scheibe, A., S. Gunther, and R. Imbihl, *Selectivity changes due to restructuring of the Pt(533) surface in the Ammonia + Oxygen reaction.* Catal. Lett. , 2003. **86**(1-3): p. 33-37.
13. Scheibe, A., M. Hinz, and R. Imbihl, *Kinetics of ammonia oxidation on stepped platinum surfaces II. Simulation results.* Surf. Sci., 2005. **576**: p. 131-144.
14. Scheibe, A., U. Lins, and R. Imbihl, *Kinetics of ammonia oxidation on stepped platinum surfaces. I. Experimental results.* Surf. Sci., 2005. **577**: p. 1-14.
15. Zeng, Y. and R. Imbihl, *Structure sensitive reaction - ammonia oxidation over Pt.* To be submitted.
16. Imbihl, R., et al., *Catalytic ammonia oxidation on platinum: mechanism and catalyst restructuring at high and low pressure* Physical Chemistry Chemical Physics, 2007. **9**(27): p.

3522-3540.

17. Kondratenko, V.A. and M. Baerns, *Mechanistic and kinetic insights into N2O decomposition over Pt gauze.* J. Catal., 2004. **225**(1): p. 37-44.
18. Kraehnert, R., *Ammonia Oxidation over Polycrystalline Platinum: Surface Morphology and Kinetics at Atmospheric Pressure*. 2005, der Technischen Universitaet Berlin: Berlin. p. 167.
19. Stacey, M.H., Catalysis 1980. **3**: p. 98.
20. Chilton, T.H., *The manufacture of nitric acid by the oxidation of ammonia Chemical Engineering Progress Monograph Series No. 3*. Vol. 56. 1960, New York: American Institute of Chemical Engineers.
21. Asscher, M., et al., *A Molecular Beam Surface Scattering Study of Ammonia Oxidation on the Pt(111) Crystal Face.* J. Phys. Chem., 1984. **88**: p. 3233-3238.
22. Bradley, J.M., A. Hopkinson, and D.A. King, *Control of Biphasic Surface Reaction by Oxygen Coverage: The Catalytic Oxydation of Ammonia over Pt(100).* J. Phys. Chem., 1995. **99**: p. 17032-17042.
23. Fogel, Y.M., et al., *Use of secondary ion emission to study the catalytic oxidation of ammonia on platinum.* Kinetika i Kataliz, 1964. **5**(3): p. 496-504.
24. Pignet, T. and L.D. Schmidt, *Kinetics of ammonia oxidation on Pt, Rh and Pd.* J. Catal., 1975. **40**: p. 212-225.
25. Baerns, M., et al., *Bridging the pressure and material gap in the catalytic ammonia oxidation: structural and catalytic properties of different platinum catalysts.* J. Catal., 2005. **232**: p. 226-238.
26. Gland, J.L. and V.N. Korchak, *Ammonia Oxidation on a Stepped Platinum Single-Crystal Surface.* J. Catal., 1978. **53**: p. 9-23.
27. Löffler, D.G. and L.D. Schmidt, *Kinetics of NH3 decomposition on single crystal planes of Pt.* Surf. Sci., 1976. **59**(1): p. 195-204.
28. Pignet, T. and L.D. Schmidt, *Selectivity of NH3 oxidation on platinum.* Chemical Engineering Science, 1974. **29**(5): p. 1123-1131.
29. Flytzani-Stephanopoulos, M., L.D. Schmidt, and R. Caretta, *Steady state and transient oscillations in ammonia oxidation on platinum.* J. Catal., 1980. **64**: p. 346.
30. Ostermaier, J.J., J.R. Katzer, and W.H. Manogue, *Crystallite Size Effects in the Low-Temperature Oxidation of Ammonia Over Supported Platinum.* J. Catal., 1974. **33**: p. 457-473.
31. Morrow, B. and I. Cody, *Infrared study of adsorption and oxidation of ammonia on platinum* J. Catal., 1976. **45**(2): p. 151-162.
32. Hannevold, L., et al., *Reconstruction of platinum-rhodium catalysts during oxidation of ammonia* Applied Catalysis a-General, 2005. **284**(1-2): p. 163-176.
33. Löffler, D.G. and L.D. Schmidt, *Kinetic of NH3 decomposition on Polycrystalline Pt.* J. Catal., 1976. **41**(3): p. 440-454.
34. Sexton, B.A. and G.E. Mitchell, *Vibrational spectra of ammonia chemisorbed on Pt(111) I. Identification of chemisorbed states.* Surf. Sci., 1980. **99**: p. 523-538.
35. Sexton, B.A. and G.E. Mitchell, *Vibrational spectra of ammonia chemisorbed on platinum (111) II. The electron scattering mechanism.* Surf. Sci., 1980. **99**(3): p. 539-552.
36. Bradley, J.M., A. Hopkinson, and D.A. King, *A molecular beam study of ammonia*

adsorption on Pt(100). Surf. Sci., 1997. **371**: p. 255-263.

37. Gland, J.L. and E.B. Kollin, *Ammonia adsorption on the Pt(111) and Pt(s)-6(111)x(111) surfaces.* Surf. Sci., 1981. **104**: p. 478-490.
38. Guthrie, W.L., J.D. Sokol, and G.A. Somorjai, *The decomposition of ammonia on the flat (111) and stepped (557) platinum crystal surfaces.* Surf. Sci. , 1981. **109**(2): p. 390-418.
39. Gohndrone, J.M., et al., *Ammonia adsorption and decomposition on several faces of platinum.* J. Vac. Sci. Technol. A, 1989. **7**(3): p. 1986-1990.
40. Jennison, D.R., P.A. Schultz, and M.P. Sears, *Ab initio calculations of adsorbate hydrogen-bond strength: ammonia on Pt(111).* Surf. Sci., 1996. **368**: p. 253-257.
41. Fisher, G.B., *The electronic structure of two forms of molecular ammonia adsorbed on Pt(111).* Chemical Physics Letters, 1981. **79**(3): p. 452-458.
42. Novell-Leruth, G., et al., *DFT Characterization of Adsorbed NHx Species on Pt(100) and Pt(111) Surfaces.* J. Phys. Chem. B, 2005. **109**: p. 18061-18069.
43. Sun, Y.-M., et al., *Electron-induced surface chemistry: Production and characterization of NH2 and NH species on Pt(111).* Journal of Vacuum Science & Technology A: Vacuum, Surfaces and Film, 1996. **14**(3): p. 1516-1521.
44. Papapolymerou, G. and V. Bontozoglou, *Decomposition of NH3 on Pd and Ir. Comparison with Pt and Rh.* J. Mol. Catal. A: Chem., 1997. **120**: p. 165-171.
45. Richardson, D.J., et al., *A Study of Ammonia Decomposition Over Pt/Alumina.* Trans IChemE, Part A, Chemical Engineering Research and Design, 2004. **82**(A10): p. 1397–1403.
46. Bonzel, H.P., G. Broden, and G. Pirug, *Structure sensitivity of NO adsorption on a smooth and stepped Pt(100) surface.* J. Catal., 1978. **53**: p. 96-105.
47. Bonzel, H.P. and G. Pirug, *Photoelectron spectroscopy of NO adsorbed on Pt(100).* Surf. Sci., 1977. **62**: p. 45-60.
48. Campbell, C.T., G. Ertl, and J. Segner, *A molecular beam study on the interaction of NO with a Pt(111) surface.* Surf. Sci., 1982. **115**: p. 309-322.
49. Ge, Q. and D.A. King, *Energetics, geometry and spin density of NO chemisorbed on Pt(111).* Chemical Physics Letters, 1998. **285**: p. 15-20.
50. Gland, J.L. and V.N. Korchak, *The Catalytic Reduction of Nitric Oxide with Ammonia over a Stepped Platinum Single Crystal Surface.* J. Catal., 1978. **55**: p. 324-336.
51. Gland, J.L. and B.A. Sexton, *Nitric oxide adsorption on the Pt(111) surface.* Surf. Sci., 1980. **94**: p. 355-368.
52. Tsukahara, N., et al., *Adsorption states of NO on the Pt(111) step surface.* Surf. Sci., 2006. **600**: p. 3477-3483.
53. Backus, E.H.G., et al., *Adsorption and dissociation of NO on stepped Pt (533).* Journal of Chemical Physics, 2004. **121**(16): p. 7946-7954.
54. Park, Y.O., R.I. Masel, and K. Stolt, *An XPS study of CO and NO adsorption on Pt(410).* Surf. Sci., 1983. **131**: p. L385 -389.
55. Ge, Q. and M. Neurock, *Structure Dependence of NO Adsorption and Dissociation on Platinum Surfaces.* J. Am. Chem. Soc., 2004. **126**: p. 1551-1559.
56. Sugisawa, T., et al., *Adsorption and decomposition of NO on Pt (112).* Applied Surface Science, 2001. **169-170**: p. 292-295.
57. Lombardo, S.J., F. Esch, and R. Imbihl, *The NO+NH3 reaction on Pt(100): steady state and*

oscillatory kinetics. Surf. Sci., 1992. **271**: p. L367-L372.

58. Katona, T., L. Guczi, and G.A. Somorjai, *The Reduction of Nitric Oxide by Ammonia over Polycrystalline Platinum Model Catalysts in the Presence of Oxygen.* J. Catal., 1992. **135**: p. 434-443.
59. Lombardo, S.J., T. Fink, and R. Imbihl, *Simulations of the nitric oxide + ammonia and nitric oxide + hydrogen reactions on platinum(100): steady-state and oscillatory kinetics.* J. Chem. Phys., 1993. **98**(7): p. 5526-5539.
60. van Tol, M.F.H., et al., *Oscillatory behaviour of the reduction of nitric oxide by ammonia over the Pt(100) single-crystal surface: the role of oxygen, comparison with the NO-H2 reaction and a general reaction mechanism for NO reduction by NH3 over Pt.* Surf. Sci., 1992. **274**: p. 63-81.
61. Kim, M., D.A. King, and S.J. Pratt, *In Situ Characterization of the Surface Reaction between Chemisorbed Ammonia and Oxygen on Pt(100).* J. Am. Chem. Society, 2000. **122**(10): p. 2409-2410.
62. Weststrate, C.J., et al., *Ammonia oxidation on Pt(410).* J. Catal., 2006. **242**: p. 184-194.
63. Mieher, W.D. and W. Ho, *Thermally activated oxidation of NH3 on Pt(111): intermediate species and reaction mechanisms.* Surf. Sci., 1995. **322**: p. 151-167.
64. Somorjai, G.A., *The experimental of the role of surface restructuring during catalytic reactions.* Catal. Lett., 1992. **12**: p. 17-34.
65. Somorjai, G.A., *The structure sensitivity and insensitivity of catalytic reactions in light of the adsorbate induced dynamic restructuring of surfaces.* Catal. Lett., 1990. **7**: p. 169-182.
66. Lang, B., R.W. Joyner, and G.A. Somorjai, *Low energy electron diffraction studies of high index crystal surfaces of platinum* Surf. Sci., 1972. **30**(2): p. 440-453.
67. Ertl, G. and J. Kueppers, *Low energy electrons and surface chemistry*. 1985, Weinheim: VCH.
68. Chorkendorff, I. and J.W. Niemantsverdriet, *Concepts of Modern Catalysis and Kinetics*. 2003, Weinheim: Wiley-VCH.
69. Niemantsverdriet, J.W., *Spectroscopy in catalysis: an introduction*. 1993, Weinheim: VCH.
70. Henzler, M., *LEED-investigation of step arrays on cleaved germanium (111) surfaces.* Surf. Sci., 1970. **19**(1): p. 159-171.
71. Brune, D., et al., eds. *Surface characterization*. Auger electron spectroscopy, ed. C.-O.A. Olsson, S.E. Hoernstroem, and S. Hogmark. 1997, Wiley-VCH: Weinheim.
72. Christmann, K., *Introduction to surface physical chemistry*. 1991, Darmstadt: Steinkopff
73. Artsyukhovich, A.N., V.A. Ukraintsev, and I. Harrison, *Low temperature sticking and desorption dynamics of oxygen on Pt(111).* Surf. Sci., 1996. **347**: p. 303-318.
74. Campbell, C.T., et al., *A molecular beam study of the adsorption and desorption of oxygen from Pt (111)surface.* Surf. Sci, 1981. **107**(1): p. 220-236.
75. Derry, G.N. and P.N. Ross, *A work function change study of oxygen adsorption on Pt(111) and Pt(100).* J. Chem. Phys. , 1985. **82**(6): p. 2772-2778.
76. Blakely, D.W. and G.A. Somorjai, *The stability and structure of high miller index platinum crystal surfaces in vacuum and in the presence of adsorbed carbon and oxygen* Surf. Sci., 1977. **65**(2): p. 419-442.
77. Avery, N.R., *An EELS and TDS study of molecular oxygen desorption and decomposition on*

Pt(111). Chem. Phys. Lett., 1983. **96**(3): p. 371.

78. Bonzel, H.P. and R. Ku, *On the kinetic of oxygen adsorption on a Pt(111) surface.* Surf. Sci., 1973. **40**(1): p. 85-101.
79. Egl, A.-P., F. Eisert, and A. Rosen, *The temperature dependence of the initial sticking probability of oxygen on Pt(111) probed with second garmonic generation.* Surf. Sci, 1997. **382**: p. 57-66.
80. Gland, J.L., B.A. Sexton, and G.B. Fischer, *Oxygen interaction with the Pt(111) surface.* Surf. Sci., 1980. **95**: p. 587-602.
81. Griffiths, K., et al., *Interaction of O2 with Pt(100) 1. Equilibrium measurements.* Surf. Sci., 1984. **138**: p. 113.
82. Kokalj, A., A. Lesar, and M. Hodoscek, *Interaction of oxygen with the Pt (111) surface: a cluster model study.* Chemical Physics Letters, 1997. **268**: p. 43-49.
83. Lynch, M. and P. Hu, *A density functional theory study of CO and atomis oxygen chemisorption on Pt(111).* Surf. Sci., 2000. **458**: p. 1-14.
84. Ohno, Y. and T. Matsushima, *Dissociation of oxygen admolecules on platinum (110)(1×2) reconstructed surfaces at low temperatures.* Surf. Sci., 1991. **241**: p. 47-53.
85. Parker, D.H., M.E. Bartramm, and B.E. Koel, *Study of high coverages of atomic oxygen on the Pt(111) surface.* Surf. Sci., 1989. **217**(3): p. 489-510.
86. Parkinson, C.R., M. Walker, and C.F. McConville, *Reaction of atomic oxygen with a Pt(111) surface: chemical and structural determination using XPS, CAICISS and LEED.* Surf. Sci., 2003. **545**: p. 19-33.
87. Zhdanov, V.P. and B. Kasemo, *Simulation of oxygen desorption from Pt(111).* Surf. Sci., 1998. **415**: p. 403-410.
88. Derry, G.N. and P.N. Ross, *High coverage states of oxygen adsorbed on Pt(100) and Pt(111) surfaces.* Surf. Sci., 1984. **140**(1): p. 165-180.
89. Barteau, M.A., E.I. Ko, and R.J. Madix, *The adsorption of CO, O2, and H2 on Pt(100)-(5×20).* Surf. Sci., 1981. **102**(1): p. 99-117.
90. Deskins, N.A., J. Lauterbach, and K.T. Thomson, *Lifting the Pt(100) surface reconstruction through oxygen adsorption: a density functional theory analysis.* J. Chem. Phys., 2005. **122**(18): p. 184709.
91. Gee, A.T. and B.E. Hayden, *The dynamics of O2 adsorption on Pt(533): Step mediated molecular chemisorption and dissociation.* Journal of Chemical Physics, 2000. **113**(22): p. 10333-10343.
92. Lindauer, G., P. Légaré, and G. Maire, *On the interaction of oxygen with Pt single crystals; LEED study of step coalescence.* Surf. Sci., 1983. **126**: p. 301-306.
93. Rar, A. and T. Matsushima, *Desorption and dissociation of oxygen admolecules on a stepped platinum (533) surface.* Surf. Sci., 1994: p. 89-96.
94. Savchenko, V.I. and N.I. Efremova, *On the kinetics of oxygen adsorption over stepped Pt surface.* Reaction Kinetics and Catalysis Letters, 1995. **56**(1): p. 97-105.
95. Schwaha, K. and E. Bechtold, *The adsorption of oxygen on the stepped Pt(S)-[9(111)×(111)] face.* Surf. Sci., 1977. **65**: p. 277-286.
96. Wang, H., et al., *Adsorption and dissociation of oxygen on Pt(335).* Surf. Sci., 1997. **372**: p. 267-278.

97. Godowski, P.J., et al., *Investigation of the CO + NO reaction over the Cu(001) surface.* Chemical Physics Letters, 2005. **406**: p. 441-445.
98. Wee, A.T.S., et al., *SIMS study of NO, CO adsorption on Cu(100) and Cu(210) surfaces.* Surf. Sci., 1994. **304**: p. 145-158.
99. Wickham, D.T., B.A. Banse, and B.E. Koel, *The adsorption of nitric oxide and nitrogen dioxide on polycrystalline platinum.* Surf. Sci., 1989. **223**: p. 82-100.
100. Gorte, R.J., L.D. Schmidt, and J.L. Gland, *Binding states and decomposition of NO on single crystal planes of Pt.* Surf. Sci., 1981. **109**: p. 367 - 380.
101. Günther, S., et al., *In situ x-ray photoelectron spectroscopy of catalytic ammonia oxidation over a Pt(533) surface.*
102. Freyer, N., et al., *Oxygen adsorption on Pt(110)-(1×2) and Pt(110)-(1×1).* Surf. Sci., 1986. **166**: p. 206-220.
103. Gohndrone, J.M. and R.I. Masel, *A TPD study of NO decomposition on Pt(100), Pt(411) and Pt(211).* Surf. Sci., 1989. **209**: p. 44 -56.
104. Gohndrone, J.M., Y.O. Park, and R.I. Masel, *A comparison of NO decomposition on Pt(210) and Pt(410).* J. Catal., 1985. **95**: p. 244 - 248.
105. Hove, M.A.V. and G.A. Somorjai, *A new microfacet notation for high-miller-index surfaces of cubic material with terrace, step and kink structures.* Surf. Sci., 1980. **92**: p. 489-518.
106. Boudart, M., Advances in Catalysis, 1969. **20**: p. 153.
107. Flytzani-Stephanopoulos, M. and L.D. Schmidt, *Morphology and etching processes on macroscopic metal catalysts.* Progress in Surface Science 1979. **9**: p. 83-111.
108. Uchida, Y., G. Lehmpfuhl, and R. Imbihl, *Reflection electron microscopy of the catalytic etching of platinum single-crystal spheres in carbon monoxide + oxygen.* Surf. Sci., 1990. **234**(1-2): p. 27-36.
109. McCabe, R.W., T. Pignet, and L.D. Schmidt, *Catalytic etching of platinum in ammonia oxidation.* J. Catal., 1974. **32**: p. 114-126.
110. Flytzani-stephanopoulos, M., S. Wong, and L. Schmidt, *Surface Morphology of Platinum Catalysts.* J. Catal., 1977. **49**(1): p. 51.
111. Hannevold, L., et al., *Reconstruction of platinum–rhodium catalysts during oxidation of ammonia.* Appl. Catal. A, 2005. **284**(1-2): p. 163-176.
112. Nilsen, O., A. Kjekshus, and H. Fjellvag, *Reconstruction and loss of platinum catalyst during oxidation of ammonia.* Appl. Catal. A, 2001. **207**: p. 43-54.
113. Schmidt, L.D., *From chemisorption to surface reactions to catalysis in catalytic oxidation reactions.* J, Vac. Sci. Technol., 1975. **12**(1): p. 341.

List of abbreviations

AES	Auger Electron Spectroscopy
CPD	Contact Potential Difference
DFG	Deutsche Forschungsgemeinschaft (German Research Foundation)
DFT	Density Function Theory
EDX	Energy Dispersive X-ray analysis
FWHM	Full width at Half Minimum
LEED	Low Energy Electron Microscopy
PEEM	Photoelectron Emission Microscopy
QMS	Quadrupole Mass Spectrometer
sccm	The unit of the flow rate, cm^3/min
SEM	Scanning Electron Microscopy
STM	Scanning Tunnelling Microscopy
TDS	Thermal Desorption Spectroscopy
TPD	Temperature-programmed Desorption
TPRS	Temperature-programmed Reaction Spectrum
UHV	Ultrahigh Vacuum
UV	Ultraviolet

List of publications

- Catalytic ammonia oxidation on platinum: mechanism and catalyst restructuring at high and low pressure
  Imbihl, R.; Scheibe, A.; Zeng, Y. F.; Guenther, S.; Kraehnert, R.; Kondratenko, V. A.; Baerns, M.; Offermans, W. K.; Jansen, A. P. J.; Van Santen, R. A.
  Physical chemistry chemical physics 9 (2007) 3522

- Homogeneous and front-induced surface transformations during catalytic oxidation of ammonia over Pt(100)
  Rafti, Matias; Lovis, Florian; Zeng, YingFeng; Imbihl, Ronald
  Chemical Physics Letters 446 (2007) 323

- Structure sensitive reaction—ammonia oxidation over Pt
  Zeng, YingFeng; Imbihl, Ronald
  To be submitted

Curriculum Vitae

Personal

Name	Zeng, Yingfeng
Birth	Nov. 28, 1974 in Nanchang, China
Nationality	Chinese
Marital Status	Married

Education

8.2003 – present	Ph.D. in Prof. Dr. R. Imbihl's group, Institute of physical chemistry and electrochemistry, Leibniz University of Hanover, Germany
6.2001	Master Degree in Engineering China University of Petroleum, Beijing
9.1998 – 6.2001	Prof. Chen Yuezhu's Group, State Key Laboratory of Heavy Oil Processing, Faculty of Chemical Engineering, China University of Petroleum, Beijing
6.1997	Bachelor Degree in Engineering Nanchang University
9.1993 – 6.1997	Department of Chemical Engineering, Nanchang University

Professional Experience

7. 2001 – 7. 2003	Engineer in Lubricant Company, SINOPEC Corp., Beiing, China
7.1997 – 8.1998	Engineer in Guangzhou Tianli PCB Company, Guangzhou, China

Acknowledgements

The thesis work was carried out at the Institute of Physical Chemistry and Electrochemistry, University of Hanover from August 2003 to December 2007. Here, I would like to express my gratitude to all those who gave me help to complete this thesis.

Firstly, I would like to sincerely acknowledge my supervisor Prof. Dr. Ronald Imbihl for giving me opportunity to work in his group. And I want to express my gratitude to him for valuable help, stimulating and insightful suggestions and encouragement he gave to me in all the time of research and writing of this thesis.

My gratitude goes to former colleague, Dr. Sebastian Guenther for his valuable advice, suggestion and help at the beginning of my thesis work. And I also would like to thank all of my current and former colleague in the working group of Prof. Imbihl. I am indebted to Dr. Monika Hinz, Dr. Ling Zhou, Dr. Tobias Neubrand, Dr. Axel Scheibe, Dr. Miguel Pineda, Hong Liu and Florian Lovis. I also want to thank Dr. Armin Feldhoff for his kind help on SEM. I am especially grateful to Mrs. Carmen Gatzen for her help in the work and my life in Germany. I gratefully acknowledge the stimulating and insightful discussion during those project meetings with the groups from Berlin and Eindhoven.

Thanks DFG foundation for financial support, this thesis work was supported by the DFG under the priority program 1091 “Bridging the gap between ideal and real system in heterogeneous catalysis”.

Last but certainly not least, I am forever in debted to the love and caring of my family. I would thank my parent and sister for their support during my whole research. Especially, I would like to give my special thanks to my wife Liqin whose patient love and substantial support enabled me to complete this work.